Understanding the Effects of Surface Roughness and Topology of Zinc on Biological Cell Function

Kieran Lapidge

Bachelor of Engineering
Major in Mechanical Engineering

Department of Engineering
Macquarie University

November 6, 2017

Supervisor: Dr Wei Xu

Acknowledgements

I would like to acknowledge those who have supported me through my education, and those who have influenced my chosen career path, namely my father and various people I have encountered as I have progressed through university.

I would like to thank my thesis project supervisors; Dr Wei Xu for his time and effort in guiding and assisting me in this project. I would like to say special thanks to Sue Lindsay from the Macquarie University Microscopy Lab for all her time taken to help out in the analysis phase of my project. I would like to thank Wendy Tao and Mynga Nhuyen from the materials department for their time and efforts.

Statement of Candidate

I, Kieran Lapidge, declare that this report, submitted as part of the requirement for the award of Bachelor of Engineering, Macquarie University, is entirely my own work unless otherwise referenced or acknowledged. This document has not been submitted for qualification or assessment at any academic institution.

Student's Name: Kieran Lapidge

Date: November 6, 2017

Abstract

One significant research area in rapidly advancing medical industry is the suitability of various materials for biodegradable bone implants. Amongst biodegradable solutions, zinc has seen in increased interest as it has displayed potential to be more suitable over common current materials such as magnesium. For this notion to progress, research must be done into how the surface conditions of zinc metal effects the biological cellular function in which it is to be applied. This project will see how changing the roughness and topology of zinc surface can optimise how well it is suited for bone implants. The project yielded inconclusive results, showing there is still much we research to be done in this area in order to understand just how zinc may be applied to bone implantation.

Table of Contents

List of figures

List of Tables

Introduction

The biology of the human body, as sophisticated and incredible as it is, has very real limitations with regards to both performance and recovery. With the medical industry branching into various fields of engineering, and humanity's collective desire to optimise quality of life, many of these limitations are seeing increased potential to be overcome. An ever advancing medical industry is generating great focus on materials that can be applied to serve various purposes in the human body. Such materials may be called 'biocompatible' have the potential to overcome various limitations and provide benefits to certain situations and natural processes. A biocompatible material is simply a material that can be applied to the human body and perform its intended function effectively without harming the host. More specifically, a biodegradable material is a biocompatible material that degrades (wastes away) as it performs its purpose.

Bone function and repair is a common field where these materials are utilised. They are often required for support and repair after the bone has incurred trauma such as breakage, fracture, tumour removal and surgical alterations. In this context, such implanted materials are usually metals. These metal implants can fall under one of two categories; permanent and biodegradable. Permanent bone implants are constructed with metals that will not corrode in the body. Although the bone does heal onto the surface, the implant will eventually require replacing after the system has aged, which is an invasive and expensive process. Biodegradable implants however slowly corrode away upon implementation and the bone will heal to take its place as it does so. The result will be an entirely healed bone once the metal has completely wasted away.

For this process to work effectively however, there must be a functional biological interaction between the bone and metal interface. The successfulness of this interaction depends largely on various material properties and conditions. The topology of the material surface is one such key feature.

Metals have been an increasing research area for bone implants as they have proven capable of displaying effective biodegradability, and other properties necessary for implants such as strength and durability. Most research and development has gone into magnesium and magnesium alloys due to its compatibility for this application, however it has been recognised lately that there may be much potential in the use instead of zinc and zinc alloys. Zinc has been recognised as it offers desirable mechanical properties, and has been realised to offer favourable biocompatible properties such as a lower toxicity potential. It is therefore of interest to conduct more research into the actual potential zinc metals have for biodegradable bone implants.

One particular area of interest is on how the topology of zinc metal affects the biological effectiveness of the implant. Changes to the surface conditions such as roughness and topological patterns of metals have been shown to influence how effectively bone cells will interact with it, although most of this research has been towards magnesium metals. This is true both on a

microscale and nanoscale, and research indicates the same is true for zinc. Since the initial successfulness of bone cell integration has a substantial bearing on how the implant will perform over its entire lifetime, further research into this area potentially has a large impact in progress in the field.

Project overview

Research into the topic, especially with iron and magnesium, has shown that topographies of metal biodegradable bone implants, at both a microscale and nanoscale, play a crucial role in how effectively the bone cells will bond to and interact with the material. This interaction has a substantial bearing on how the implant will perform over its entire lifetime.

This project aims to further understanding on how the topology and surface roughness of zinc metal effects cellular biological function when used as biodegradable bone implants. This ideally will progress an understanding on how these surface conditions can be leveraged to optimise how effectively a bone implant will function.

Through this project, the surface of samples of zinc metal will be physically manipulated to yield various topology conditions. The samples will then be suspended in biological solution that simulates the body biology matter in which they are to be applied. During this time, the cellular matter will interact with the zinc. The results of this interaction will then be analysed.

The manipulation of the zinc surface will be done two ways;

1. Grinding/sanding to a uniform and consistent surface roughness (non-ordered topology)
2. Ordered physical surface indentation (ordered topology)

Each method will be used to create a variety of different surface roughness's and topologies. Samples will also be prepared using combinations of the two methods for greater variety.

Primarily, how well the cells adhere and cultivate to the metal are of interest. Applicable equipment will be used to analyse and quantify biological effectiveness of the various samples.

Project goals

The primary goal of this project is to make a meaningful contribution to the progression of understanding on how the surface roughness and topology of zinc metal effects biological cell function for osseointegration. This may have influences primarily on two more broad focuses including:

1. A better understanding of how metal topology effects cell interaction in biocompatible materials (specifically zinc).
2. Development knowledge on the suitability of zinc for biodegradeable bone implants.

On a broader scale, this project may have influences in a number of secondary goals/outcomes. These may include:

- Link between surface wettability and cell integration
- Zinc toxicity in biological environments
- Provision of a greater source of reference material on experimented topographies for future work and reference
- Greater insight on osseointegration for zinc and zinc alloys
- Observe effects surface roughness has on cell proliferation
- Observe effects surface roughness has on the fate of adhered cells

Background Information

Much of the foundation of knowledge and practice of surface modification of biodegradable materials has been focused on magnesium alloys. This is not just for surface modification but of the use of the material as an implant in general. Much of the understanding on topology and its effects with respects to biocompatibility with therefore be based on research and observation on other materials. Since the potential of zinc for biodegradable implants has been realised, there has been a growth in zinc specific research, although much of this research is still in its moderate stages of development. The field of cell-surface interaction is well researched as it applies heavily within the medical industry. Analysis of this knowledge is necessary in understanding and efficiently conducting the project to explore how this can be applied to zinc metals.

Zinc as a Biodegradable Implant

There has not been a large amount of research conducted into zinc alloys for use of biodegradable implants, however interest does seem to be increasing for various reasons. Most previous research and practice has been into magnesium alloy solutions. There has been increasing notation however of how magnesium alloys behave with increasing percentage content of zinc. With Zinc noted to have a more desirable corrosion with respect to biodegradability, this is one primary factor into the necessity to research deeper into zinc alternatives.

Zinc started gaining attention as it is one of an array of metals that is commonly alloyed in small percentages with magnesium implants. This was done primarily in order to alter the corrosion resistance of the metal, and hence its biocompatibility. Zinc being a more noble (less reactive) metal than magnesium positively affects the corrosion resistance and strength of magnesium [1]. As well as this, zinc is naturally fairly abundant within the human body as it is involved with bodily function. This means toxicity is generally less of an issue, especially when taking into account zinc lower corrosion rate. The recommended dietary allowance (RDA) and recommended upper limit for zinc are 15 and 40 mg day−1, respectively [1]. The consumption of zinc in amounts higher than these values is generally considered relatively non-toxic, and amounts approaching 100 mg per day can be tolerated for some time [1]. These figures become relevant when analysing biocompatibility. As zinc percentage in magnesium based alloys continued increasing with favourable results, zinc based alloys were indicated as having potential, which seemed favourable as zinc manufacturability was also more cost efficient. In a test conducted comparing various alloys in simulated bodily fluid (SBF), zinc based alloys consistently corroded 3-5 times faster than that of magnesium [1]. In this experiment, the surfaces of all of the alloys were covered by relatively compact layers of corrosion products. Due to internal stress these layers are cracked and locally detached from the surface in some areas.

Cell Surface interaction

The nature of any implant surface has a large effect on the cell's response and interaction with it. A substantial amount of research has been carried out on manipulating cell responses through surface topographical modification, notably recently. Aspects to be considered relevant to cell and surface interaction include cell proliferation (the cell's readiness to divide and grow), migration (orchestrated movement of cells in particular directions to specific locations), and differentiation (cells changing from one type to another) [2]. In the context of bone implants, implant failures are frequently attributed to poor osseointegration between bones and implant surfaces [3]. A number of surface modification methods have been established in order to improve implant integration, including modification of surface topography, chemistry, wettability and charge [2]. Random patterned surfaces are difficult to reproduce. For example, even surfaces with the same surface roughness parameter Ra can have two distinctly different surface profiles [4]. Limited research has so far shown that limited evidence suggests that ordered patterned surfaces could lead to enhanced metabolic activities and elongated cellular morphology compared to random counterparts [5]. Recent advances in technology however have improved techniques available for ordered surface topology manipulation. Electron beam lithography (EBL) is one such method that can exercise very fine control over laser etching into metal surfaces.

The bone and the implant will interact simultaneously at different scales. Emerging evidence has shown that surface topographies at both microscale and nanoscale play a crucial role in regulating morphology, adhesion, differentiation, migration, proliferation and eventually, the fate of cell [2], and some studies have shown that nano features are more effective in improving osseointegration than micro scaled surfaces [6]. This contributed to the necessity for finetuned surface modification methods such as Electron beam lithography. However there still exists no clear conclusions on the optimum geometry and surface topography scale [2]. Figure 1 below shows how interaction of the bone and implant surface differ at different scales.

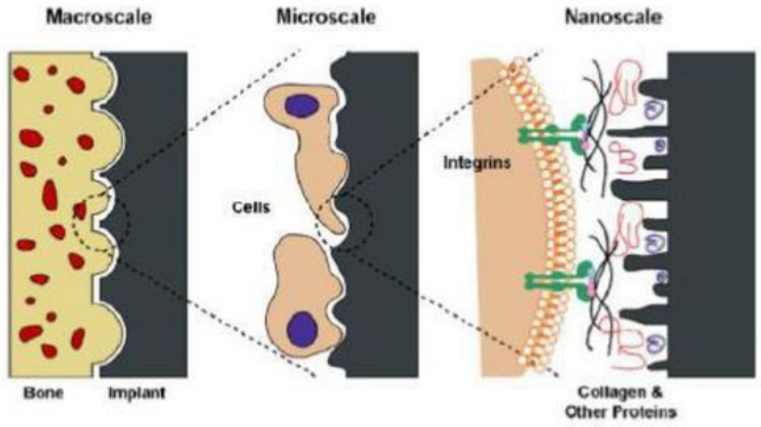

Figure 1 - Interaction of bone and implant surfaces at different scales

Semi ordered and ordered patterns fall into 7 categories; dots, tubes, protrusions, pits, grooves, intricate matrices and hierarchical micro-nano topographies. Multiple experiments have compared the general effectiveness of each method, with somewhat conclusive results.

Dots are small protrusions on a surface, with diameter significantly larger than the depth. Experiments have shown that the degree of osteogenesis was indicated by the size of the 'focal adhesion', and that degree of osteogenesis was proportional to the increased focal adhesion size [8][9].

Pits are like small holes in the material. The effectiveness seems to change with the pit diameter, and the symmetry of pit arrays. 30-40 nanometer diameter pits were observed to be more osteogenic than that of smaller diameters [10]. It has also been reported that 120-nm diameter nanopits arranged in a square order prevented osteoblast adhesion and spreading compared to randomly arranged counterparts [11].

Effectiveness of etched grooves in a material is determined by altering the groove's ridge width, groove width, depth, pitch, and pattern density. It is a common method of surface topology modification. Cell morphology is typically elongated along the grooves. In general, decreasing groove width and increasing groove depth encourage formation of elongated cells and vice versa [2]. In general comparison of 13 micropatterned surfaces, Justesen et al. concluded that the vertical dimension (i.e. height) exerted more effects on cell responses (morphology and spreading) than the lateral dimensions [12].

Experimental Procedures

The project methodology was laid out in a and practical process. Following this process involved discrete and systematic phases in order to make sure the process was coherent in conducting and also documenting. The Zinc metal acquired for the experimentation was of high quality %wrt to keep results highly relevant to zinc. Rods were acquired as they enabled an easy and efficient manufacturing process to provide small samples with a high surface area for experimentation. Of all the samples manufactured, not all would yield results, due to the touchy nature of biological experimentation.

The procedure can be divided into 4 main phases:

1. Zinc preparation and surface modification
2. Pre-cell culture analysis
3. Cell culture testing
4. Post-cell culture analysis

Zinc preparation and surface modification

Cutting zinc to shape

The zinc rods were cut into cylindrical pieces 2.5mm long and 10mm in diameter using a Struers ACCUTOM cutting machine located in the Materials Department.

Figure 2 - Struers ACCUTOM cutting machine

After manually mounting the rod, the machine was able to digitally control movement of the cutting blade and rod mount, providing a series of cuts yielding pieces consistently accurate to 2.5mm.

Figure 3 - Zinc samples cut using Struers ACCUTOM cutting machine

This length was selected as it provided a sufficiently strong and rigid structure with enough length for easy manual control of the pieces throughout the subsequent steps in the project, yet small as to minimise necessary bio-material costs and maximise practicality. The material costs for the zinc itself was relatively minimal and not a primary concern. 50 pieces were cut overall, providing more than would be ideally required for the experiment so there were extra pieces in case they were later needed.

Modifying Zinc Surface Roughness

A systematic variety of topologies was desired in order to produce a favourable array of results. The manipulation of the zinc surface was done two ways:

1. Grinding/sanding to a uniform and consistent surface roughness (non-ordered topology)
2. Ordered surface indentation (ordered topology)

Grinding/Sanding

5 grades of surface roughness were produced. Various grit measures of silicon carbide sandpaper were used to conceive 4 of these levels of roughness. During this process, it was important to make sure that the top and bottom surfaces of the zinc pieces stayed level and parallel, and that

that relevant grit roughness had been achieved. In order to unsure the surface stayed level during the sanding, a specialised brass device was used.

Figure 4 - Brass and ceramic sanding device used to assist sanding

A lining of tape would adhere to the platform, and the bottom of the zinc sample would be adhered to this tape lining via a small amount of industrial glue. The central pillar of the device could then be raise dor lowered relative to its outer rim via its internal thread. The platform would be adjusted so that the top surface of the zinc sample protruded slightly above the outer rim. The device was then used to sand the sample across the sandpaper that was fixed on a flat and rigid surface. The outer rim of the device is composed of ceramic that is negligibly effected by sanding, so when the top of zinc sample sanded down to the level of the outer rim it cannot go any further, producing a flat sanded sample.

The 5^{th} grade of surface roughness was unable to be produced via this sanding method. In order to achieve this, a machine polisher was to be used. A Struers TEGRAMIN machine, located in the Materials Department was utilised for this. This machine required that the zinc samples first be fixed in a plastic-like rigid mount, so that is was compatible with its machinery. For this, a Struers Citopress Mounting Press was used, also located in the Materials department

To mount the zinc samples, they were place on the mounting press platform and lowered into the machine. A specialised powder substance is then poured in the cavity around the sample. The machine is then closed, and heat and pressure are applied to the powder substance, turning it to a hard solid substance around the zinc sample, only leaving the top surface of the zinc exposed.

Figure 5 - Struers Citopress mounting press machine

Once the zinc sample has been mounted it can then be polished. The mounted block is placed in the metal bracket of the polisher, and a program is run, sanding and polishing the substance. The final level of polishing was achieved using a fine diamond abrasive pad compatible with the equipment. This was done using a diamond matrix liquid abrasive.

Figure 7 - Struers TEGRAMIN

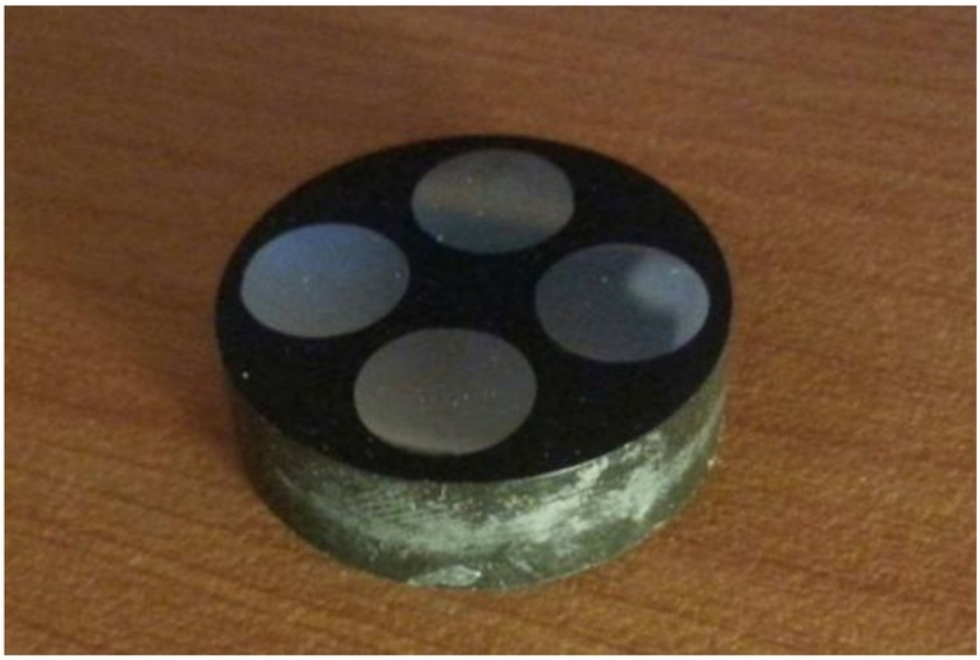

Figure 6 - 4 pieces of zinc mounted using mounting press

Ordered Pattern Impacting

In order to produce the ordered surface indentation patterns, a Struers DuraScan G5 hardness testing machine was used, located in the Materials Department.

Figure 8 - Struers DuraScan Hardness Tester

This machine utilises a diamond indenter and a fine controlled xy plane platform to move the object that is being indented. The force the indenter presses with is digitally controlled, accurately pressing with a user defined force, with a greater force producing a larger dent in the surface. This allowed dimensionally accurate lattices of indents to be created in the material surface. The equipment used a HV value to measure the force at which the indenter in applied. HV = kgf/mm^2.

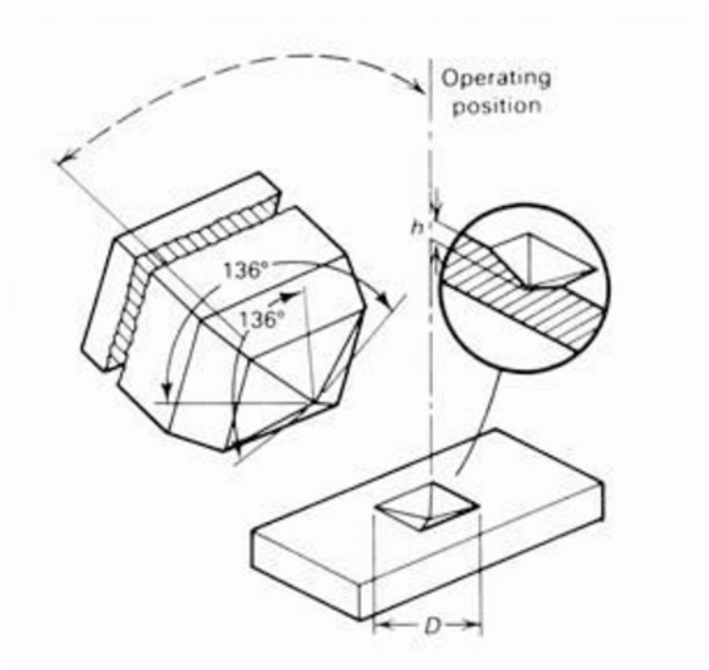

Figure 9 - Diagram of a the pyramidal diamond indenter of a Vickers hardness tester

This method combined with an array of different surface roughness's produced a diverse variety of surface topologies. Each sample was engraved with a number on the bottom surface to individually identify them. These numbers were noted for reference. 3 samples were made for each surface condition to improve precision of results. Below is a table listing all the samples and corresponding surface topology conditions.

Table 1 - All created zinc samples with their corresponding topologies

GRIT (P)	PATTERN	SAMPLE NUMBER
120	no pattern	#1,2,3
320	no pattern	#4,5,6
800	no pattern	#7,8,9
800	0.05HV, 100um between each impact	#10,11,12
800	0.2HV, 150um between each impact	#13,14,15
1200	no pattern	#16,17,18
1200	0.05HV, 60um between each impact	#19,20,21
1200	0.1HV, 80um between each impact	#22,23,24
polished	no pattern	A
polished	0.01HV, 40um between each impact 0.025HV, 60um between each impact 0.1HV, 100um between each impact	B1 B2 B3
polished	0.01HV, 40um between each impact 0.025HV, 60um between each impact 0.1HV, 100um between each impact	C1 C2 C3
polished	0.01HV, 40um between each impact 0.025HV, 60um between each impact 0.1HV, 100um between each impact	D1 D2 D3

Pre-Cell Culture Analysis

Reference Marking and Microscope Imaging

Since the indent patterns only covered a portion of the area of each sample surface, it was important to make sure the area could be later located, as it was unsure how visible the zinc surface would be after the cell culture testing. A reference mark on the relevant samples was made on the relevant samples by using a fine cutting blade to cut a groove in the side of the metal. This groove was visible when looking directly at the top surface of the sample. The relevant samples were then photographed using an Olympus SZX16 Stereomicroscope located in the microscopy lab, so that the modified area was able to be accurately located later in the project.

Figure 10 - Olympus SZX16 Stereomicroscope

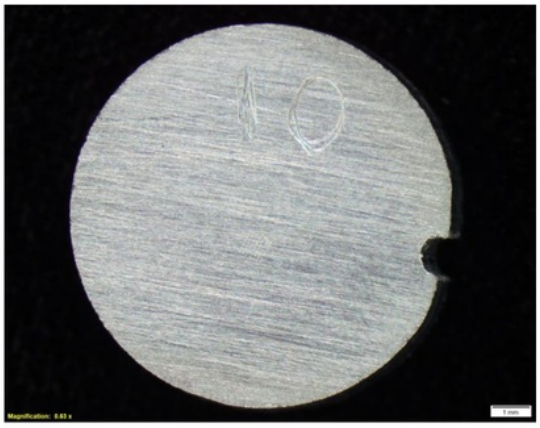

Figure 11 - Microscope image of zinc sample showing surface topology and reference mark

SEM Imaging

A PHENOM XL Benchtop Scanning Electron Microscope was then used to conduct high magnification and detailed imaging of the zinc surface topologies. This system loads the samples into a vacuumed chamber and provides a resolution of < 20nm. An acceleration voltage of 10kV, and a backscatter (BSD), as well as a secondary (SED) detector was used to conduct imaging at magnifications ranging from 250x to 4000x.

Figure 12 - PHENOM XL Benchtop SEM

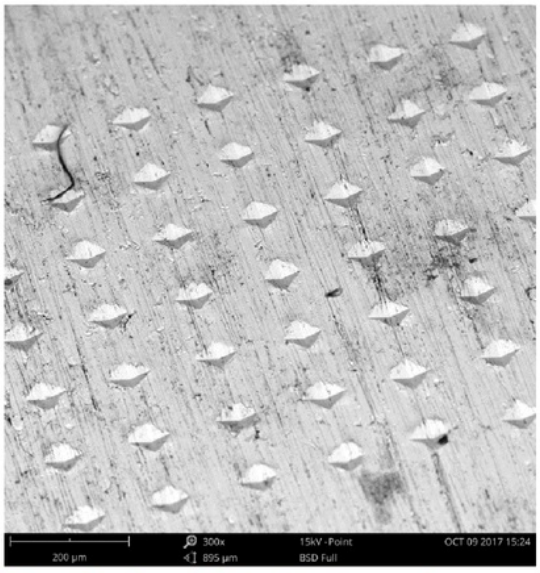

Figure 13 – Image of ordered pattern on zinc surface taken via SEM

This imaging process provided an appropriate reference analysis on the zinc surface, on which could be compared later to the cell culture results.

Wettability Testing

A Kruss Drop Shape Analyser DSA30 was used to perform measurements on the zinc surfaces to provide further quantification on the surface conditions. This equipment places a small drop of water (distilled water was used) on the material surface and used a high quality camera to observe the shape of the drop.

Figure 14 – Kruss Drop Shape Analyser DSA30

The image is displayed on a connected computer and the appropriate software is then able to perform calculations to quantify aspects of the material based on the shape of the drop. This method yielded measures of:

- **Interfacial Tension (IFT) -** the force that holds the surface of a particular phase together, measured in dynes per cm, where one dyne is equal to 10^{-5} N
- **Droplet contact angle (Theta)**– the angle made between the interface of the droplet and the surface

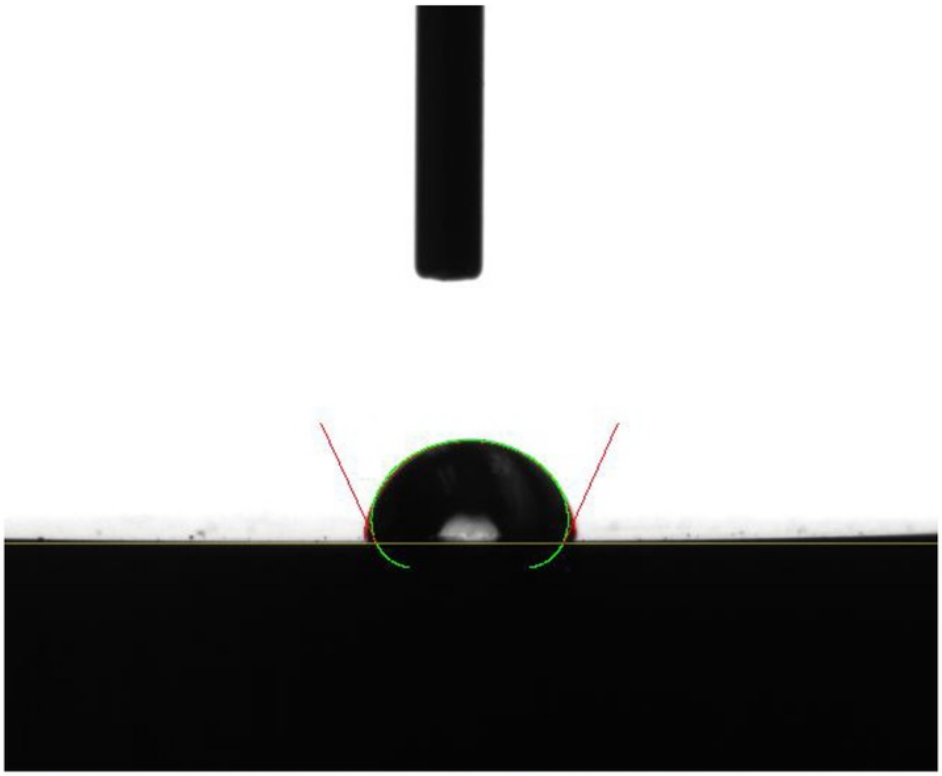

Figure 15 - Image of water droplet on zinc surface taken by Kruss Drop Shape Analyser

These measures provided a better analysis and understanding of the surface properties. Doing so aimed to better understand links between specific zinc surface properties and its biodegradable effectiveness.

Cell Culture Testing

The pieces were then packaged and sent for cell culture testing. Care was taken to ensure the zinc surfaces would not be damaged or altered during transport. Out of all samples produced, only a portion of them were selected for testing. This was due to cost and practical limitations of the nature of the testing process. Out of the original spectrum, the table below displays the array of samples chosen for testing. This selection was determined to maximise variety in terms of aims of the experiment, and minimise the overall number of pieces used.

Table 2 - Zinc Samples selected for cell culture testing (shown in red)

GRIT (P)	PATTERN	SAMPLE NUMBER
120	no pattern	#1,2,3
320	no pattern	#4,5,6
800	no pattern	#7,8,9
800	0.05HV, 100um between each impact	#10,11,12
800	0.2HV, 150um between each impact	#13,14,15
1200	no pattern	#16,17,18
1200	0.05HV, 60um between each impact	#19,20,21
1200	0.1HV, 80um between each impact	#22,23,24
polished	no pattern	A
polished	0.01HV, 40um between each impact 0.025HV, 60um between each impact 0.1HV, 100um between each impact	B1 B2 B3
polished	0.01HV, 40um between each impact 0.025HV, 60um between each impact 0.1HV, 100um between each impact	C1 C2 C3
polished	0.01HV, 40um between each impact 0.025HV, 60um between each impact 0.1HV, 100um between each impact	D1 D2 D3

The process consisted of three primary phases;

1. Cleaning
2. Cellular solution exposure
3. Fixing and Drying

Cell culture testing was conducted at an external institution.

Cleaning

The material was cleaned of any external impurities and biological matter that may have affected the experiment. Any impurities on the zinc surface may decrease the reliability of the results, and any live matter such as bacteria or microorganisms may have large affects on the biological function of the cellular interaction.

The prepared zinc samples were cleaned with acetone,ethanol and distilled water in an ultrasonic bath for 15 minutes at each step, and dried with N_2 gas. All the samples were sterilized using an autoclave at 120 °C and exposed UV light in a sterilized fume hood for 20 min.

Cellular Solution Exposure

Human fetal osteoblast line (hFOB 1.19) was used in this study (ATCC, CRL-11372). They were cultured in the medium of mixed Dulbecco's Modified Eagle's and Ham's F12 (DMEM/F12, Thermofisher Scientific), supplemented with 10 % (v/v) fetal bovine serum (Interpath Services) and 0.3 mg/ml Geneticin selective antibiotics G418 (Thermofisher Scientific) at 34°C in a humidified atmosphere of 5% CO_2. The complete growth medium was replaced every other day. At Day 3, the confluent cells were subcultured using TrypLE™ Express Enzyme (Invitrogen). A total of 1.5×10^5/100 µl cells were seeded on each disk in a 24-well culture plate for the study of cell number and viability.

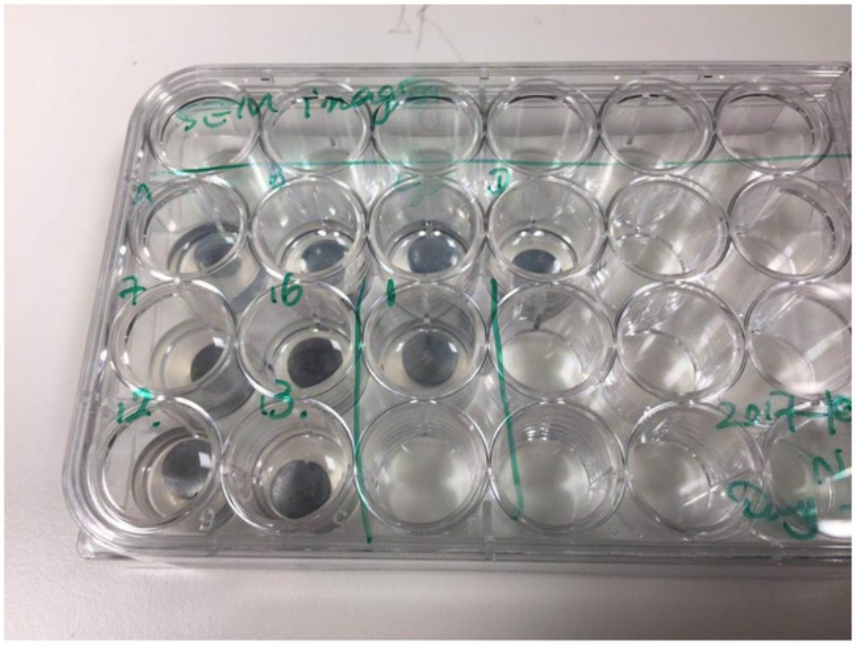

Figure 16 - Zinc samples in containment after 3 day cell culture testing

Fixing and Drying

After culturing for 3 days, cell-seeded zinc samples were rinsed with sodium cacodylate and then fixed with 0.1M cacodylate buffer that contains 2 % (v/v) paraformaldehyde and 2.5 % (v/v) glutaraldehyde for 30 min. They were dehydrated in a graded series of ethanol (from 30% to 100%). Finally, all substrates were chemically dried with 100% hexamethyldisilazane (Sigma-Aldrich) for overnight. This process is required to preserve the cells as they are after cell culture testing, allowing a proper analysis of the biological interaction.

Post-Cell Culture Analysis

Analysis of the samples that exhibited successful cell seeding was then conducted. The cells that did not seed successfully were disregarded, not deemed useful for further study. Out of the successful pieces, some stayed of cell counting, and the remaining were sent back for further analysis.
Analysis of the cell culture post-testing consisted of 3 methods:

1. Cell count
2. Microscope imaging
3. SEM imaging and element composition analysis

Cell count

A cell count was conducted on the samples displaying uniform non-ordered surface topology (all sanded and not indented samples) only. Since the ordered patterns did not cover the entire zinc surface, a cell count from them would not yield useful information.

This process included a live cell count and a dead cell count in both the medium and on the zinc. This would indicate how many cells there were in the system compared to the initial conditions, and give values on percentage viability.

Microscope Imaging

The Olympus SZX16 Stereomicroscope in the microscopy lab was used to take low magnification images of the zinc surfaces. This method gave a magnified natural coloured image, giving a basic representation of the density and behaviour of the cellular matter before undergoing further more detailed analysis. An overall but underdeveloped representation on cell culture success was able to be clearly seen. On samples containing ordered indent patterns, the reference mark was used to locate the pattern when necessary. Below shows a basic example of the nature of imaging captured by this method.

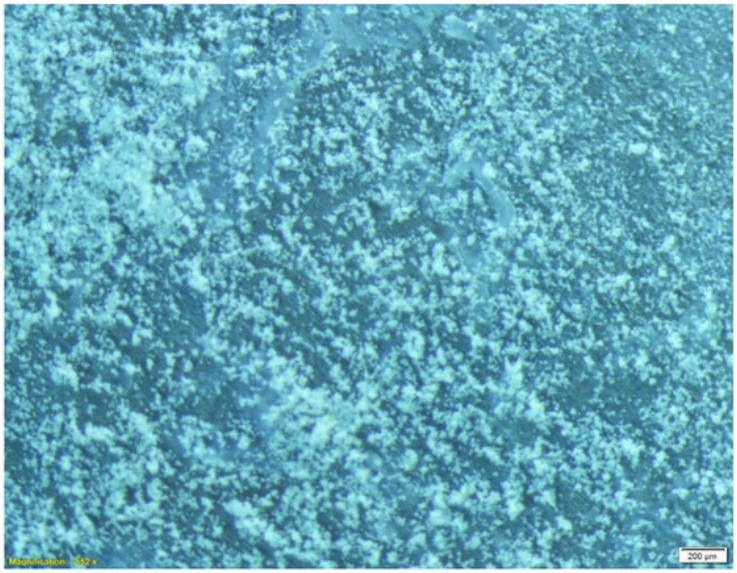

Figure 17 - Example of image captured by Olympus microscope of cell culture on zinc surface

SEM Imaging and Element Composition Analysis

The PHENOM XL Benchtop Scanning Electron Microscope was then used to both perform an element composition analysis and perform high magnification imaging simultaneously. Once an image had been captured via SEM, linking software conducted a point element composition analysis at chosen spots on this image. This identified the composition at single points rather than a general area. Carbon and nitrogen rich points indicated solid biological matter, indicating cells. This high magnification imaging allowed a detailed view of the behaviour of the cellular matter.

These methods combined give an appropriate quantification of the cell culture successfulness.

Results

Results of the project will be divided corresponding to the experimental procedure.

Pre-Cell Culture Results

SEM imaging

Points were chosen that gave a good representation of the general topology of the sample surfaces. Only imaging for samples that were selected for cell culture testing are included in this report.

For SEM images of zinc surface topologies, see Appendix A.

Wettability testing

3 tests were performed for each surface condition. For wettability testing images, see Appendix B.

Table 3 below provides all results obtained via wettability analysis:

Table 3 - Wettability test results for different surface topologies

Surface Condition	Contact Angle (degrees)	Interfacial Tension (dynes/cm)
120P grit, No ordered pattern:	65.3	39.38
	65.9	9.93
	68.3	78.05
800P grit, No ordered pattern	96.7	11.14
	94.9	3.43
	95.3	7.93
800P grit, 0.05HV, 100 micrometers between indents	91.4	91.4
	96.3	4.04
	99.3	2.33
800P grit, 0.02HV, 150 micrometers between indents	92.8	5.48
	82.7	82.7
	81.8	5.58
1200P grit, No ordered pattern	98.4	5.33
	99.5	10.33
	95.1	6.73
Polished, No ordered pattern	106.8	2.2
	109.2	4.17
	105.1	1.67
Polished, 0.01HV, 40 micrometers between indents	100	4.78
	102.4	1.33
	103.7	3.72
Polished, 0.025HV, 60 micrometers between indents	94	11.97
	93.9	120.51
	95.2	1.31
Polished, 0.1HV, 100 micrometers between indents	90.7	4.59
	92.2	5.23
	95.5	3.09

Post-Cell Culture Results

Cell Count

Initially, 1.5x10^5 cells were seeded on each sample. The complete growth medium was replaced every other day. At Day 3, the confluent cells were subcultured using TrypLE™ Express Enzyme (Invitrogen). The tables below show the cell count (alive and dead) both in the medium and and the zinc surface after 3 days out of the cells that exhibited successful cell culture seeding.

Table 4 - Cell count after culture for sample 2

	Disk	Medium	In total
Total:	1.7x10^5	4.6x10^4	2.16x10^5
Live:	4.0x10^4	1.3x10^4	
Dead:	1.3x10^5	3.3x10^4	
Viablity:	23%	28%	

Table 5 - Cell count after culture for sample 3

	Disk	Medium	In total
Total:	7.6x10^4	1.5x10^5	2.26x10^5
Live:	2.1x10^4	6.0x10^4	
Dead:	5.5x10^4	8.7x10^4	
Viablity:	28%	41%	

Table 6 - Cell count after culture for sample 8

	Disk	Medium	In total
Total:	2.5x10^5	2.3x10^4	2.73x10^5
Live:	8.1x10^4	8x10^3	
Dead:	1.7x10^5	1.6x10^4	
Viablity:	32%	33%	

Table 7 - Cell count after culture for sample 9

	Disk	Medium	In total
Total:	1.5x10^5	4.6x10^4	1.96x10^5
Live:	2.3x10^4	1.9x10^4	
Dead:	1.2x10^5	2.7x10^4	
Viablity:	12%	41%	

Table 8 - Cell count after culture for sample 17

	Disk	Medium	In total
Total:	6.9x10^4	3.5x10^4	1.04x10^5
Live:	2.5x10^4	9.0x10^3	
Dead:	4.5x10^4	2.6x10^4	
Viablity:	36%	25%	

Table 9 - Cell count after culture for sample 18

	Disk	Medium	In total
Total:	1.3x10^5	6.6x10^4	1.96x10^5
Live:	3.3x10^4	2.2x10^4	
Dead:	1.0x10^5	4.4x10^4	
Viablity:	25%	33%	

Microscope imaging

The microscope images taken using the Olympus SZX16 Stereomicroscope give a basic representation of the density and behaviour of the cellular matter.

For microscope images of cell culture on zinc samples, see Appendix C.

SEM & Element Composition Analysis

Once the nature of what the SEM images were displaying, a greater understanding could be gathered by looking at the images alone. The Element composition analysis function of the PHENOM XL Benchtop SEM was used to determine the composition of the matter captured in

the imaging below at the points shown. This allowed better understanding of the subsequent SEM images.

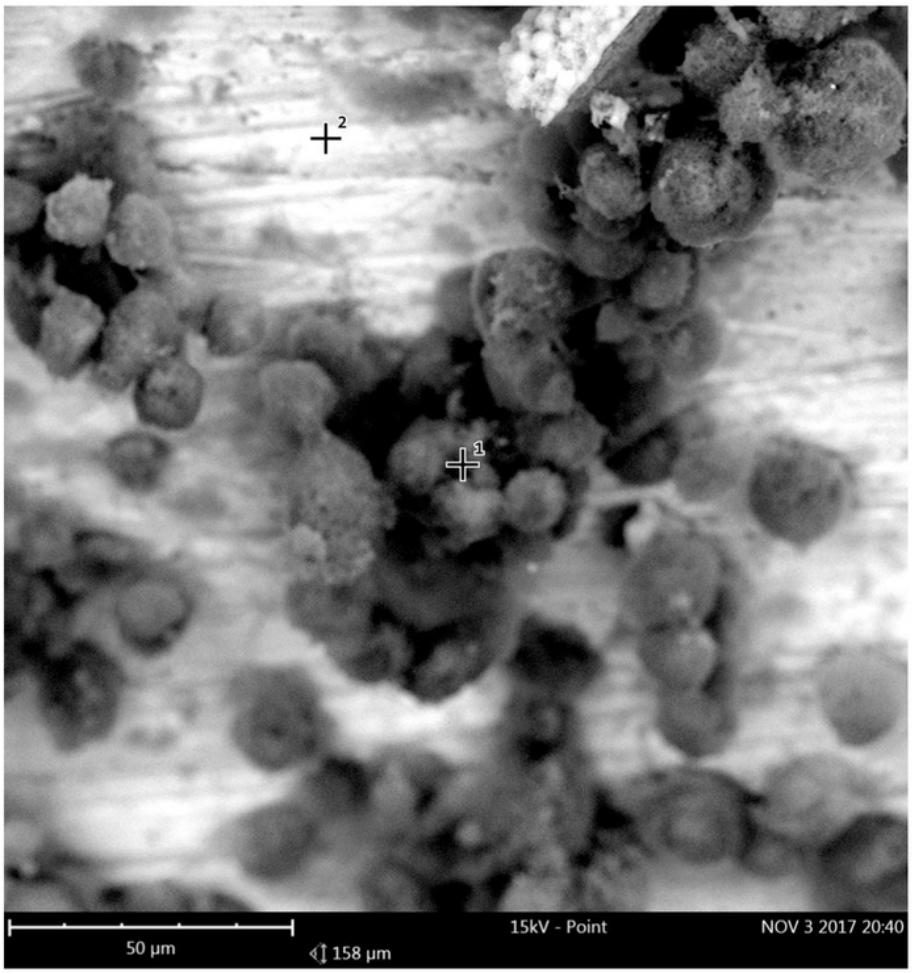

Figure 18 - Image from SEM showing two points to have element composition analysed

Below is a report summary for these two points.

Point 1

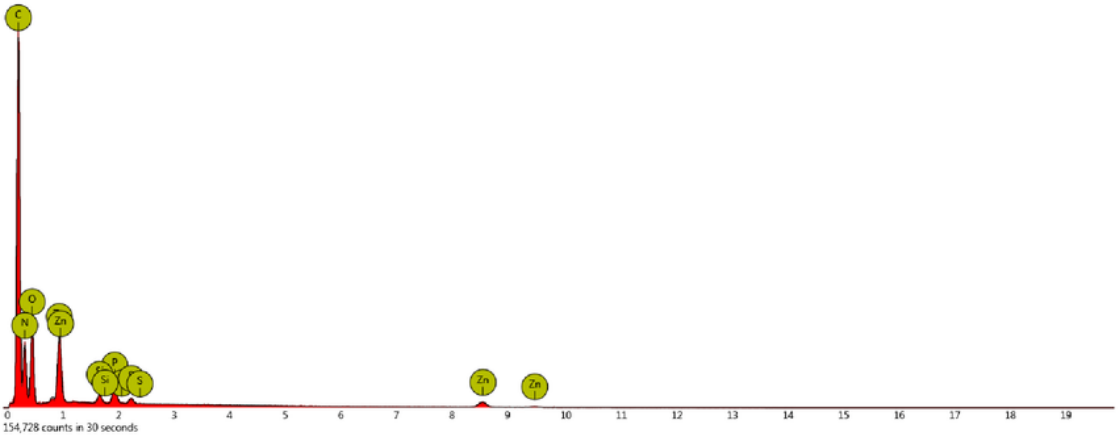

	Atomic percentage
C	50.30 %
N	30.20 %
O	17.60 %
Zn	1.21 %
P	0.40 %
Si	0.17 %
S	0.12 %

	Weight percentage
C	42.88 %
N	30.03 %
O	19.99 %
Zn	5.61 %
P	0.87 %
Si	0.34 %
S	0.28 %

Element Number	Element Symbol	Element Name	Atomic Conc.	Weight Conc.
6	C	Carbon	50.30	42.88
7	N	Nitrogen	30.20	30.03
8	O	Oxygen	17.60	19.99
30	Zn	Zinc	1.21	5.61
15	P	Phosphorus	0.40	0.87

Point 2

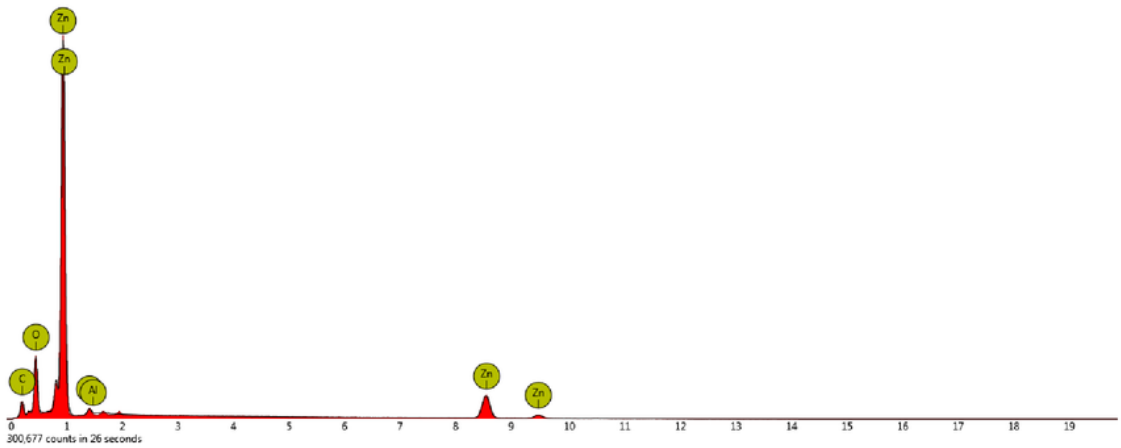

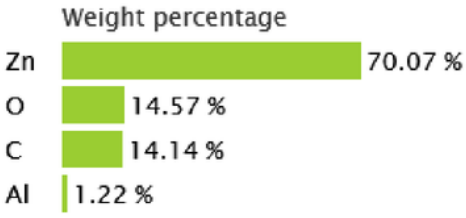

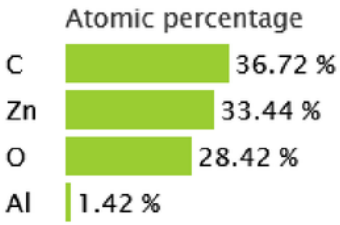

Element Number	Element Symbol	Element Name	Atomic Conc.	Weight Conc.
30	Zn	Zinc	33.44	70.07
8	O	Oxygen	28.42	14.57
6	C	Carbon	36.72	14.14
13	Al	Aluminium	1.42	1.22

A comprehensive array of SEM images was obtained for the cell culture samples. For SEM images of cell culture on zinc samples, see Appendix D.

Discussion

The Thesis project was conceptualised and carried out with no major variations from the initial project plan. Most equipment used during the experimental process and also analysis were available within the facilities of Macquarie University and so readily accessible, with the exception of the phase in the methodology in which the biomaterial was involved. This required third party experimentation in an external facility. This did not introduce any complications, however time constraints may have influenced the experimentation process (more on this below). Limitations also forced the use of the DuraScan hardness tester for use of achieving the ordered topography patters, making the process not as time efficient as it could have been, although was successful in creating desirable results. Analysis of cell culture samples was done successfully via SEM methods. The cell culture results were only partially conclusive. Analysis showed images that had differences to what was expected. This will be discussed in greater detail below.

Surface Modification

The process of obtaining the array of topologies was successful. The patterns that were formed do not fall under the applications that the DuraScan hardness tester specialises in. Impacts were created individually, with manual movement of the sample via fine control spindles. The result however was dimensionally accurate, and topologically favourable for the application. This process also had advantages over methods such as laser etching, which locally alter other properties of the metal surface, changing the experiment.

Wettability Results

The results for the wettability drop shape testing show consistent results for the contact angle corresponding to each surface condition, although quite inconsistent for the interfacial tension measurements. Results indicated as expected that the contact angle increased as the zinc surface got smoother. High contact angle refers to a low wettability, seen as the droplet tends to stay in a small ball shape instead of dispersing (wetting) over the surface. When comparing wettability measurements to corresponding cell cultivation, although images showed subjective results, there did seem to be a link between wettability and cultivation success. Generally, a higher wettability measure meant greater cell cultivation, although the degree of this varied substantially. This relationship is most notable by comparing sample 1 and sample A. Out of the samples that did not include ordered patterns, these two samples showed the highest and lowest wettibility respectively. Figure 19 and 18 below displays SEM images of sample 1 (120P grit) and sample A (polished) with corresponding wettibility measure.

Sample 1: Average contact angle = 64

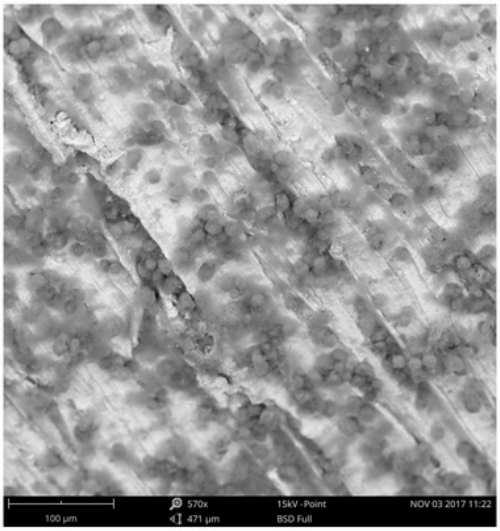

Figure 19 - SEM image of cell culture of Sample 1

Sample A: Average contact angle = 107

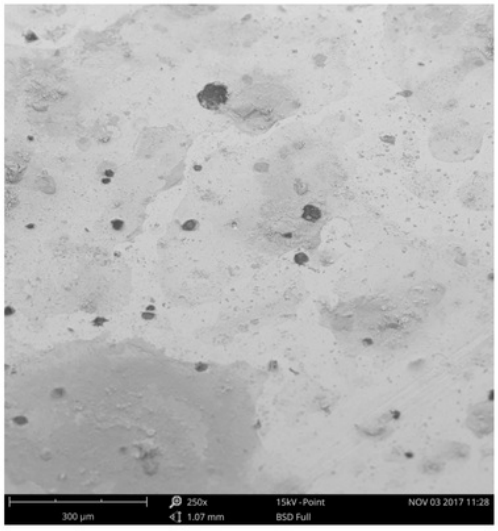

Figure 20 - SEM image of cell culrure of Sample A

Cell Count

The number of cells counted on the non-ordered topology samples gave insight to the link between surface roughness and cell viability. As both dead and alive cells were counted in both the medium solution and on the zinc surface, different trends can be observed.

For the samples tested, it can be observed that the percentage of alive to dead cells in the zinc-medium system was higher for lower surface roughness samples. However absolute numbers of cells in the system was greater for samples with higher surface roughness. This seems to indicate that cells take to adhering to the rougher surfaces more readily and cell proliferation is greater, but cell viability will be lower.

Imaging

SEM imaging produced varied and inconsistent results, although certain trends and interactions could be gathered. The primary inconsistency was the tendency for cell densities not to be uniform over a single sample topology. The main body of the cells were able to be seen clearly in detail. Interactions on a nanoscale were harder to quantify as they were more subtle and difficult to be differentiated from other materials and formations.

Although there were variations amongst results across alike topologies, consistencies most notably showed how surface features effected cellular positioning on a small scale. In samples of higher roughness, it was observed that cells were being found more consistently in and amongst physical features such as scratched. This is clearly visible in figure 18 above in. This was also evident for the more large indents made in ordered pattern topography.

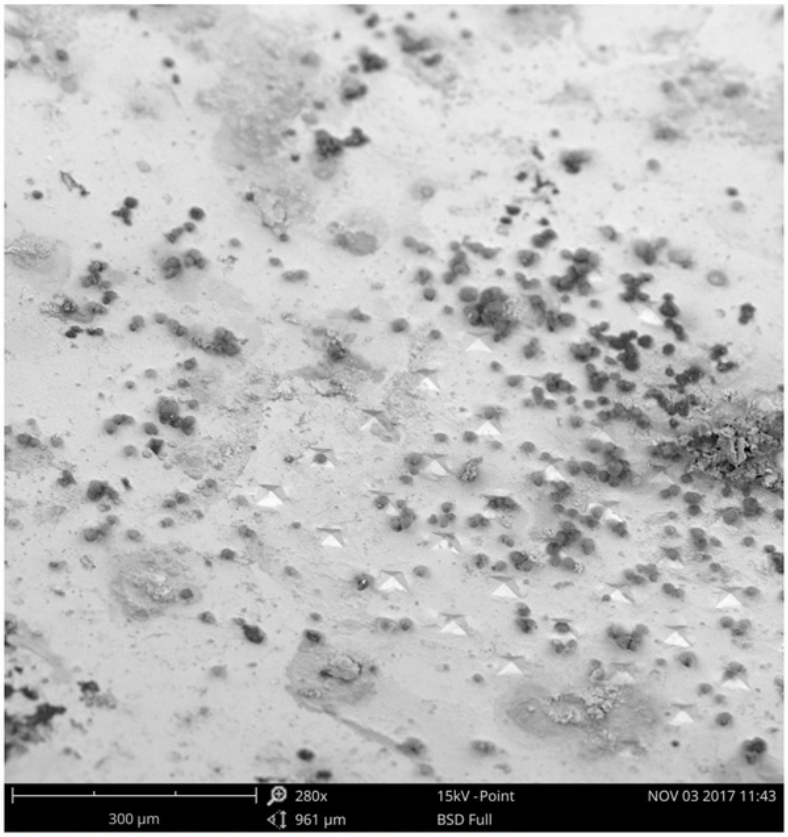

Figure 21 - SEM image of cell culture on sample B1

Figure 20 above shows well the cell behaviour around ordered impacts. It is evident that the cell density within the indent pattern area is greater than the area surrounding it.

This was not as evident in smaller impact samples however, and at times was not evident in larger indents also. In the smaller indent cases, it seems the cells were more likely to be found suspended in the substrate, unattached to the material. Perhaps due to the substrate, it seems there may be a lower limit on the indent size that has much effect on the cell culture results. Figure 21 below shows an example of a larger indent pattern with minimal effects on the cellular matter.

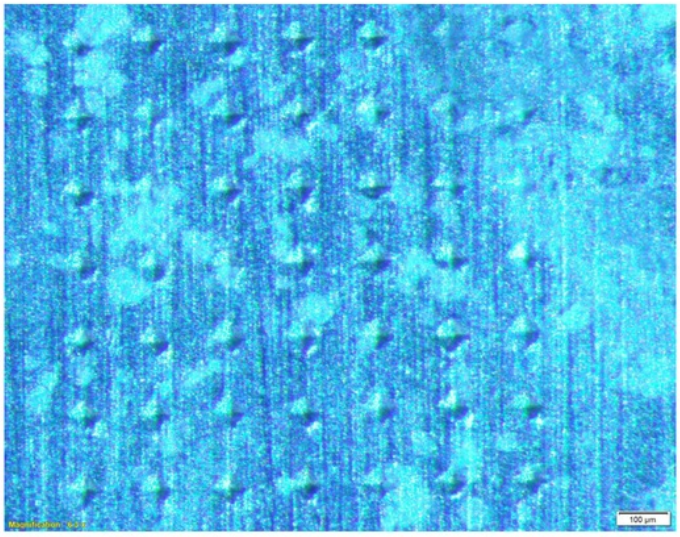

Figure 22 - Microscope image of indent topology with little effect on cellular matter

Conclusions

This thesis project aimed to develop a greater understanding of how the effects of surface roughness and topology of zinc on biological cell function.

Zinc samples of various measures of surface roughness exposed to the cellular medium displayed a spectrum of results when analysing how successfully the cells cultivated onto the zinc surface. These results were somewhat inconsistent, with similar zinc surface topologies displaying a range of cell cultivation densities. There were however evident trends that displayed successful cell interaction with features on the zinc surface.

A count of the number of alive and dead cells both on the zinc and in the medium after 3 days of exposure to the biomaterial indicated that there seemed to be relationship between cell numbers and surface roughness. A greater roughness indicated a higher amount of both alive and dead cells after 3 days. The percentage of alive to dead cells however was higher with a lower measure of roughness. These results may be relevant to wettability as wettability measures were highly correlated with surface roughness.

Wettability measure yielded consistent measures of contact angle, yet a low consistency of interfacial tension. For surfaces yielding higher wettability, the cell cultures displayed higher levels of proliferation, although there were variations in the strength of this trend. Ordered pattern indentation of the surface changed the wettability of the zinc surface, with the courser indentation patterns yielding higher wettability.

SEM imaging produced varied and inconsistent results, although certain trends and interactions could be gathered. The primary inconsistency was the tendency for cell densities not to be uniform over a single sample topology. Although there were variations amongst results across alike topologies, cells were consistently located in indented features in the surface. This was most evident in larger features, such as scratched in rougher surfaces, and larger indents in ordered indent topographies. Scales of this effect are observable in the appendices.

Future work

Future work is required in this field to progress to a sufficient understanding of how zinc may potentially be used as biodegradable bone implants. There are many different ways in which the surface of a metal can be altered to change how it may behave in a biological environment, and this report only covered as small niche in that field. The following points provide areas for further research that may address conclusions not reached in this report, or areas in which further insight may be beneficial:

Space distribution of indentations:

In noted cases, individual cell did seem to gravitate to spot points where indentations were present, however proliferation was not significant around these points. Perhaps a denser indent distribution will provide a higher cell density as it closes distance between individual cells

Longer cell growth testing period:

Time limitations allowed only a 3 period in which the zinc samples were exposed to the biomaterial. Although initial results are indicative of long term success, perhaps a longer exposure may be beneficial in result accuracy.

Wettability correlation:

The spectrum of results indicated that higher wettability (contact angle) measure correlated to higher biological function. There may be a point in which there is a limit to this relationship. A detailed analysis of a wider spectrum of wettability measures may be beneficial in developing a reliable relationship model. Also more work may be done into IFT measurement and achieving consistent values across similar surface topologies.

Cell proliferation and viability:

Result trends indicated a higher surface roughness may correlate to a higher total number of both alive and dead cells found after cell exposure, although the percentage of alive to dead cells was less. Research into the legitimacy of this phenomenon may be beneficial to establishing an optimisation between the two conditions.

References

[1] D. Vojteˇch ˚, J. Kubásek, J. Šerák, P. Novák. "Mechanical and corrosion properties of newly developed biodegradable Zn-based alloys for bone fixation, pp. 3155-3522, Jan 2011.

[2] N. Gui1, W. Xu, D. Myers, R. Shukla, H. P. Tang, M. Brant, M. Qian. "The role of semi-ordered and ordered surface topography in cell regulation for bone implant materials - a review" pp.1-49, 2016

[3] K. Kulangara, K.W. Leong, Substrate topography shapes cell function, Soft Matter 5(21) (2009) 4072-4076.

[4] M.J. Dalby, N. Gadegaard, R. Tare, A. Andar, M.O. Riehle, P. Herzyk, C.D. Wilkinson, R.O. Oreffo, The control of human mesenchymal cell differentiation using nanoscale symmetry and disorder, Nature materials 6(12) (2007) 997-1003.

[5] M. Ball, D.M. Grant, W.J. Lo, C.A. Scotchford, The effect of different surface morphology and roughness on osteoblast-like cells, Journal of Biomedical Materials Research Part A 86(3) (2008) 637-647.

[6] J. Kim, W.-G. Bae, H.-W. Choung, K.T. Lim, H. Seonwoo, H.E. Jeong, K.-Y. Suh, N.L. Jeon, P.-H. Choung, J.H. Chung, Multiscale patterned transplantable stem cell patches for bone tissue regeneration, Biomaterials 35(33) (2014) 9058-9067.

[7] R.A. Gittens, R. Olivares-Navarrete, Z. Schwartz, B.D. Boyan, Implant osseointegration and the role of microroughness and nanostructures: Lessons for spine implants, Acta Biomaterialia 10(8) (2014) 3363-3371.

[8] T. Sjöström, M.J. Dalby, A. Hart, R. Tare, R.O.C. Oreffo, B. Su, Fabrication of pillar-like titania nanostructures on titanium and their interactions with human skeletal stem cells, Acta Biomaterialia 5(5) (2009) 1433-1441.

[9] T. Sjöström, N. Fox, B. Su, Through-mask anodization of titania dot-and pillar-like nanostructures on bulk Ti substrates using a nanoporous anodic alumina mask, Nanotechnology 20(13) (2009).

[10] M.J. Dalby, N. Gadegaard, R. Tare, A. Andar, M.O. Riehle, P. Herzyk, C.D. Wilkinson, R.O. Oreffo, The control of human mesenchymal cell differentiation using nanoscale symmetry and disorder, Nature materials 6(12) (2007) 997-1003.

[11] M. Biggs, R. Richards, N. Gadegaard, C. Wilkinson, M. Dalby, The effects of nanoscale pits on primary human osteoblast adhesion formation and cellular spreading, Journal of Materials Science: Materials in Medicine 18(2) (2007) 399-404.

[12] J. Justesen, M. Lorentzen, L. Andersen, O. Hansen, J. Chevallier, C. Modin, A. Füchtbauer, M. Foss, F. Besenbacher, M. Duch, Spatial and temporal changes in the morphology of preosteoblastic cells seeded on microstructured tantalum surfaces, Journal of Biomedical Materials Research Part A 89(4) (2009) 885-894.

[13] http://optofab.org.au/lasermicro.html

Appendix

Appendix A - SEM images of zinc surface topologies

Sample 1

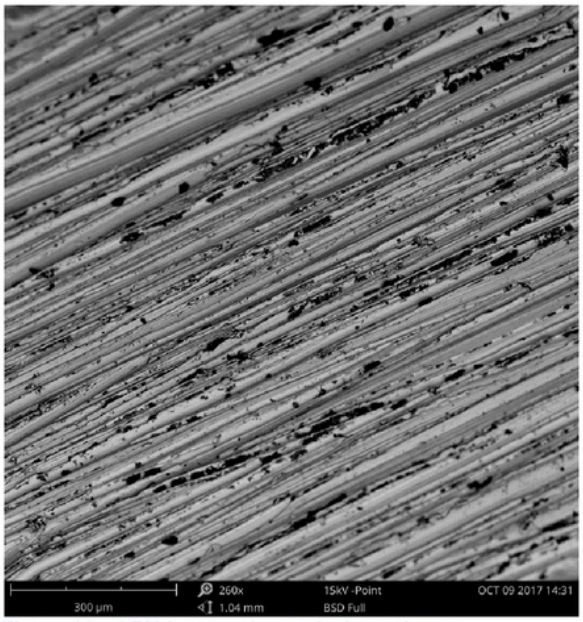

Figure 23 - SEM Image of sample 1 topology

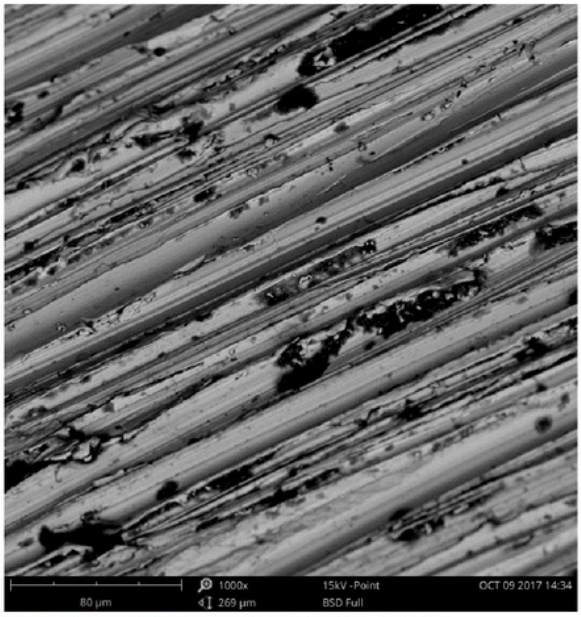

Figure 24 - SEM Image of sample 1 topology

Sample 2

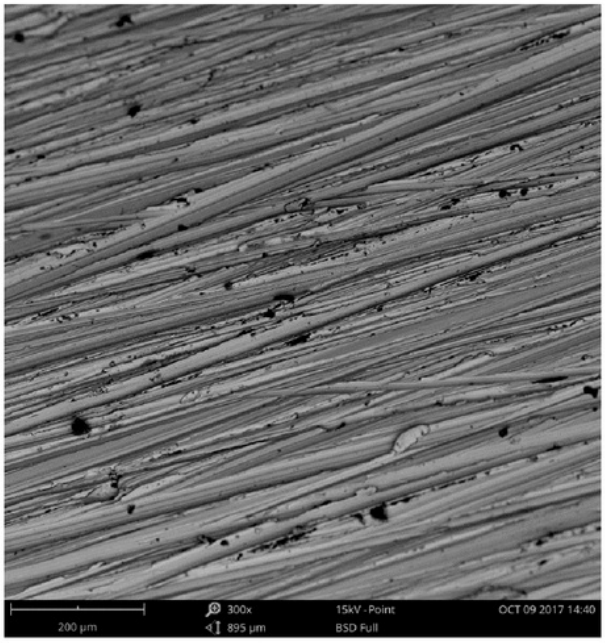

Figure 25 - SEM Image of sample 2 topology

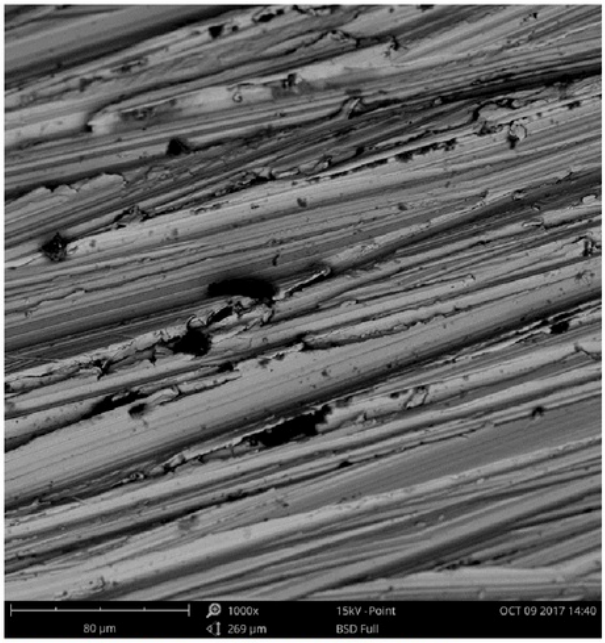

Figure 26 - SEM Image of sample 2 topology

Sample 3

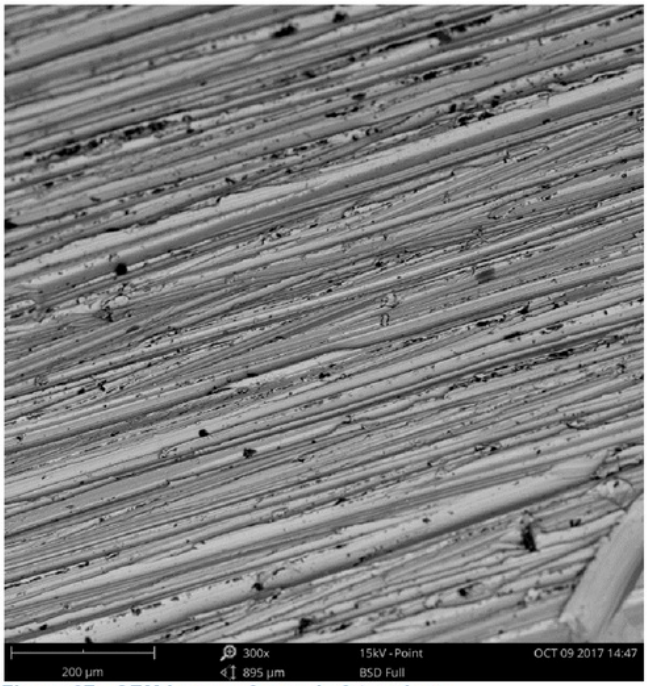

Figure 27 - SEM Image of sample 3 topology

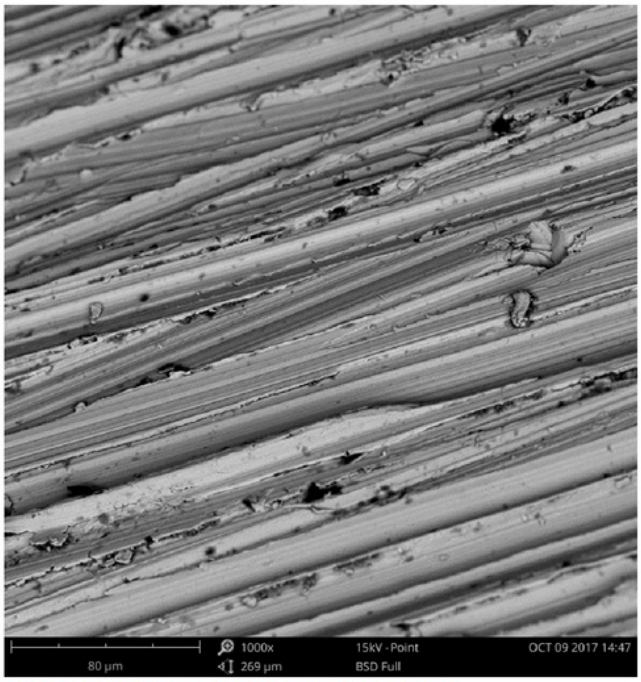

Figure 28 - SEM Image of sample 3 topology

Sample 7

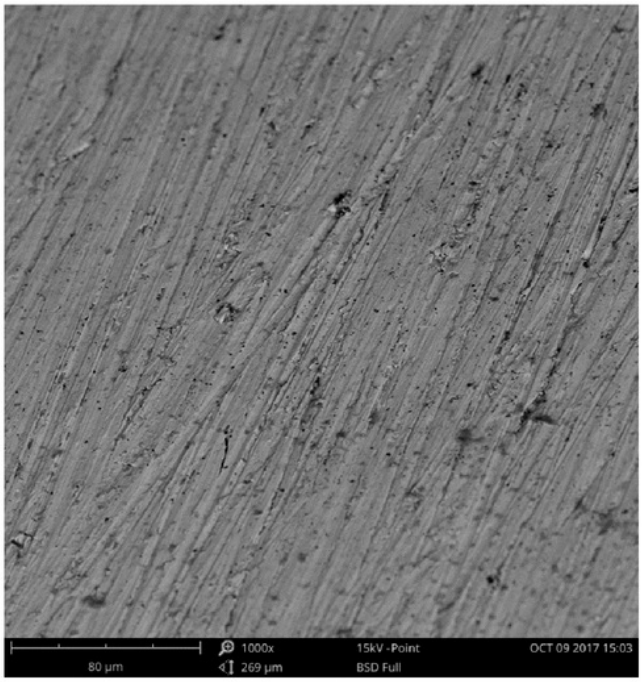

Figure 29 - SEM Image of sample 7 topology

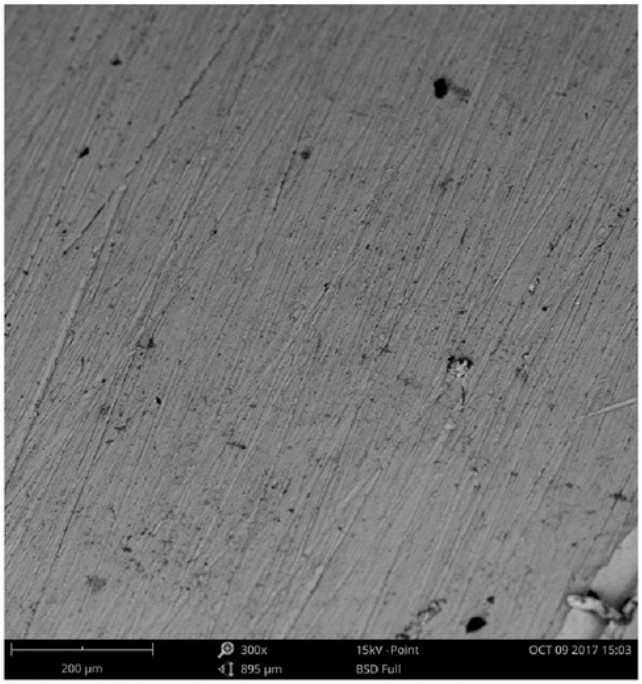

Figure 30 - SEM Image of sample 7 topology

Sample 8

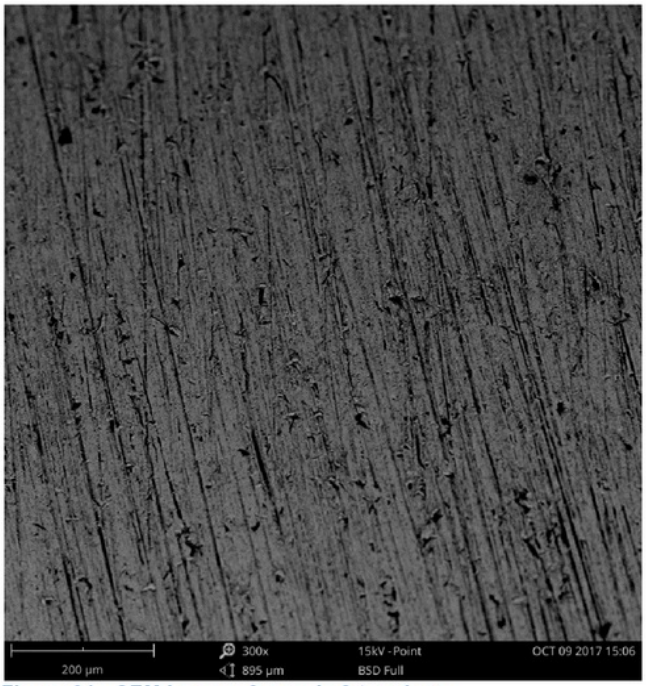

Figure 31 - SEM Image of sample 8 topology

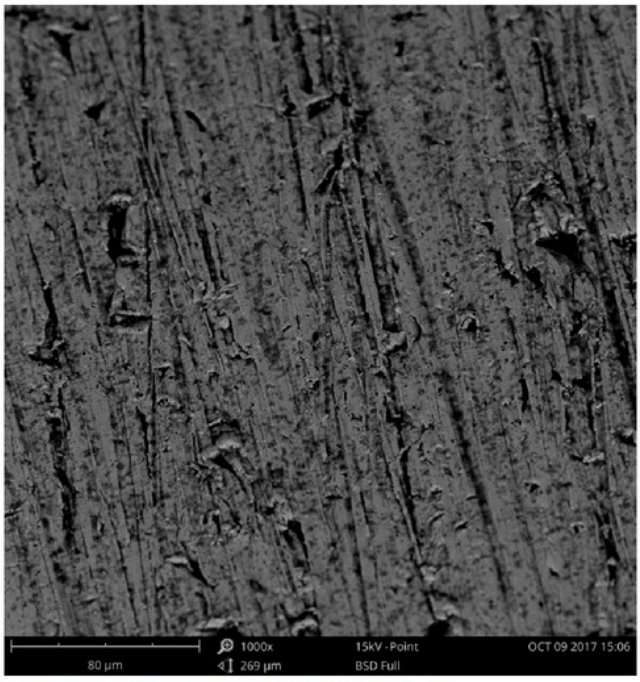

Figure 32 - SEM Image of sample 8 topology

Sample 9

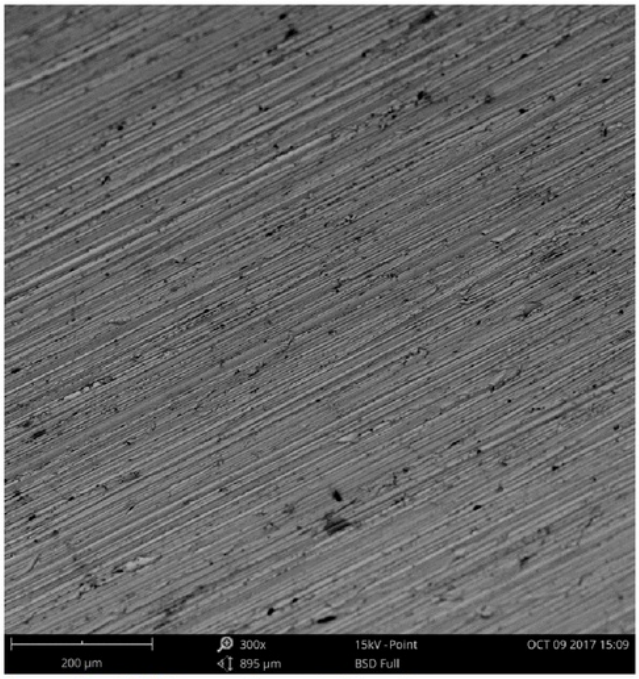

Figure 33 - SEM Image of sample 9 topology

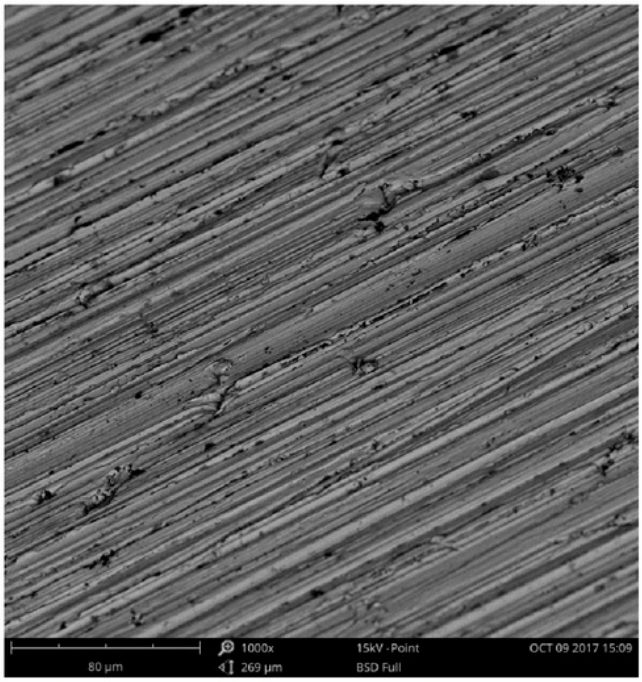

Figure 34 - SEM Image of sample 9 topology

Sample 12

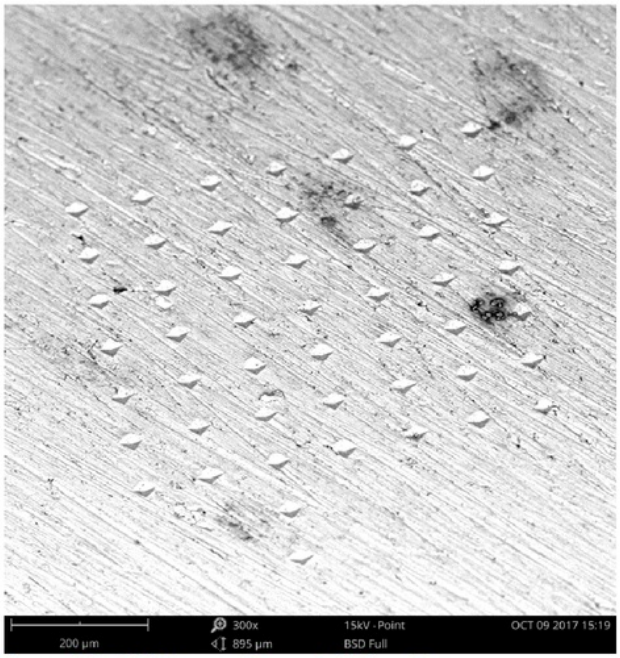

Figure 35 - SEM Image of sample 12 topology

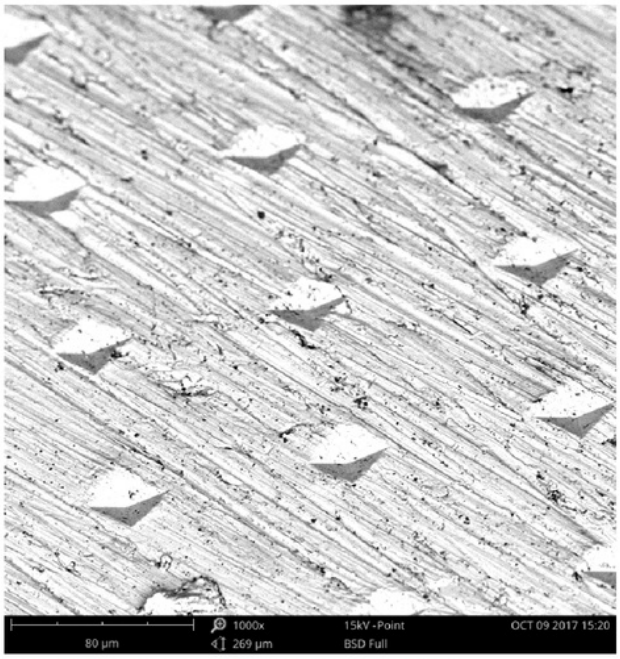

Figure 36 - SEM Image of sample 12 topology

Sample 13

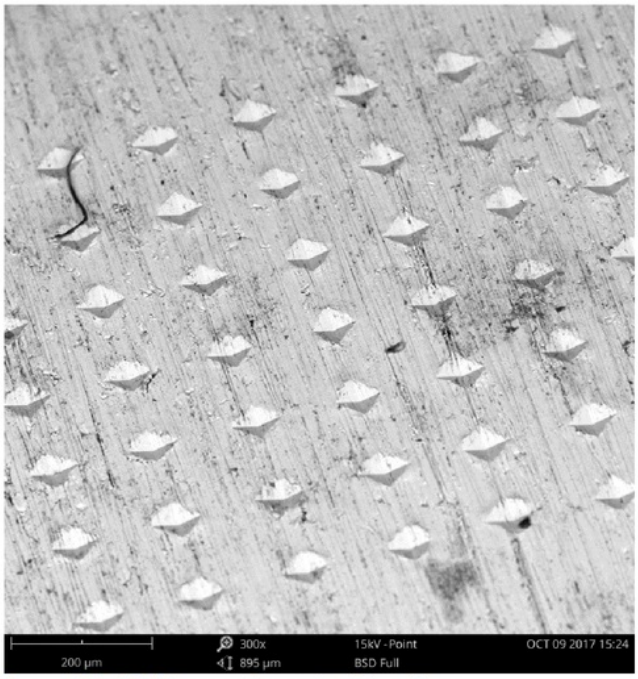

Figure 37 - SEM Image of sample 13 topology

Figure 38 - SEM Image of sample 13 topology

Sample 16

Figure 39 - SEM Image of sample 16 topology

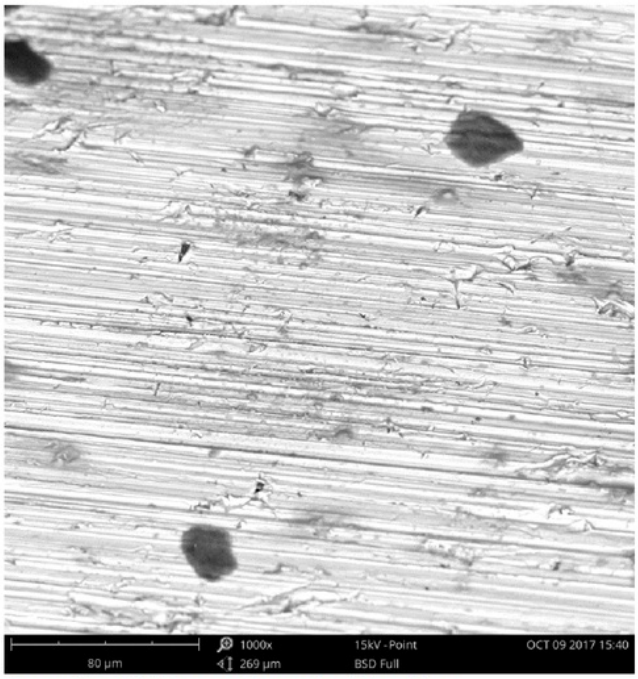

Figure 40 - SEM Image of sample 16 topology

Sample 17

Figure 41 - SEM Image of sample 17 topology

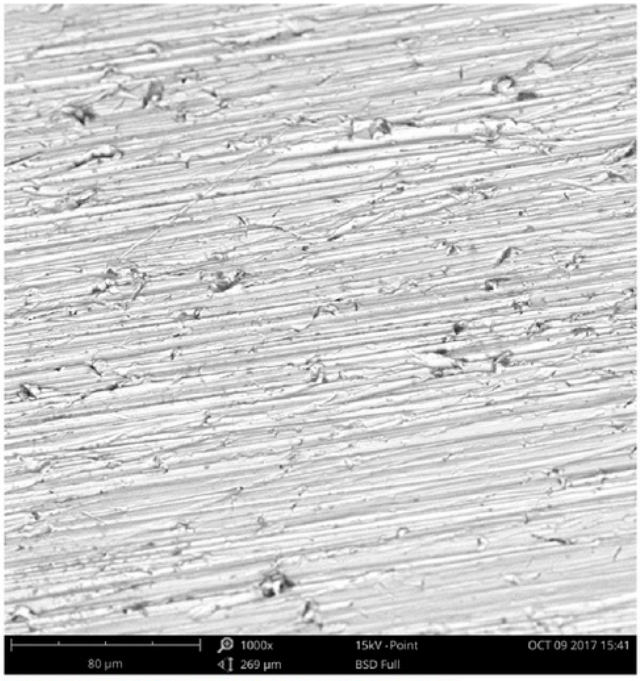

Figure 42 - SEM Image of sample 17 topology

Sample 18

Figure 43 - SEM Image of sample 18 topology

Figure 44 - SEM Image of sample 18 topology

Sample A

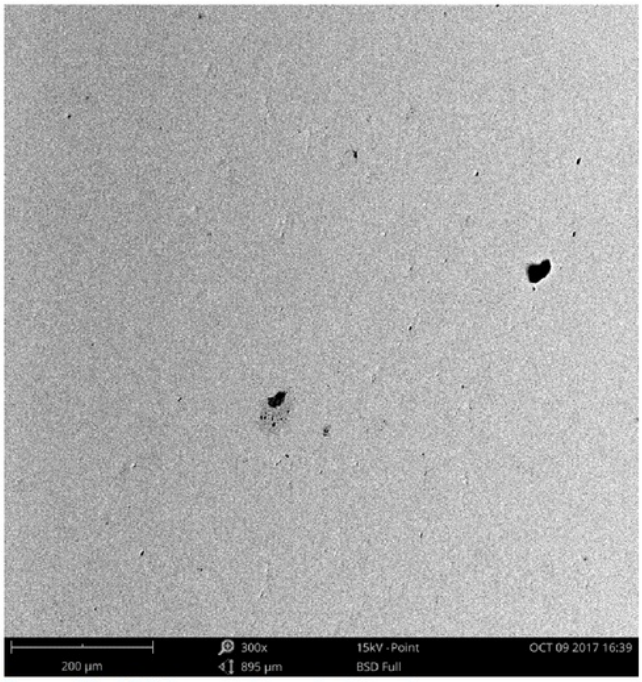

Figure 45 - SEM Image of sample A topology

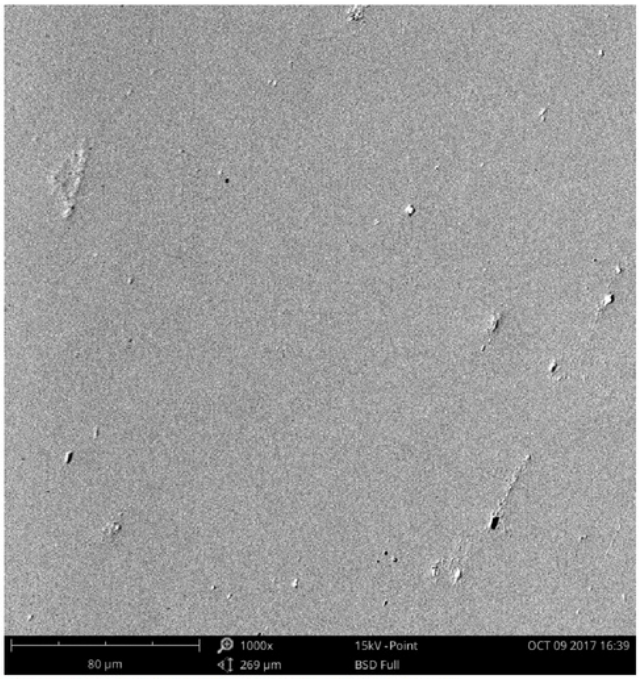

Figure 46 - SEM Image of sample A topology

Sample B1

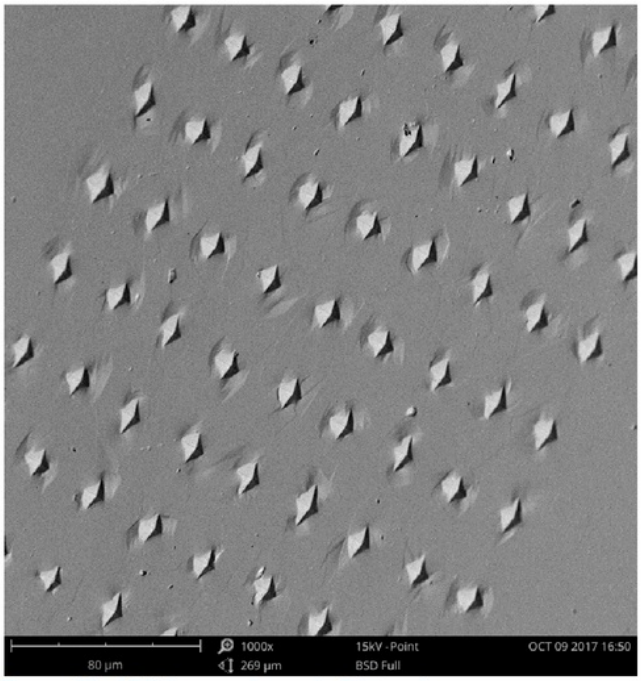

Figure 47 - SEM Image of sample B1 topology

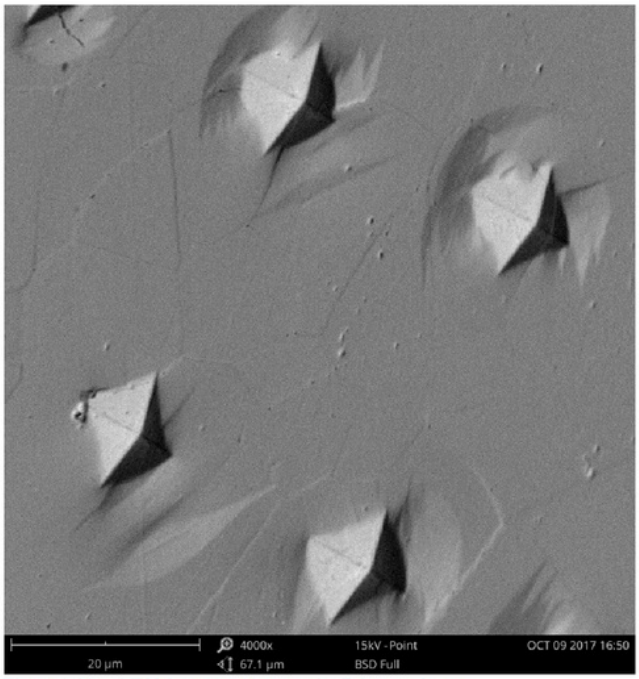

Figure 48 - SEM Image of sample B1 topology

Sample B2

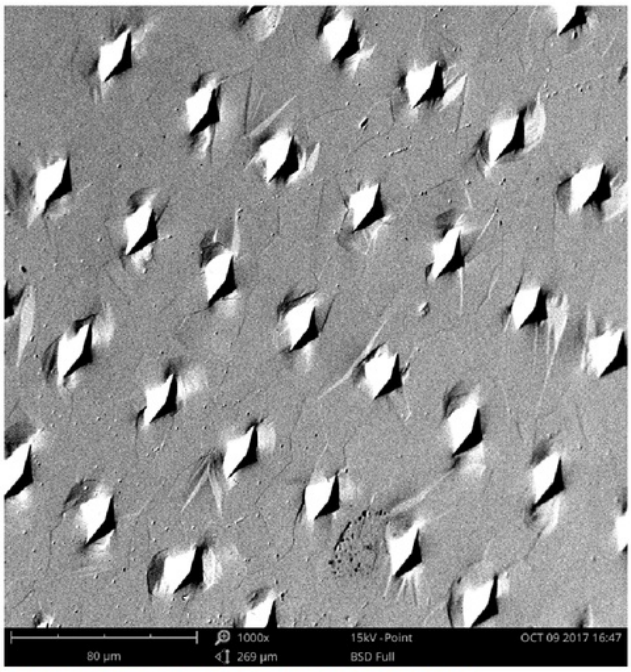

Figure 49 - SEM Image of sample B2 topology

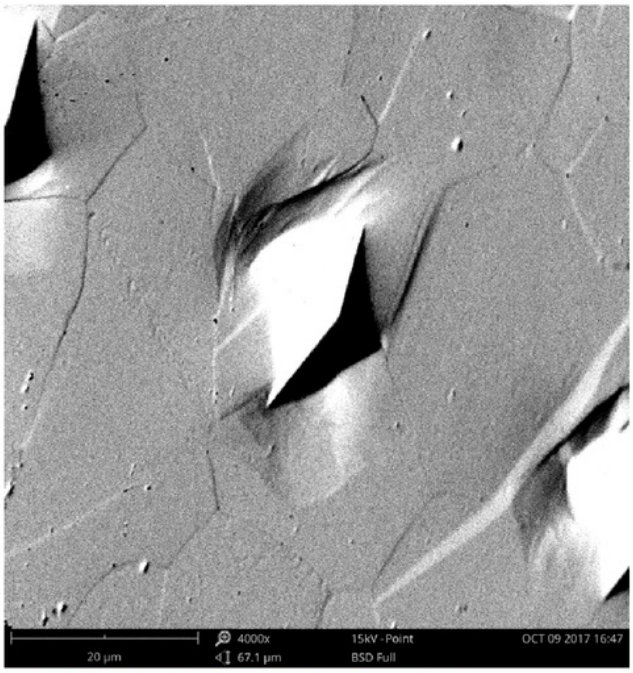

Figure 50 - SEM Image of sample B2 topology

Sample B3

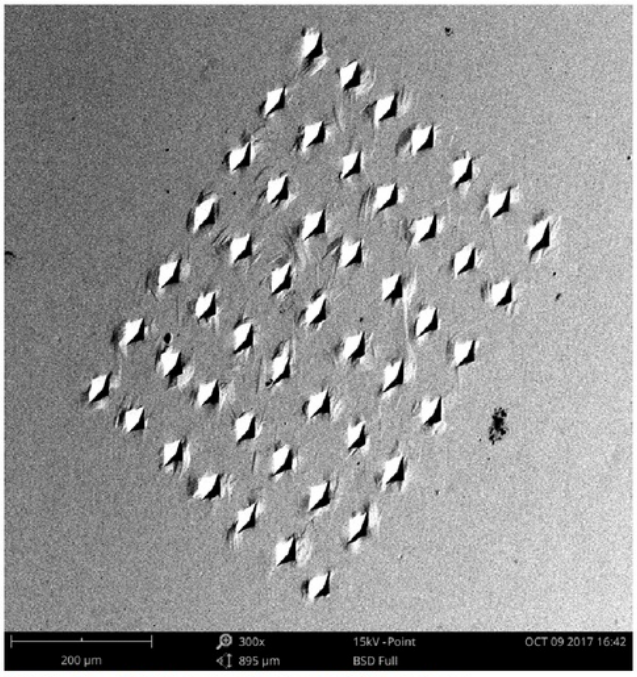

Figure 51 - SEM Image of sample B3 topology

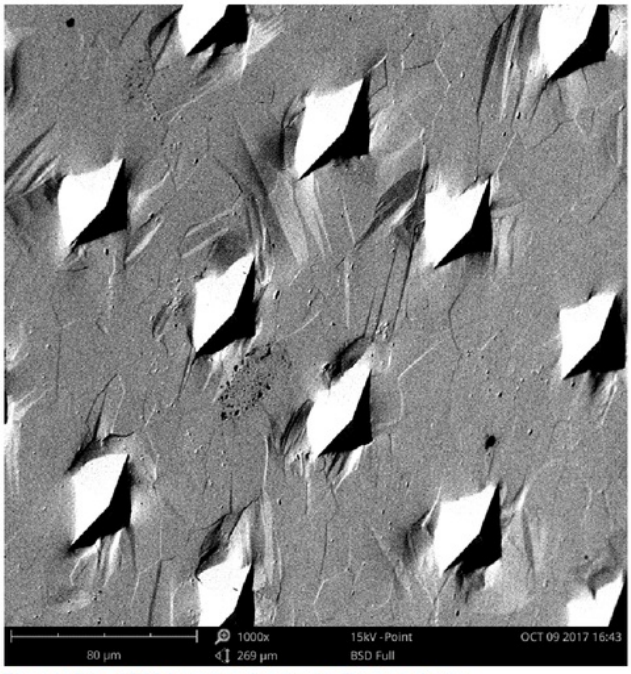

Figure 52 - SEM Image of sample B3 topology

Sample C1

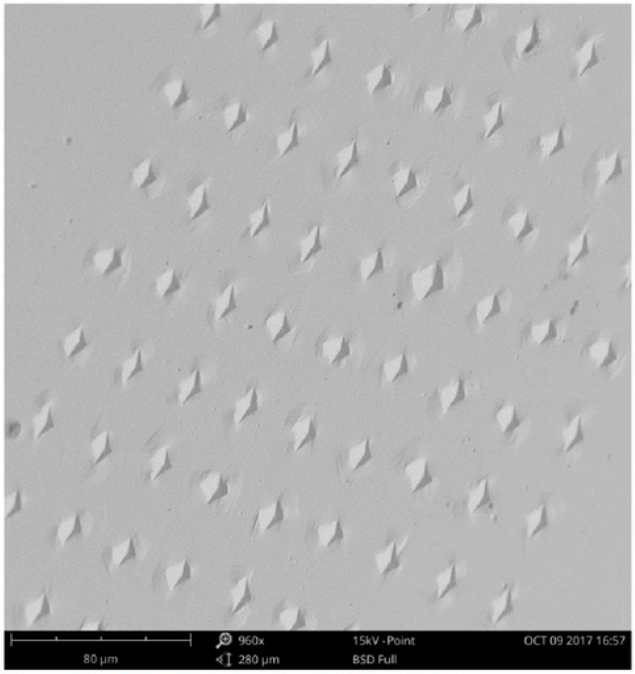

Figure 53 - SEM Image of sample C1 topology

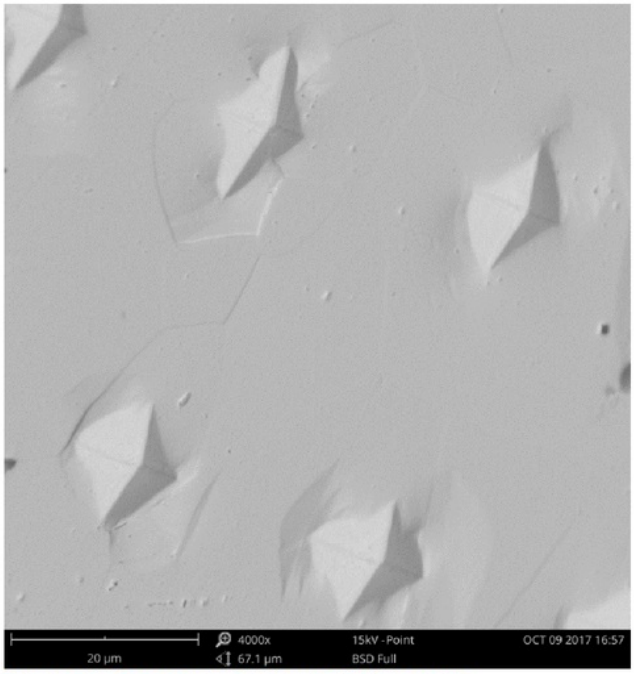

Figure 54 - SEM Image of sample C1 topology

Sample C2

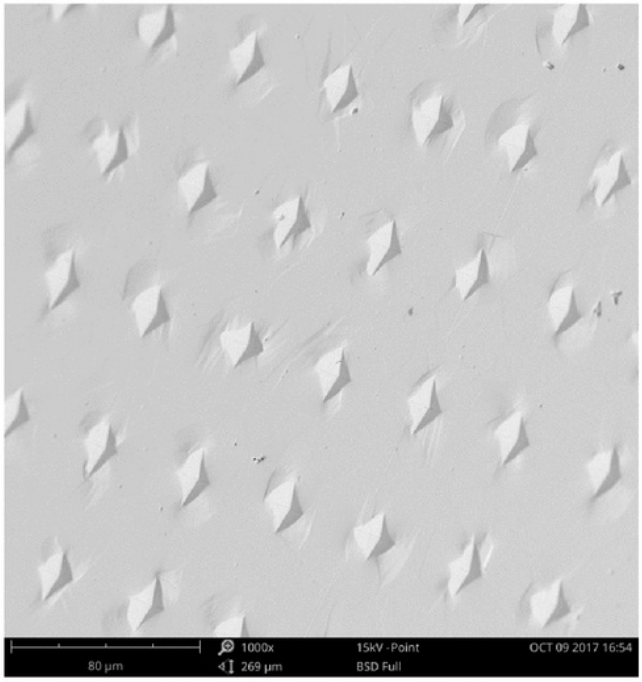

Figure 55 - SEM Image of sample C2 topology

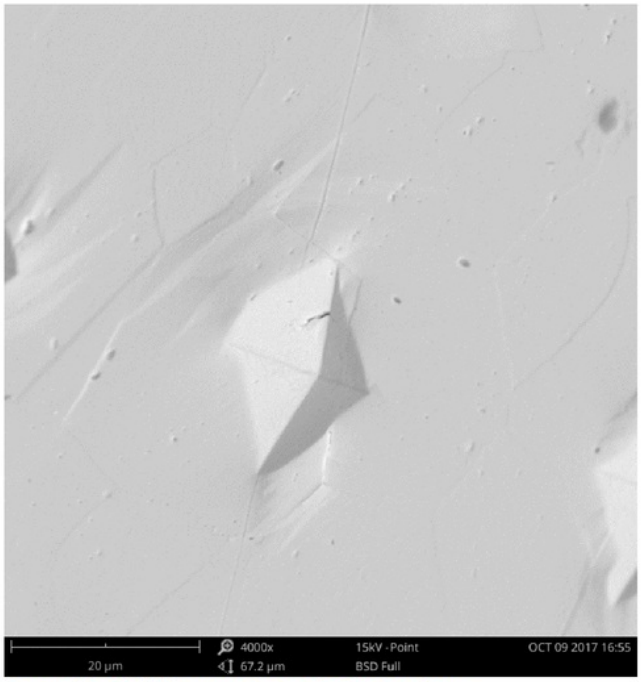

Figure 56 - SEM Image of sample C2 topology

Sample C3

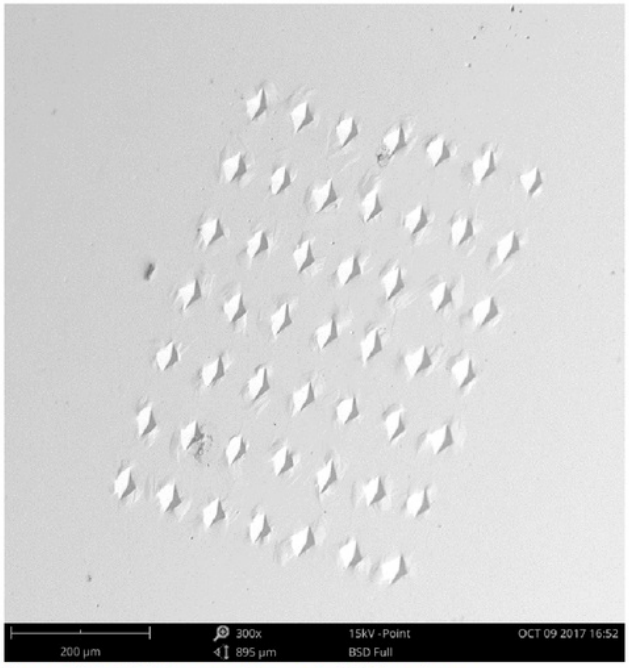

Figure 57 - SEM Image of sample C3 topology

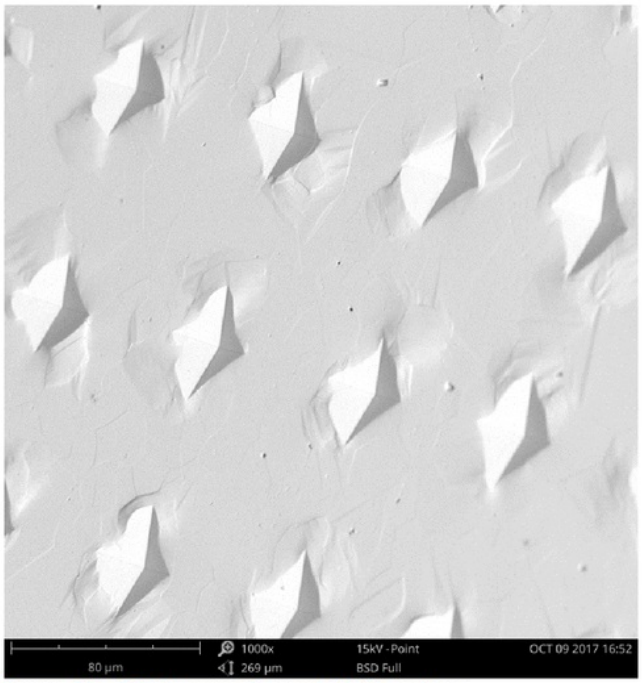

Figure 58 - SEM Image of sample C3 topology

Sample D1

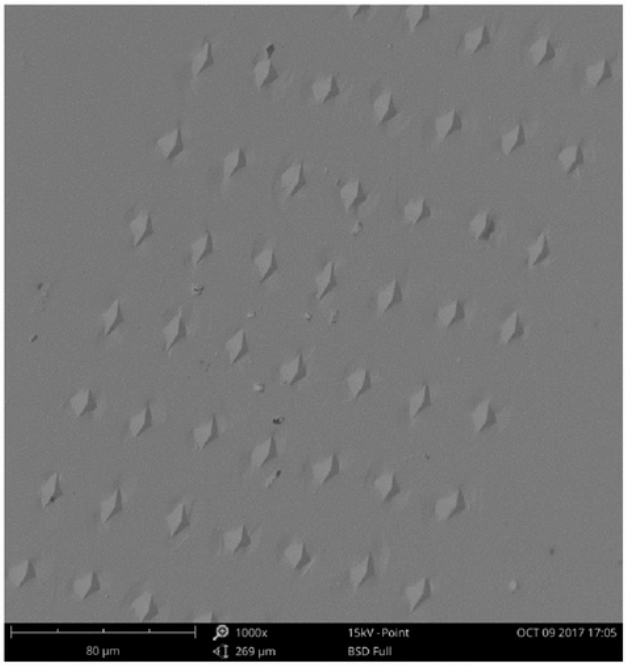

Figure 59 - SEM Image of sample D1 topology

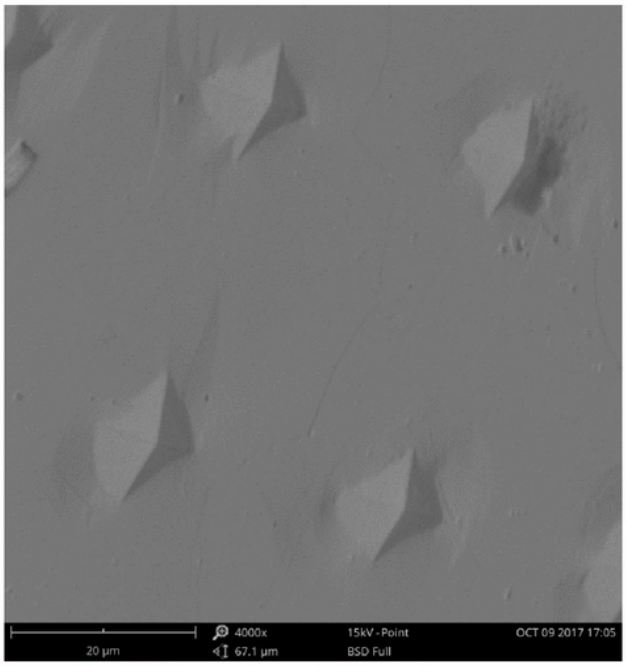

Figure 60 - SEM Image of sample D1 topology

Sample D2

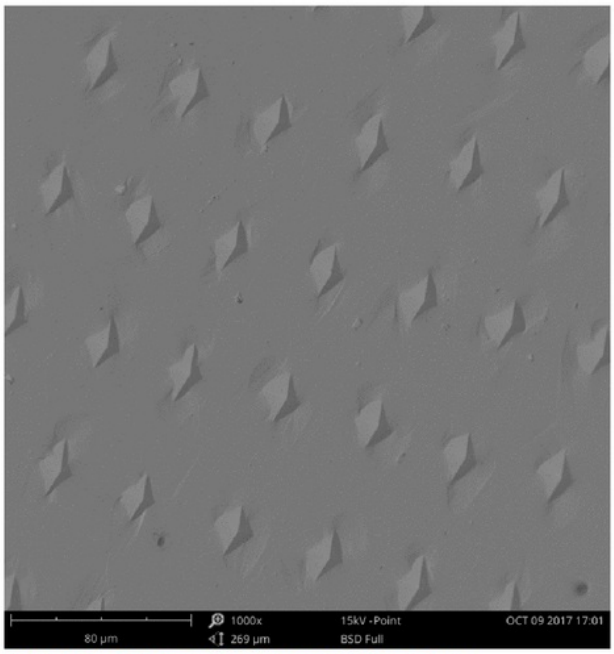

Figure 61 - SEM Image of sample D2 topology

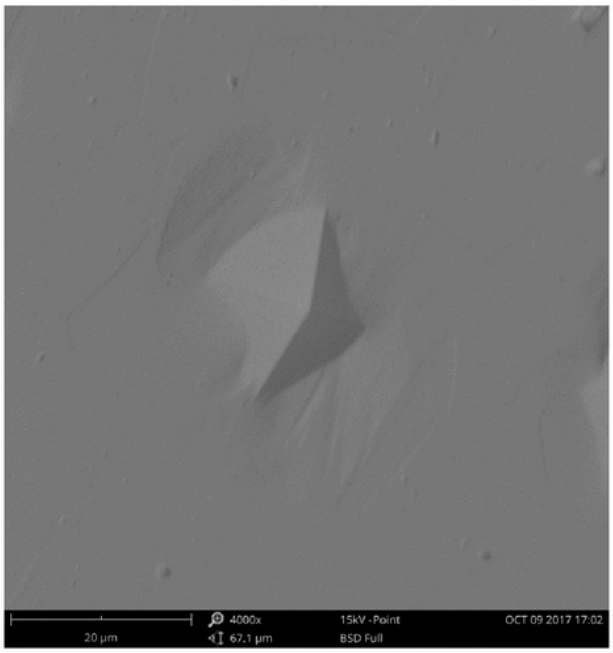

Figure 62 - SEM Image of sample D2 topology

Sample D3

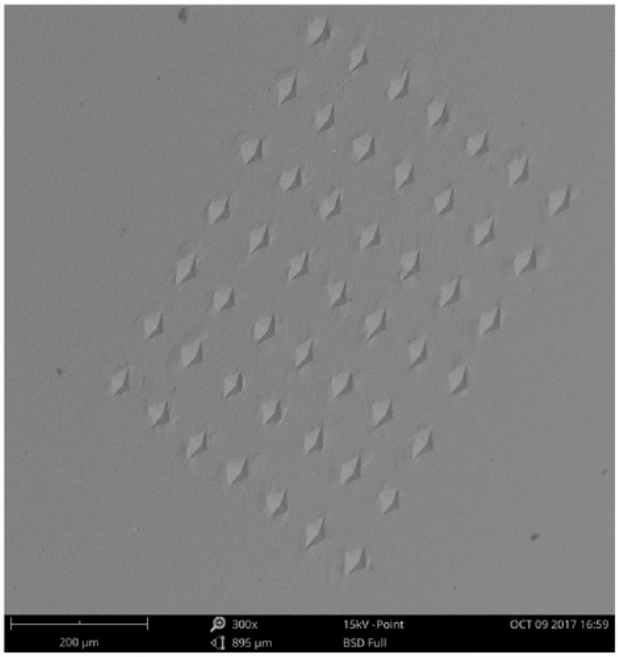

Figure 63 - SEM Image of sample D3 topology

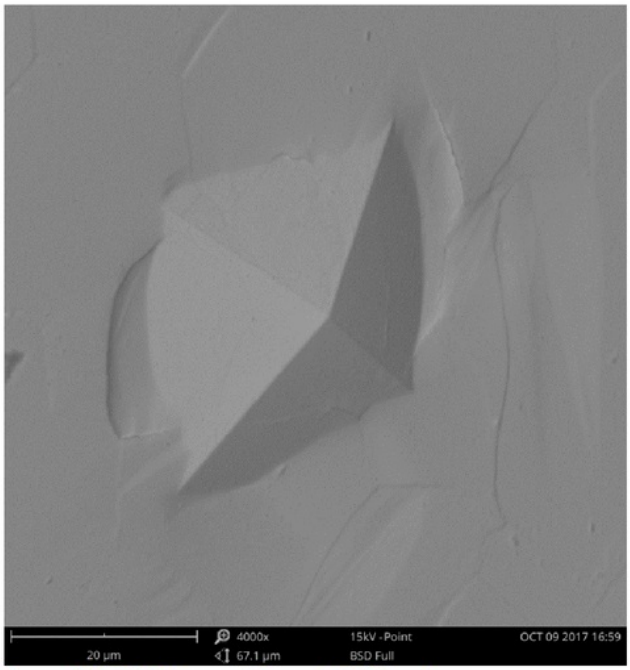

Figure 64 - SEM Image of sample D3 topology

Appendix B - Wettability testing images

Surface condition; 120P grit, No ordered pattern:

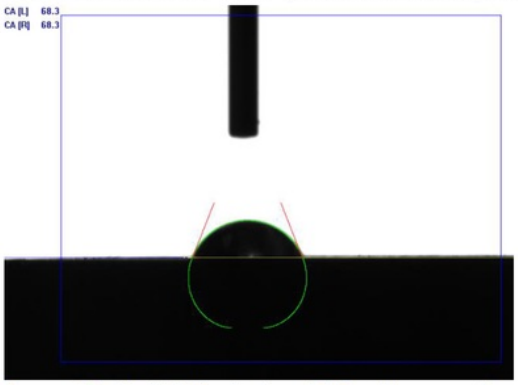

Figure 65 - Wattability test on 120P grit, non ordered topography

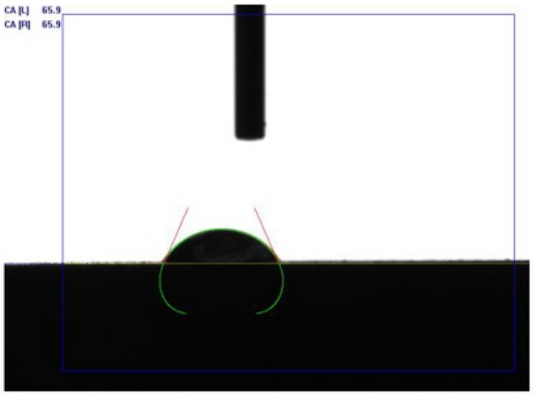

Figure 66 - Wattability test on 120P grit, non ordered topography

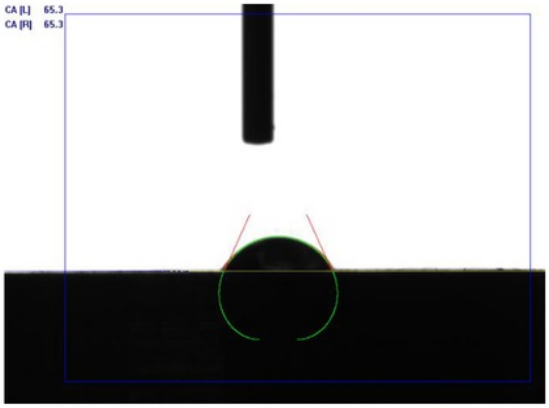

Figure 67 - Wattability test on 120P grit, non ordered topography

Surface condition; 800P grit, No ordered pattern:

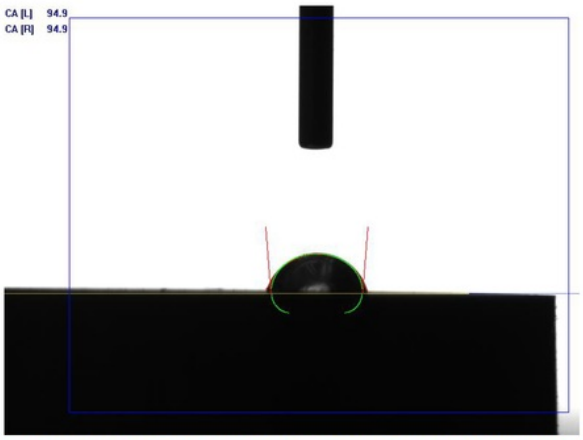

Figure 68 - Wattability test on 800P grit, non ordered topography

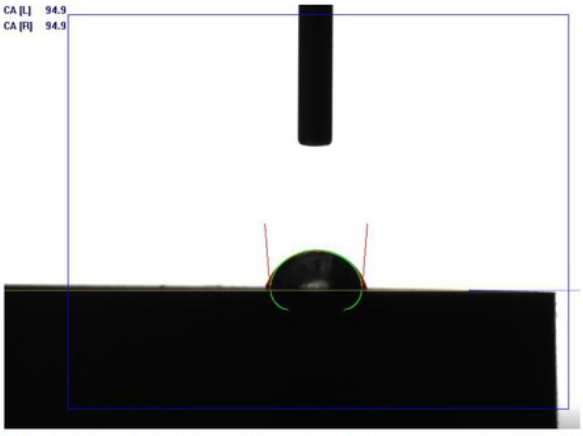

Figure 69 - Wattability test on 800P grit, non ordered topography

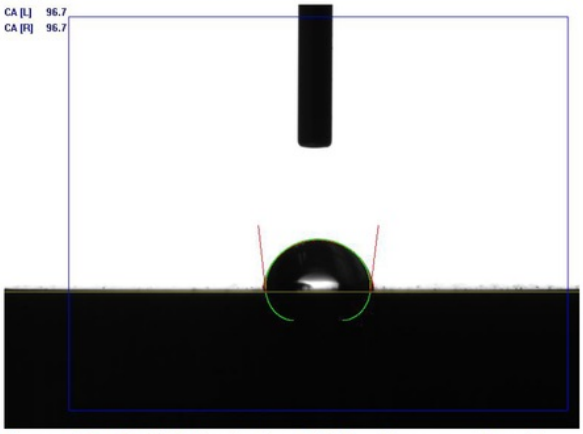

Figure 70 - Wattability test on 800P grit, non ordered topography

Surface condition; 800P grit, 0.05HV, 100 micrometers between indents:

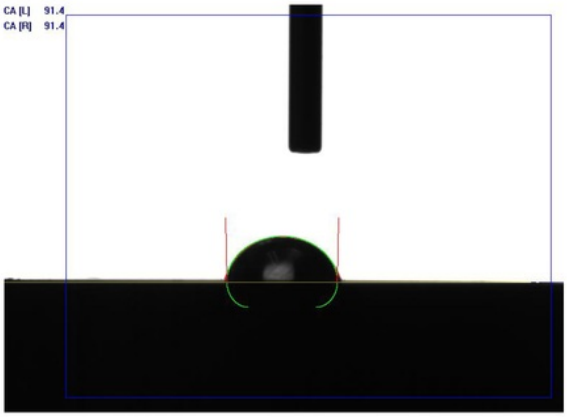

Figure 71 – Wettability test on 800P grit, 0.05HV, 100 micrometers between indents

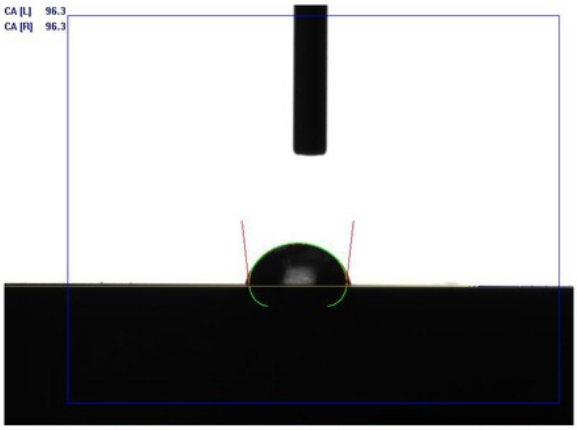

Figure 72 - Wettability test on 800P grit, 0.05HV, 100 micrometers between indents

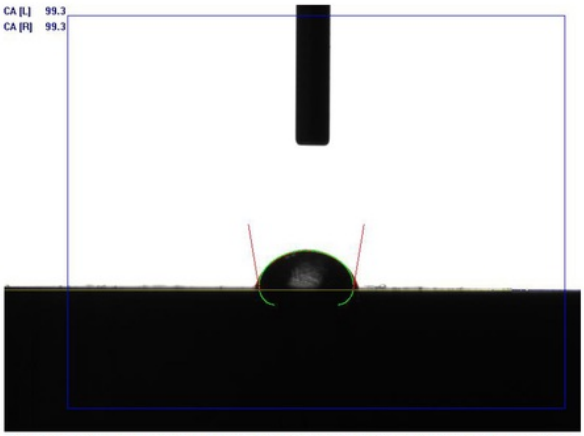

Figure 73 - Wettability test on 800P grit, 0.05HV, 100 micrometers between indents

Surface condition; 800P grit, 0.02HV, 150 micrometers between indents:

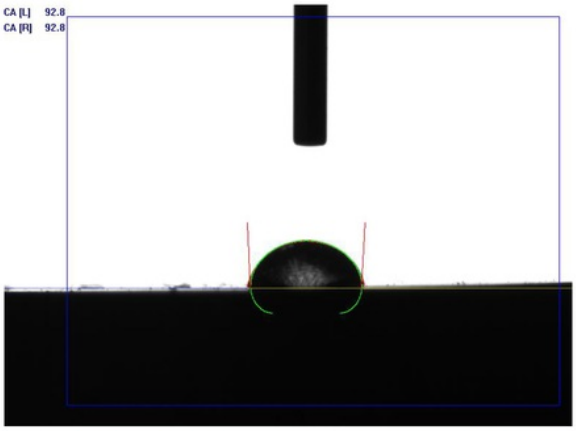

Figure 74 - Wettability test on 800P grit, 0.02HV, 150 micrometers between indents

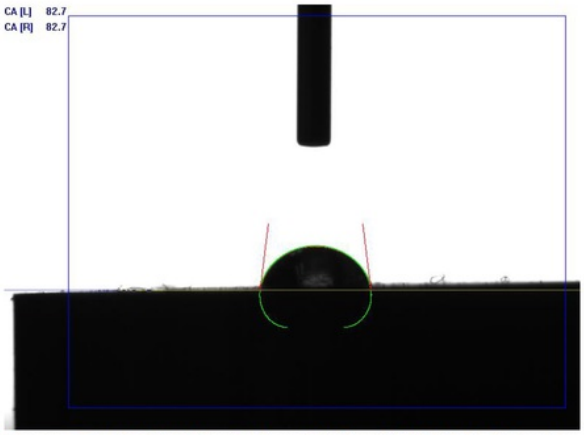

Figure 75 - Wettability test on 800P grit, 0.02HV, 150 micrometers between indents

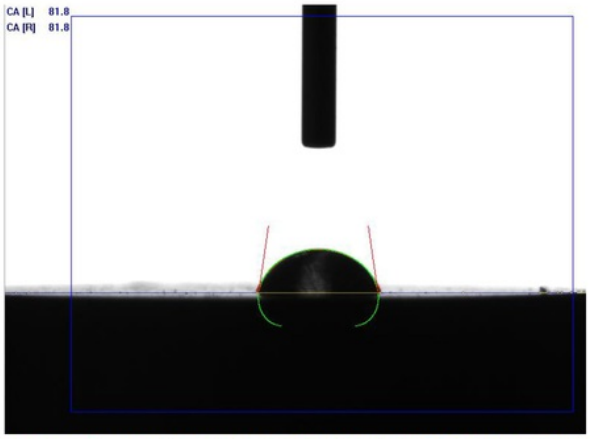

Figure 76 - Wettability test on 800P grit, 0.02HV, 150 micrometers between indents

Surface condition; 1200P grit, No ordered pattern:

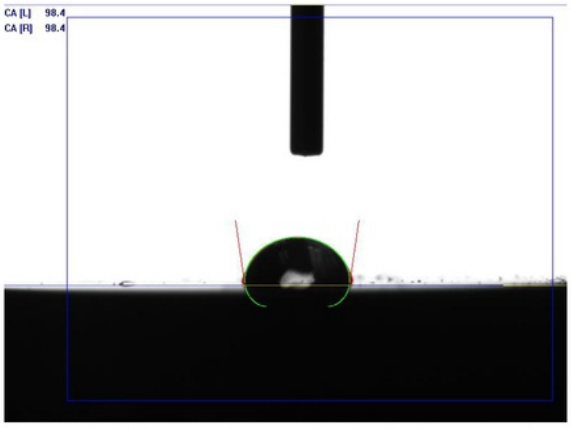

Figure 77 - Wettability test on 1200P grit, No ordered pattern

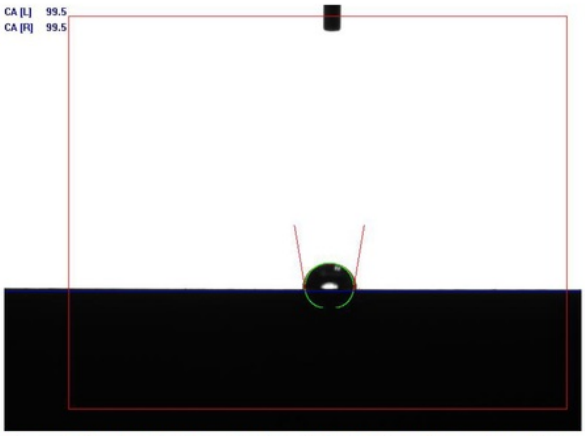

Figure 78 - Wettability test on 1200P grit, No ordered pattern

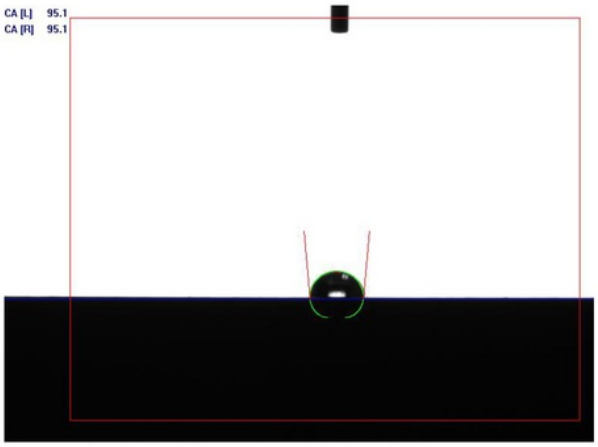

Figure 79 - Wettability test on 1200P grit, No ordered pattern

Surface condition; Polished, No ordered pattern:

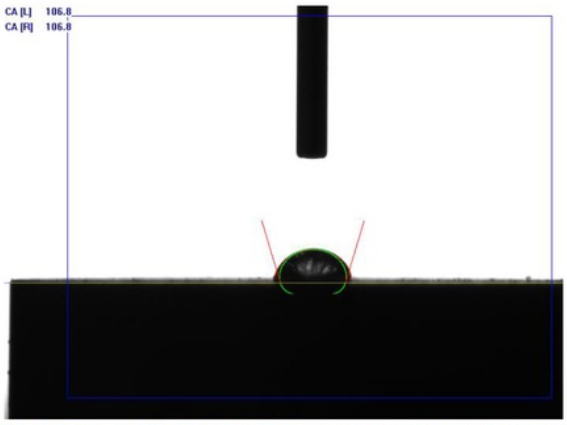

Figure 80 - Wettability test on Polished, No ordered pattern

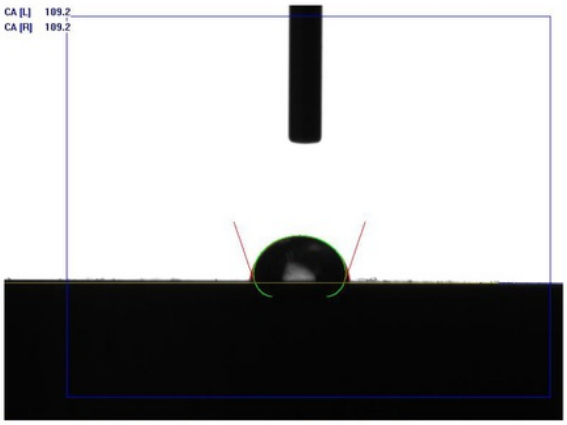

Figure 81 - Wettability test on Polished, No ordered pattern

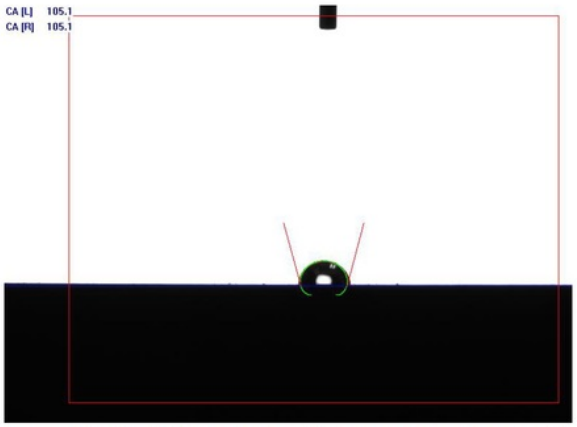

Figure 82 - Wettability test on Polished, No ordered pattern

Surface condition; Polished, 0.01HV, 40 micrometers between indents:

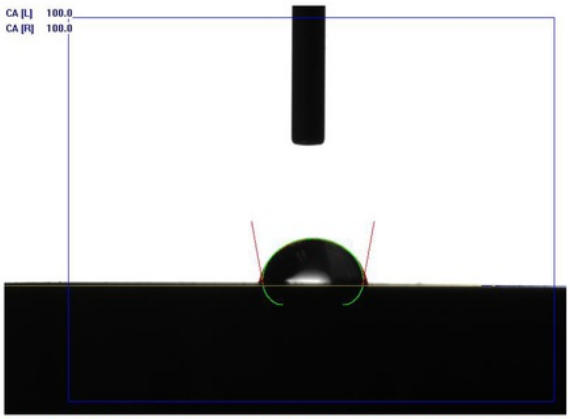

Figure 83 - Wettability test on Polished, 0.01HV, 40 micrometers between indents

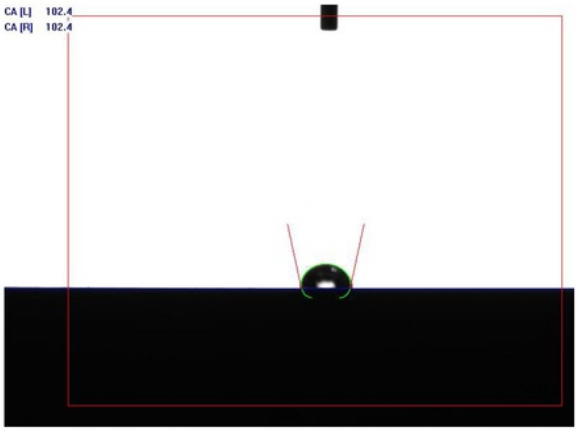

Figure 84 - Wettability test on Polished, 0.01HV, 40 micrometers between indents

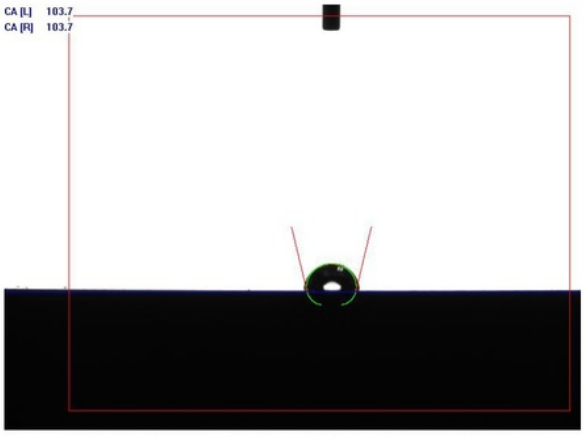

Figure 85 - Wettability test on Polished, 0.01HV, 40 micrometers between indents

Surface condition; Polished, 0.025HV, 60 micrometers between indents:

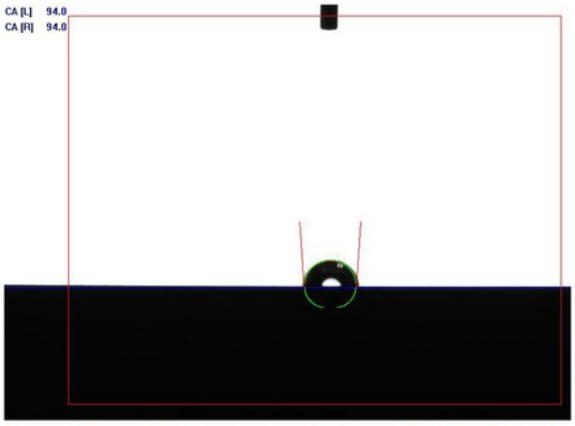

Figure 86 - Wettability test on Polished, 0.025HV, 60 micrometers between indents

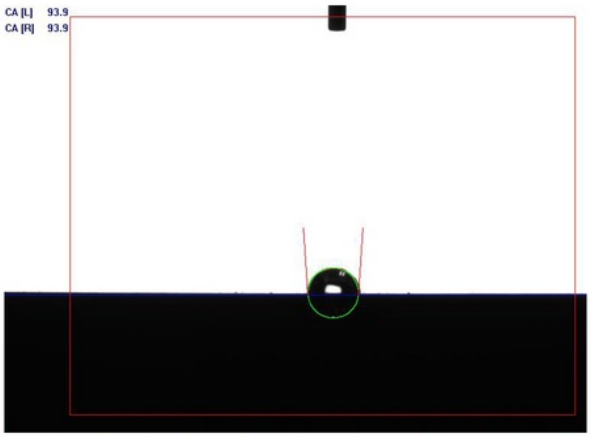

Figure 87 - Wettability test on Polished, 0.025HV, 60 micrometers between indents

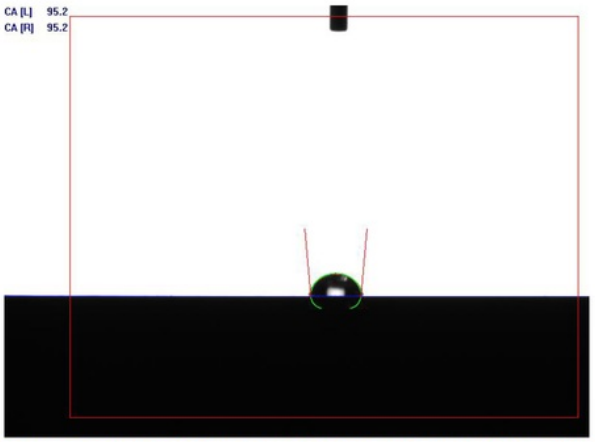

Figure 88 - Wettability test on Polished, 0.025HV, 60 micrometers between indents

Surface condition; Polished, 0.1HV, 100 micrometers between indents:

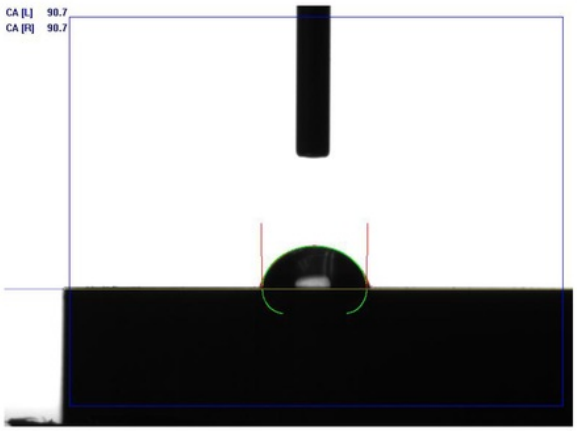

Figure 89 - Wettability test on Polished, 0.1HV, 100 micrometers between indents

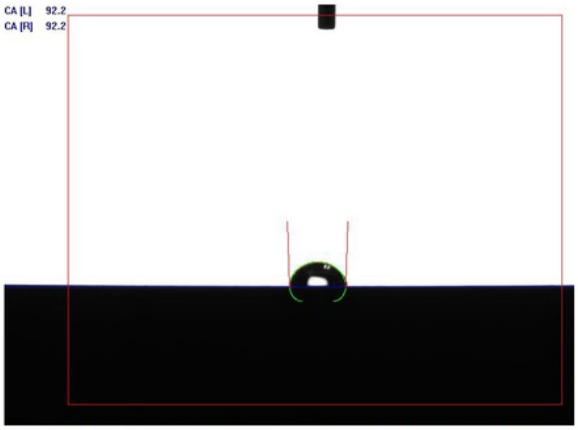

Figure 90 - Wettability test on Polished, 0.1HV, 100 micrometers between indents

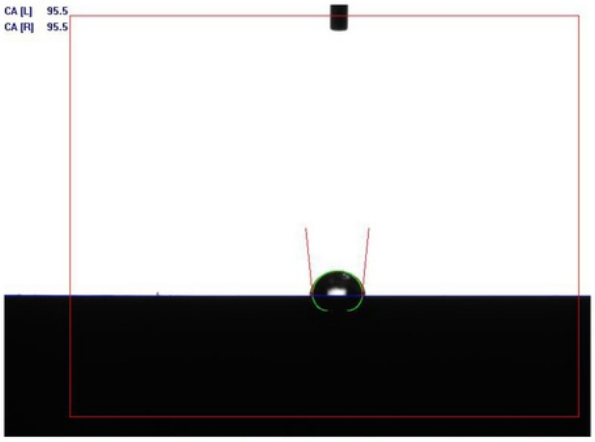

Figure 91 - Wettability test on Polished, 0.1HV, 100 micrometers between indents

Appendix C - Microscope images of cell culture on zinc samples

Sample 1

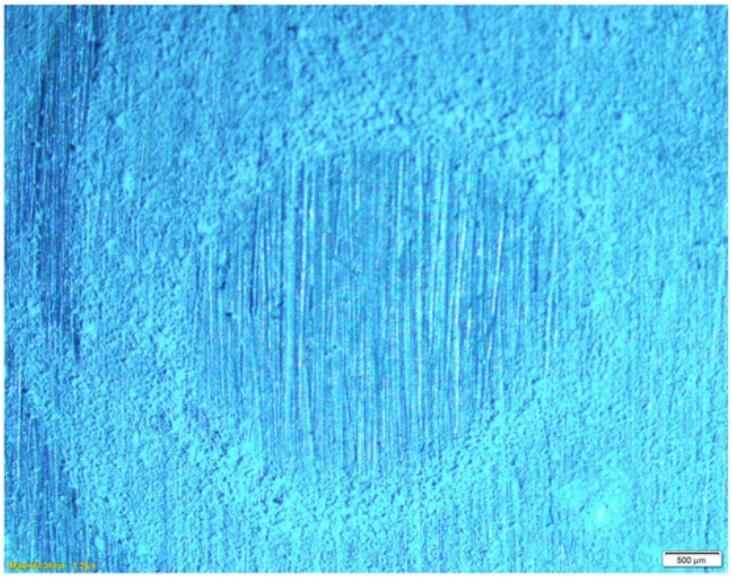

Figure 92 - Microscope image of cell culture on sample 1

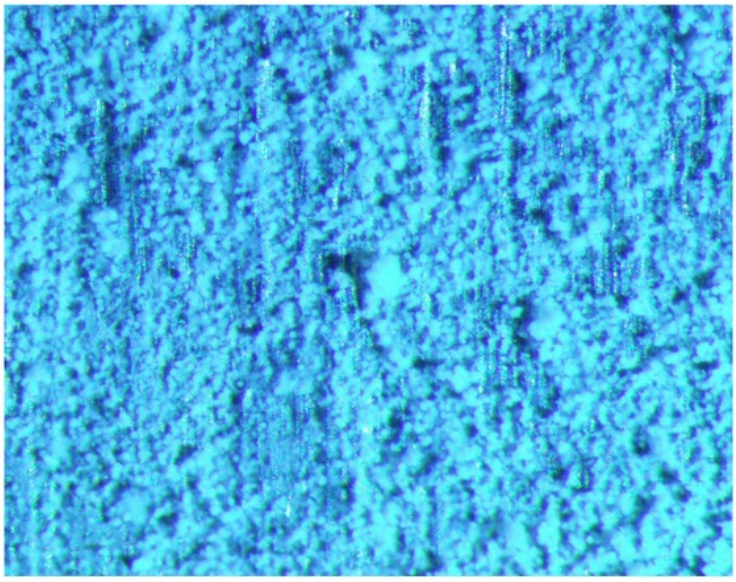

Figure 93 - Microscope image of cell culture on sample 1

Sample 7

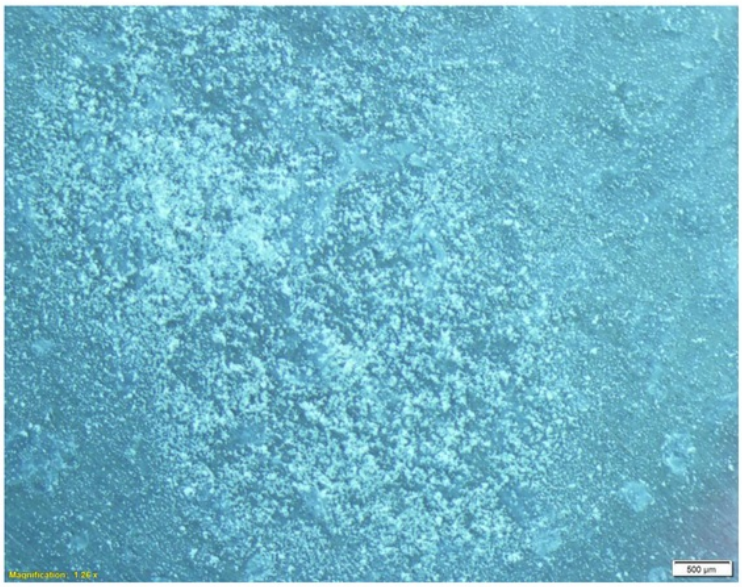

Figure 94 - Microscope image of cell culture on sample 7

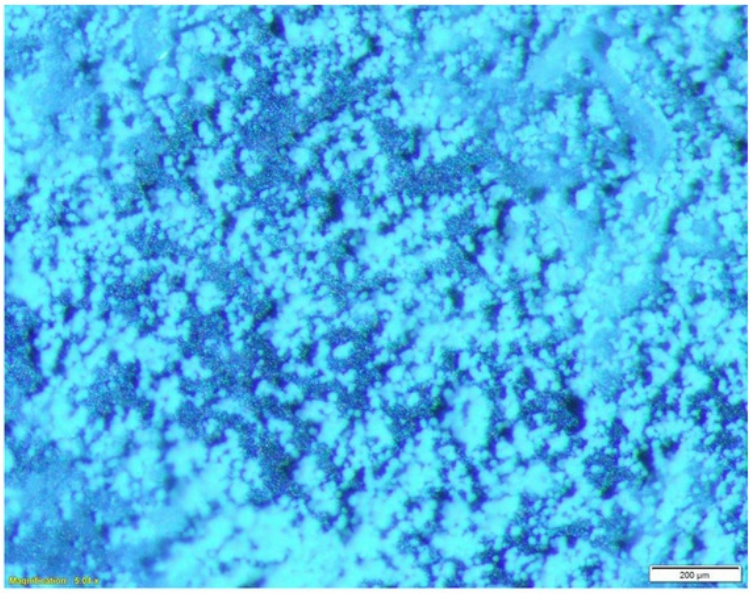

Figure 95 - Microscope image of cell culture on sample 7

Sample 12

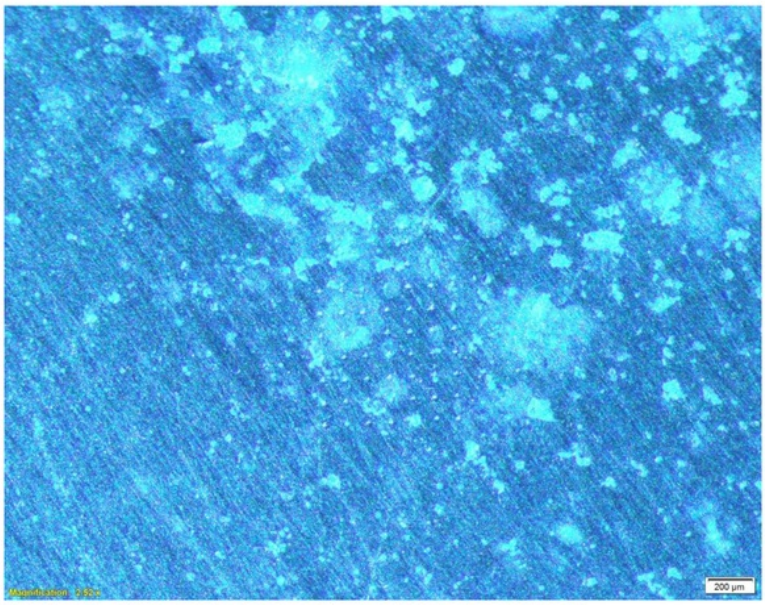

Figure 96 - Microscope image of cell culture on sample 12

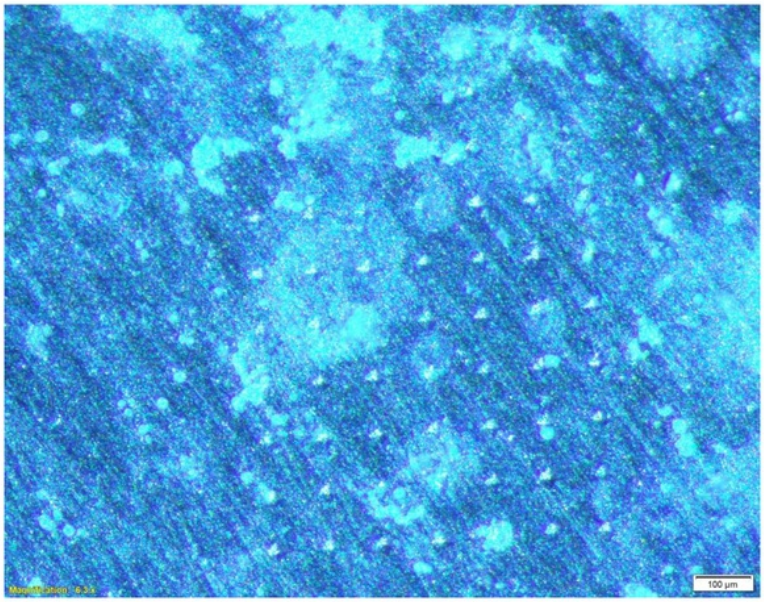

Figure 97 - Microscope image of cell culture on sample 1

Sample 13

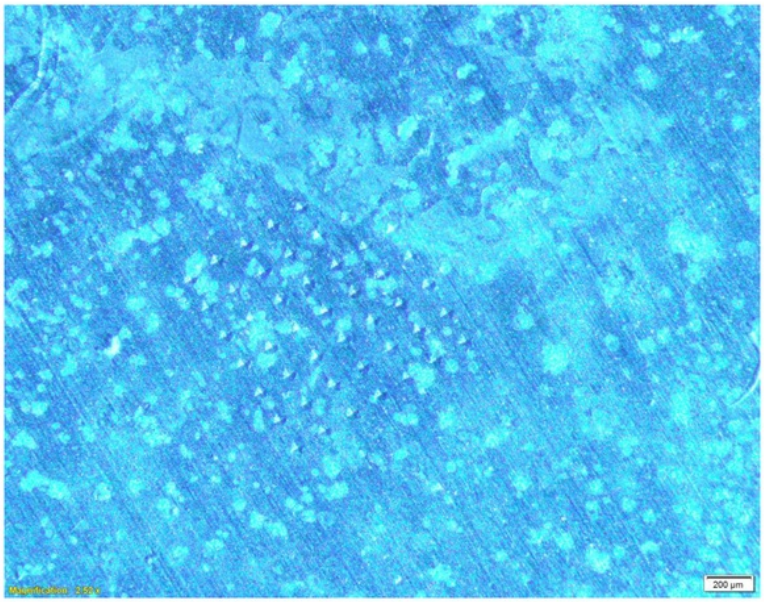

Figure 98 - Microscope image of cell culture on sample 13

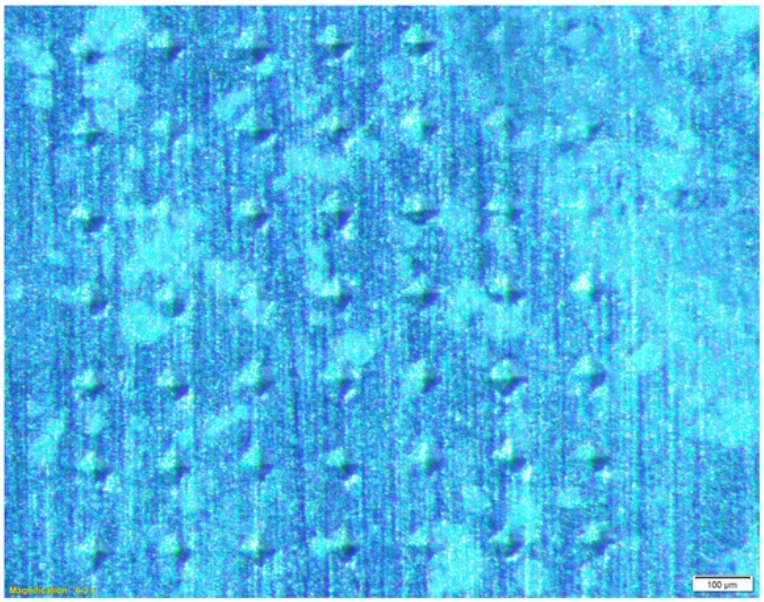

Figure 99 - Microscope image of cell culture on sample 13

Sample 16

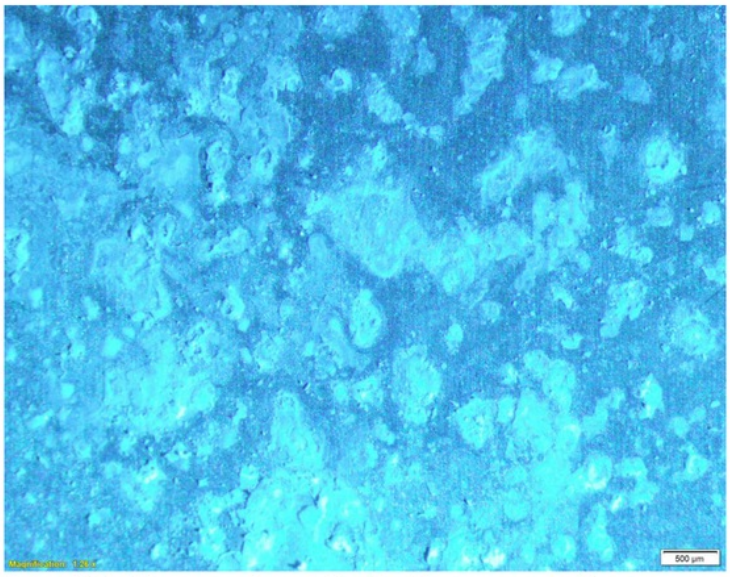

Figure 100 - Microscope image of cell culture on sample 16

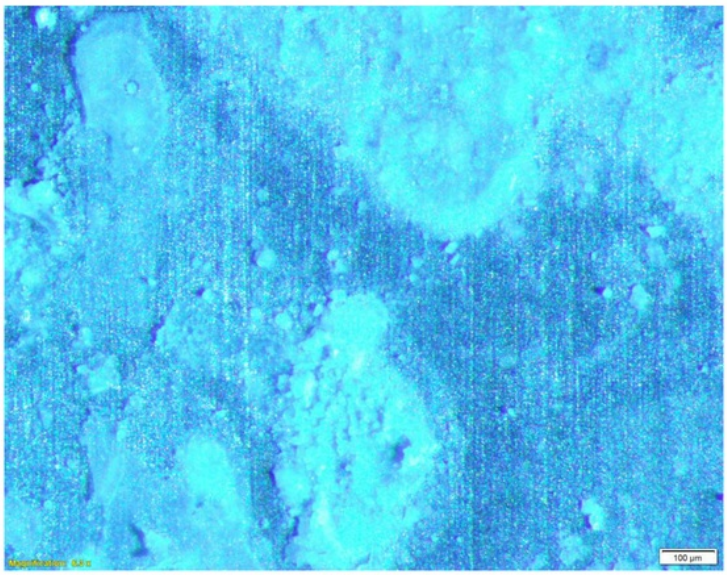

Figure 101 - Microscope image of cell culture on sample 16

Sample A

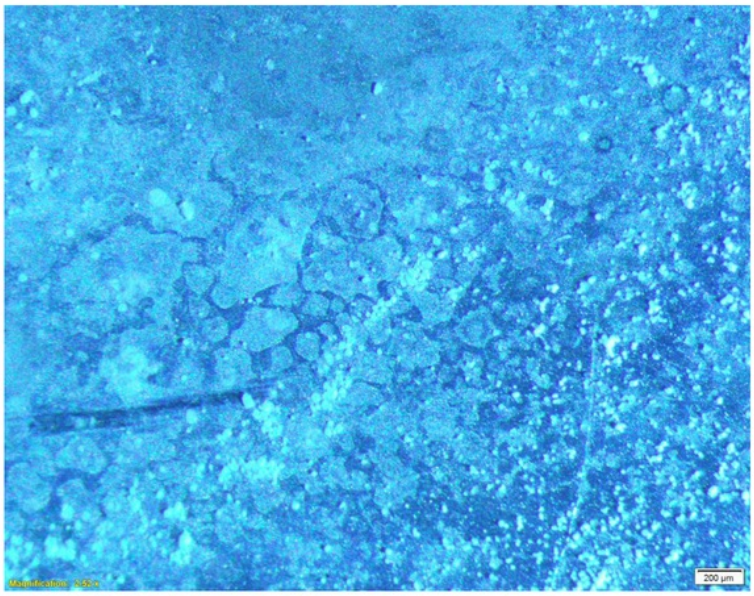

Figure 102 - Microscope image of cell culture on sample A

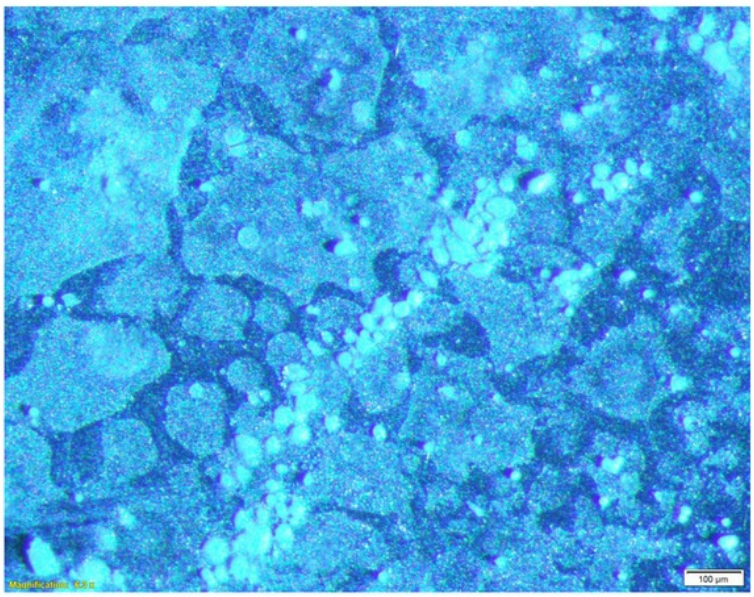

Figure 103 - Microscope image of cell culture on sample A

Sample B1

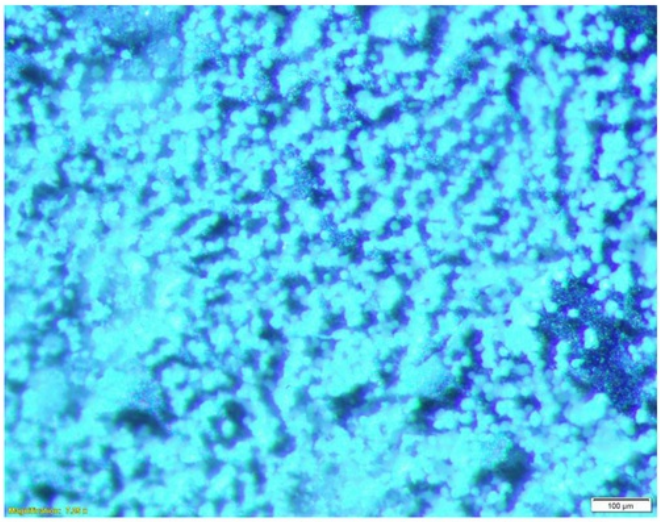

Figure 104 - Microscope image of cell culture on sample B1

Sample B2

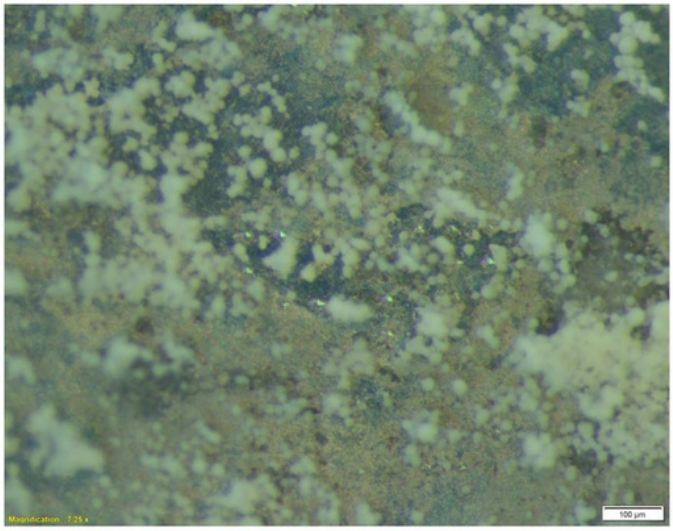

Figure 105 - Microscope image of cell culture on sample B2

Sample B3

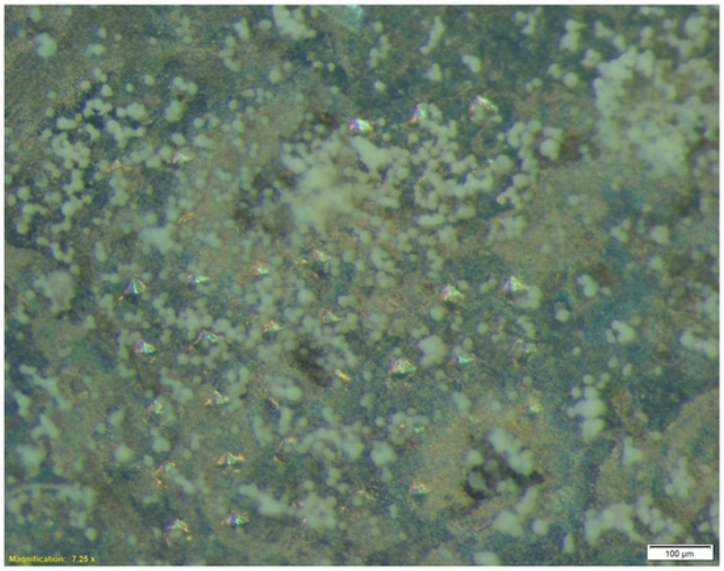

Figure 106 - Microscope image of cell culture on sample B3

Sample C1

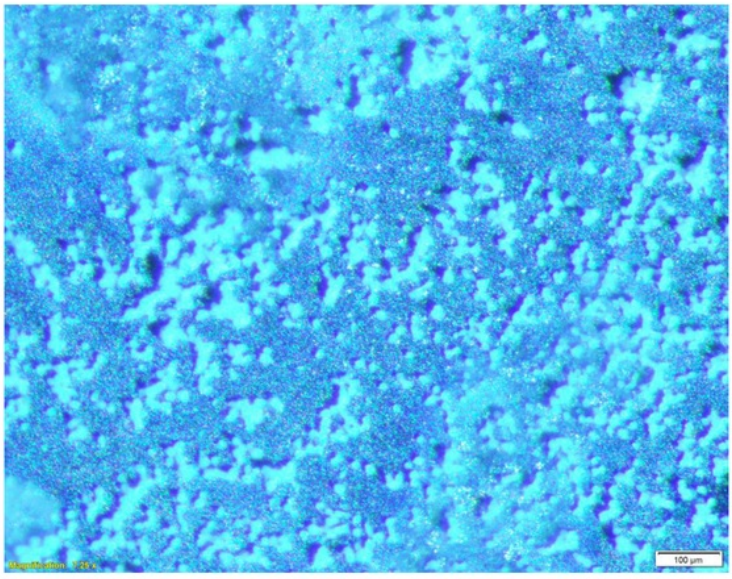

Figure 107 - Microscope image of cell culture on sample C1

Sample C2

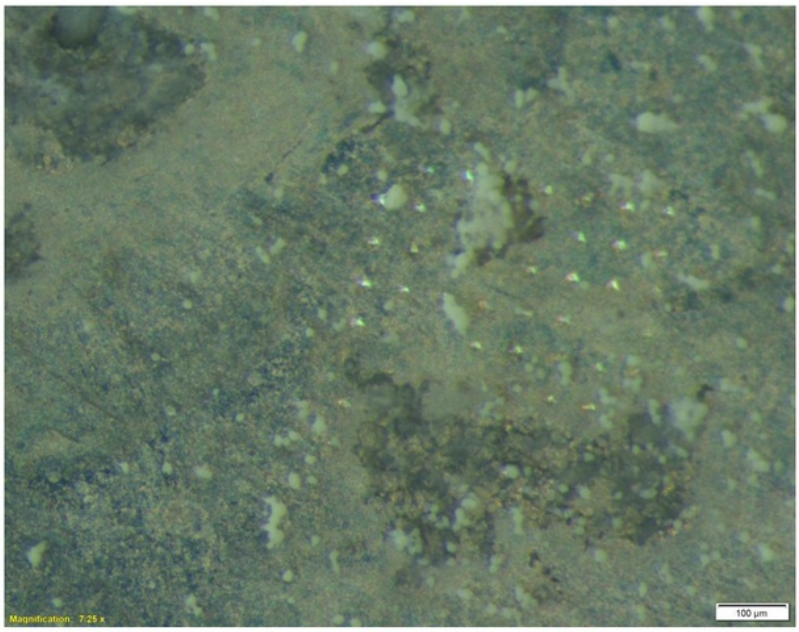

Figure 108 - Microscope image of cell culture on sample C2

Sample C3

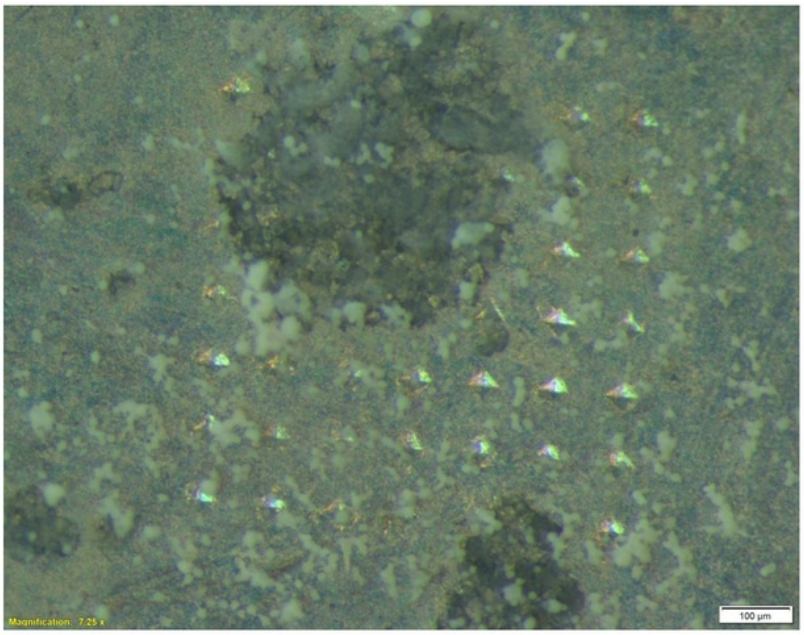

Figure 109 - Microscope image of cell culture on sample C3

Sample D1

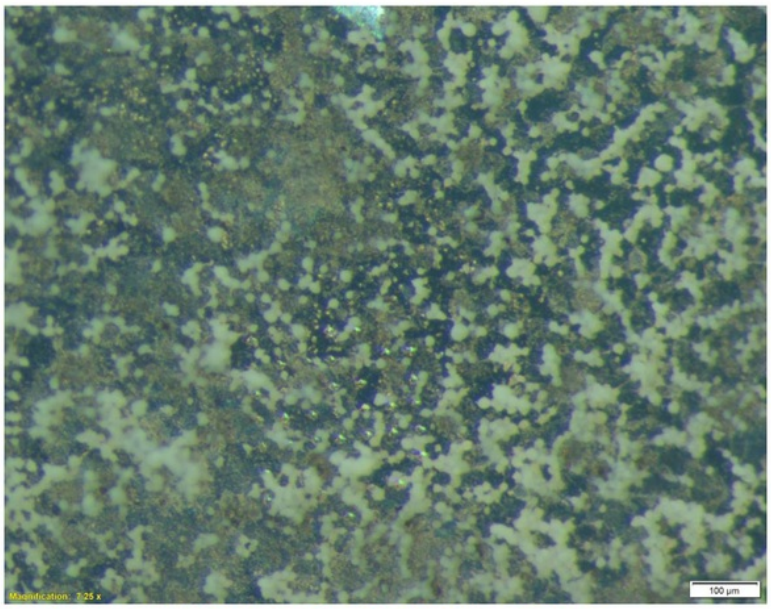

Figure 110 - Microscope image of cell culture on sample D1

Sample D2

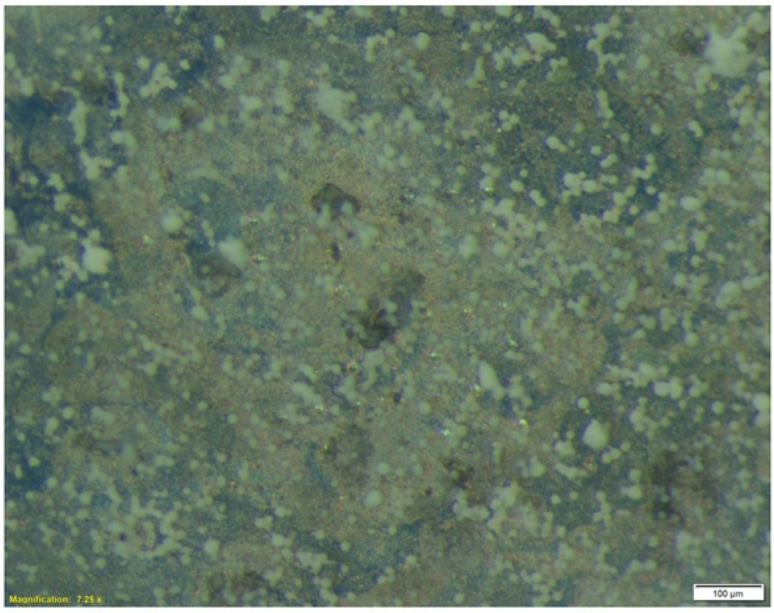

Figure 111 - Microscope image of cell culture on sample D2

Sample D3

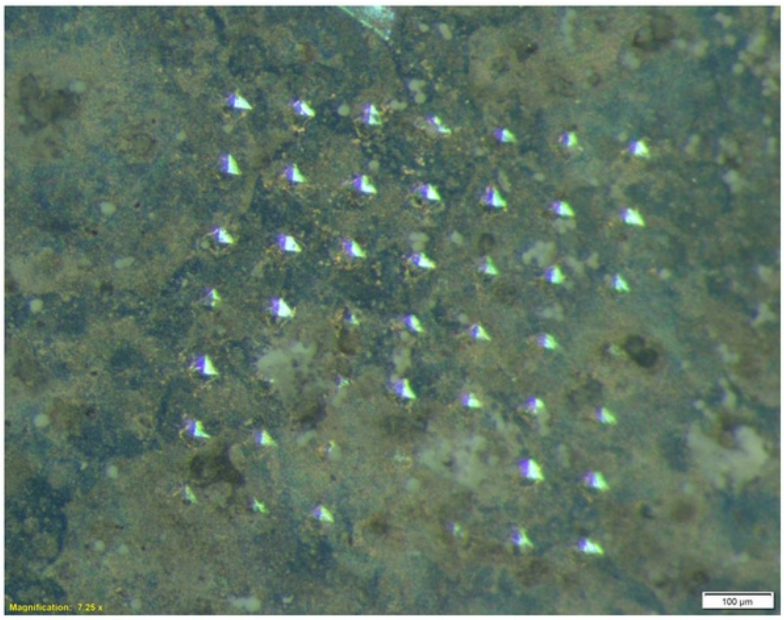

Figure 112 - Microscope image of cell culture on sample D3

Appendix D - SEM images of cell culture on zinc samples

Sample 1

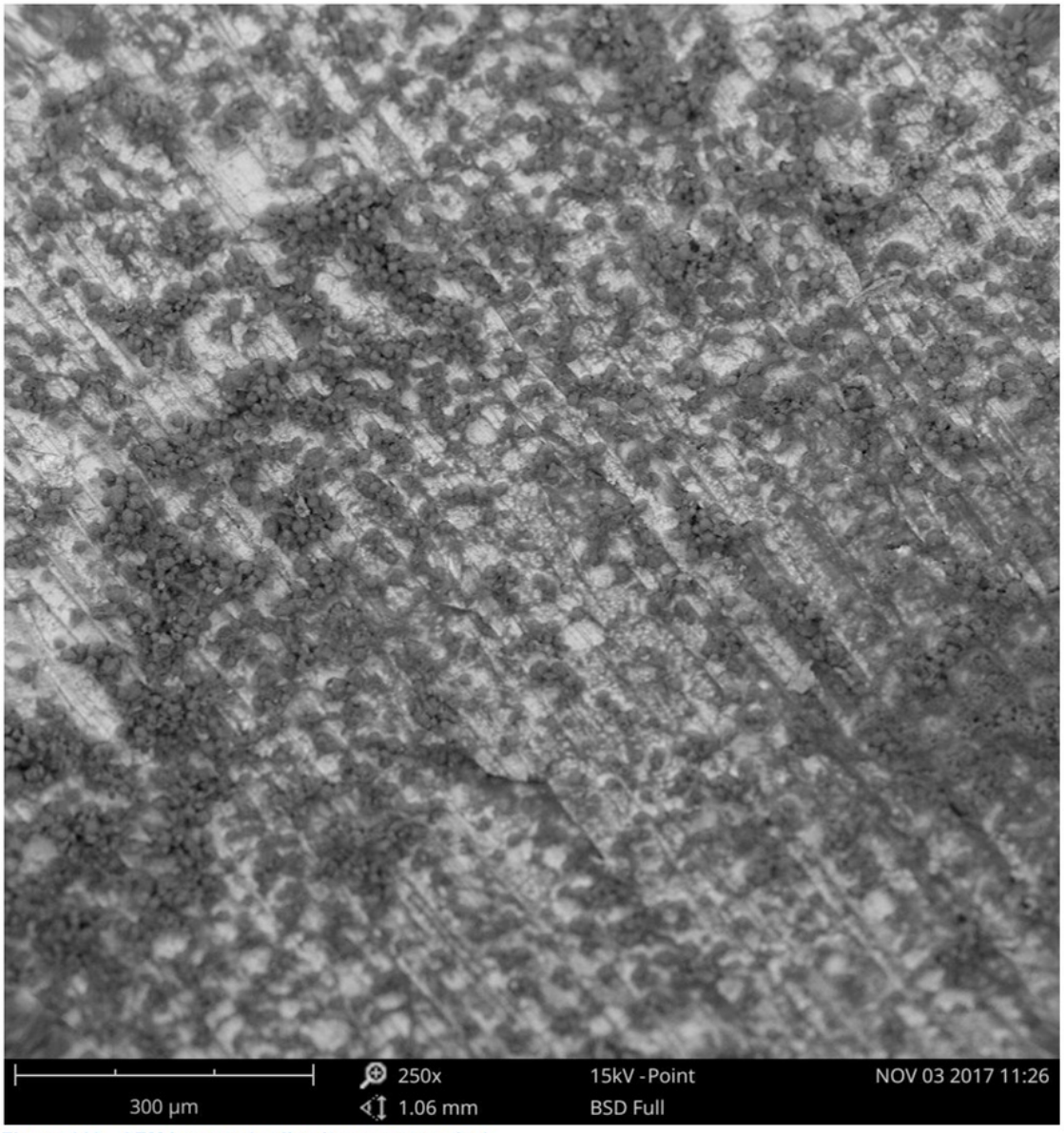

Figure 113 - SEM image of cell culture on sample 1

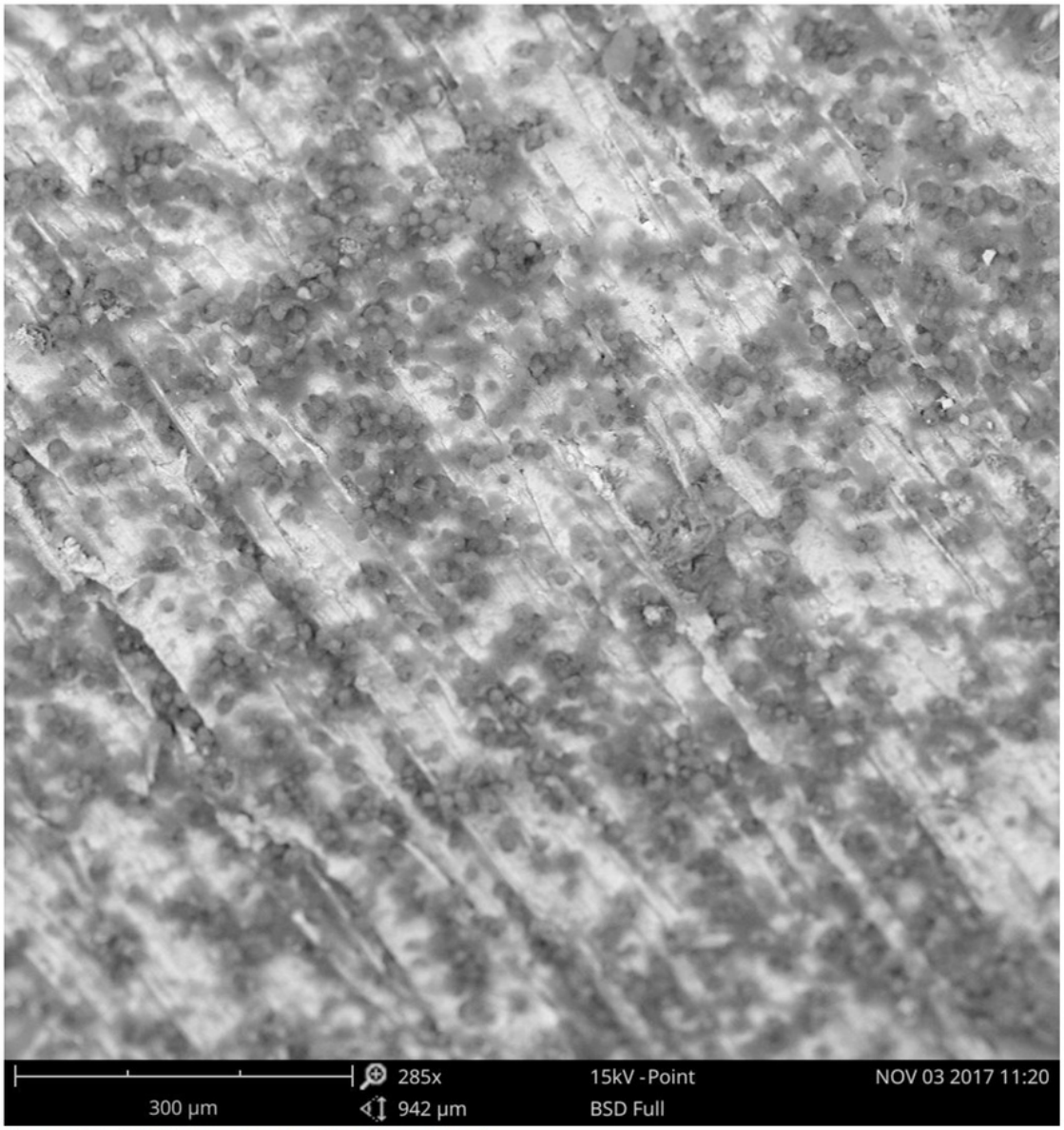

Figure 114 - SEM image of cell culture on sample 1

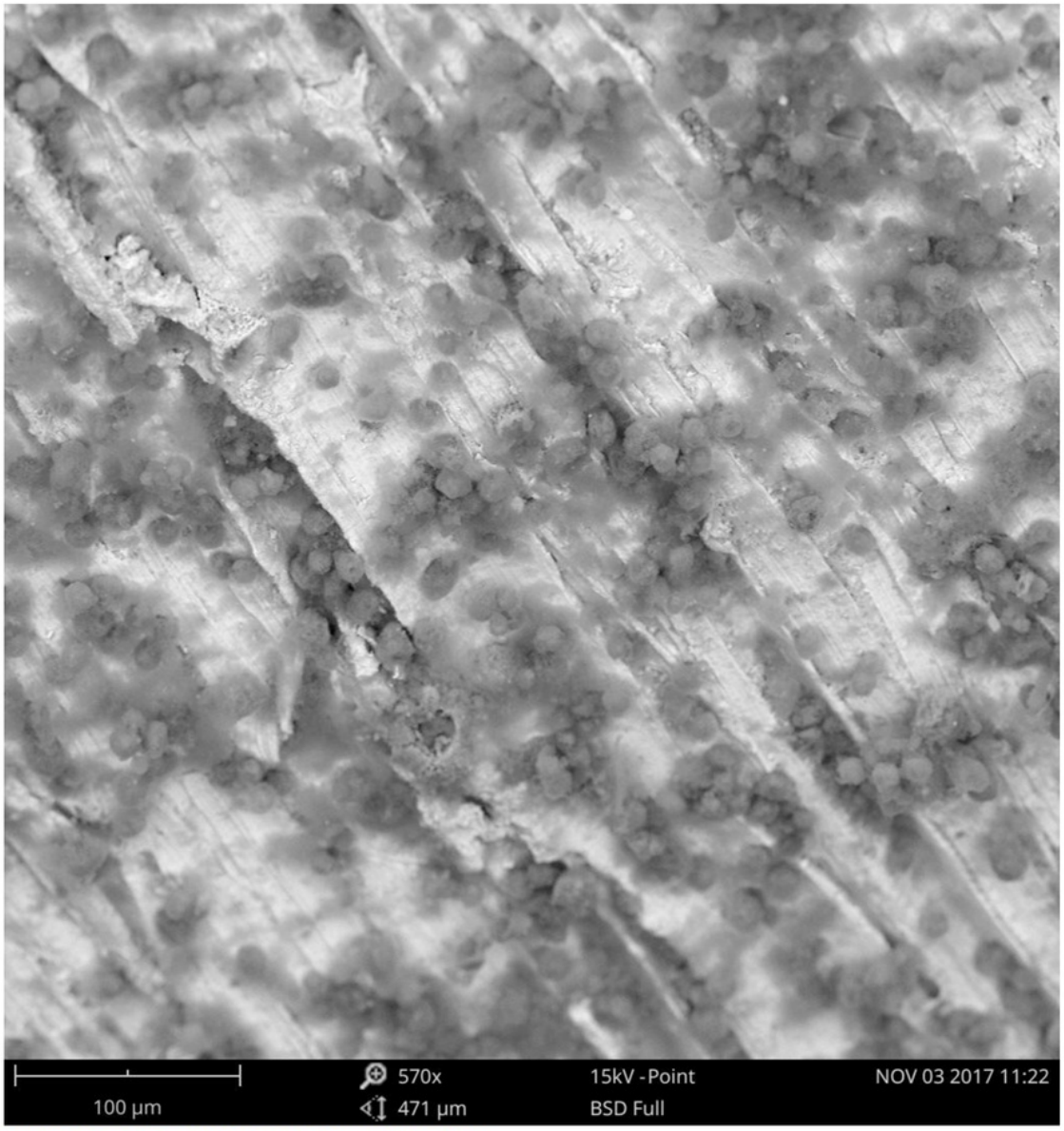

Figure 115 - SEM image of cell culture on sample 1

Sample 7

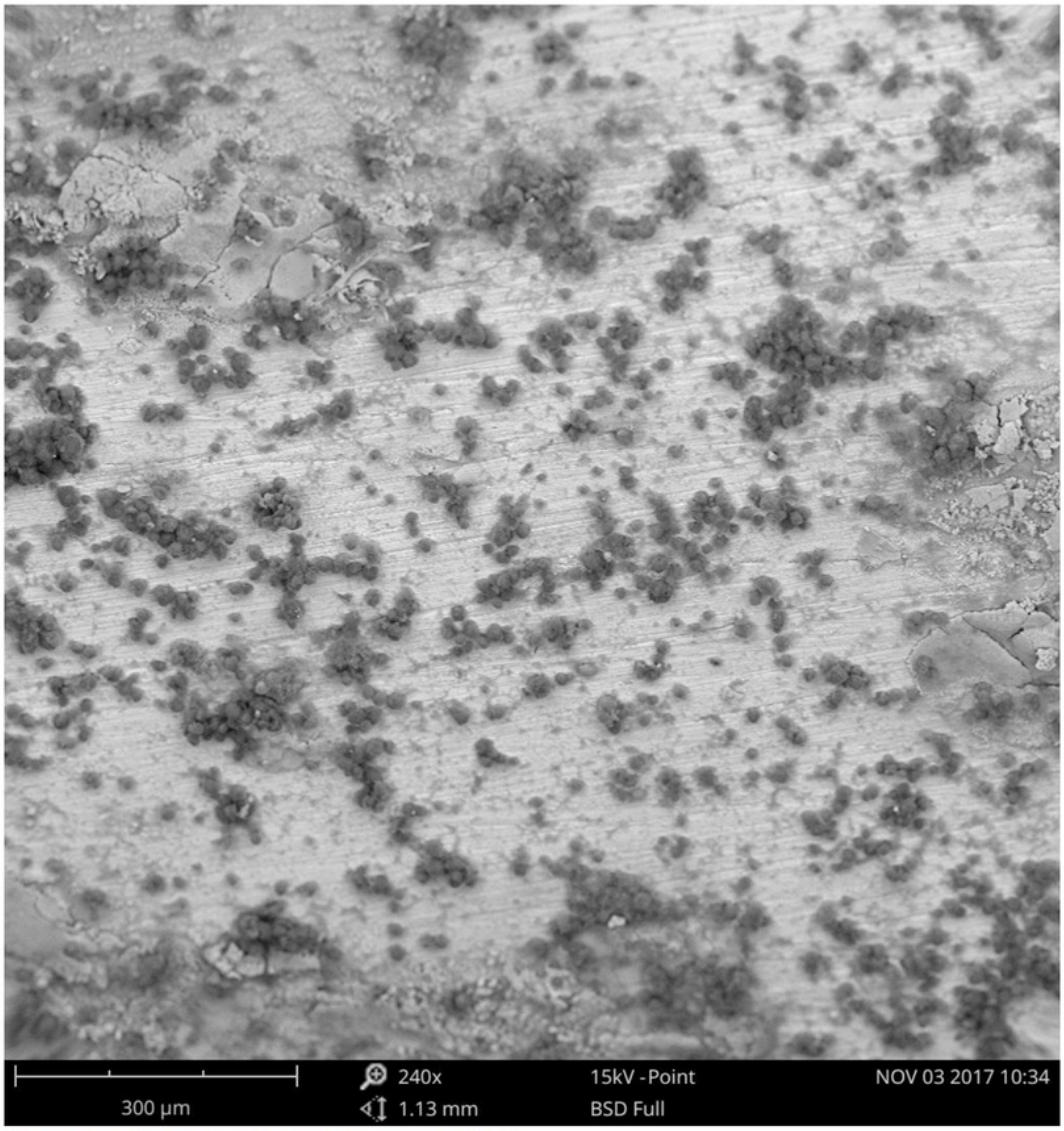

Figure 116 - SEM image of cell culture on sample 7

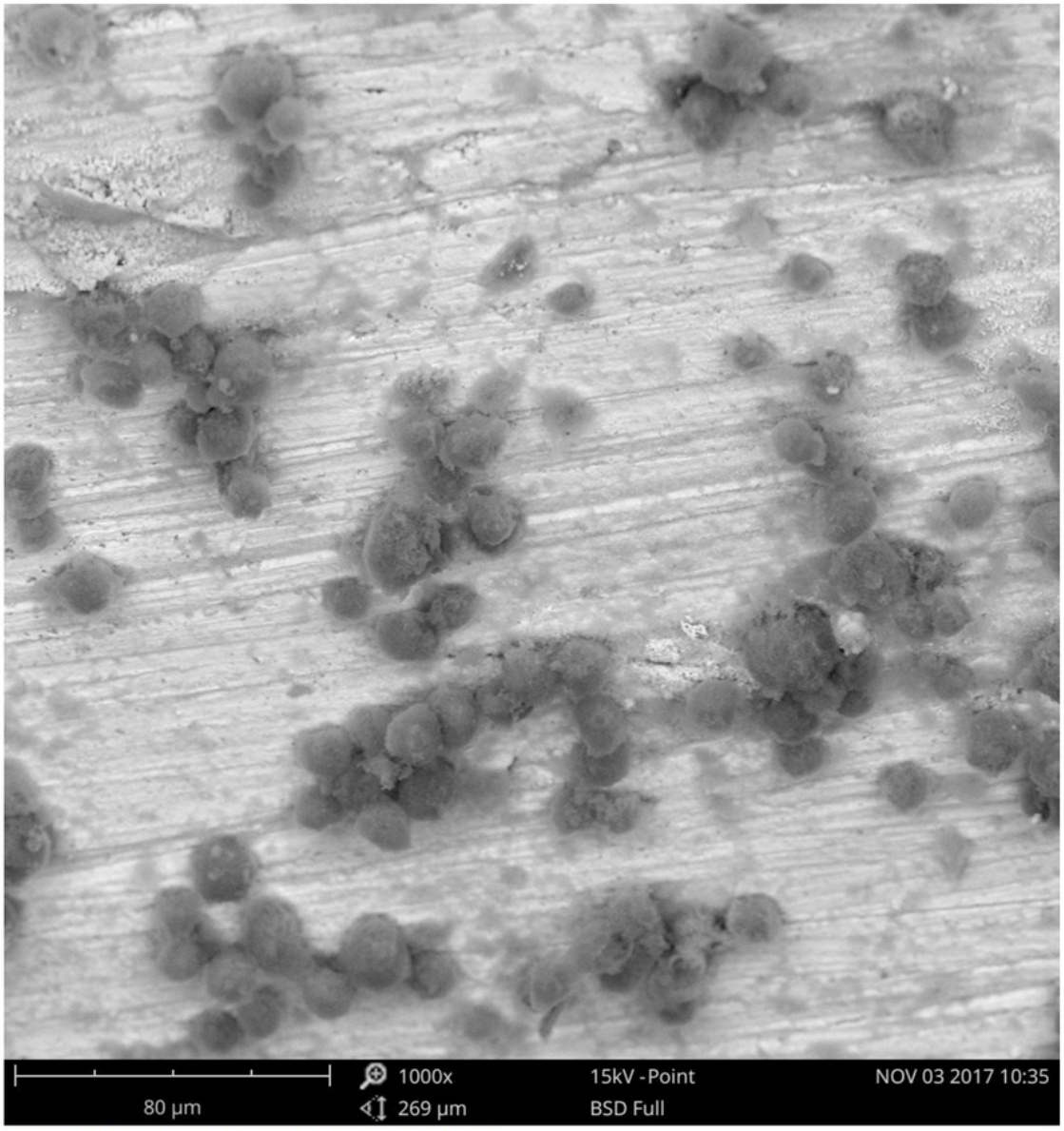

Figure 117 - SEM image of cell culture on sample 7

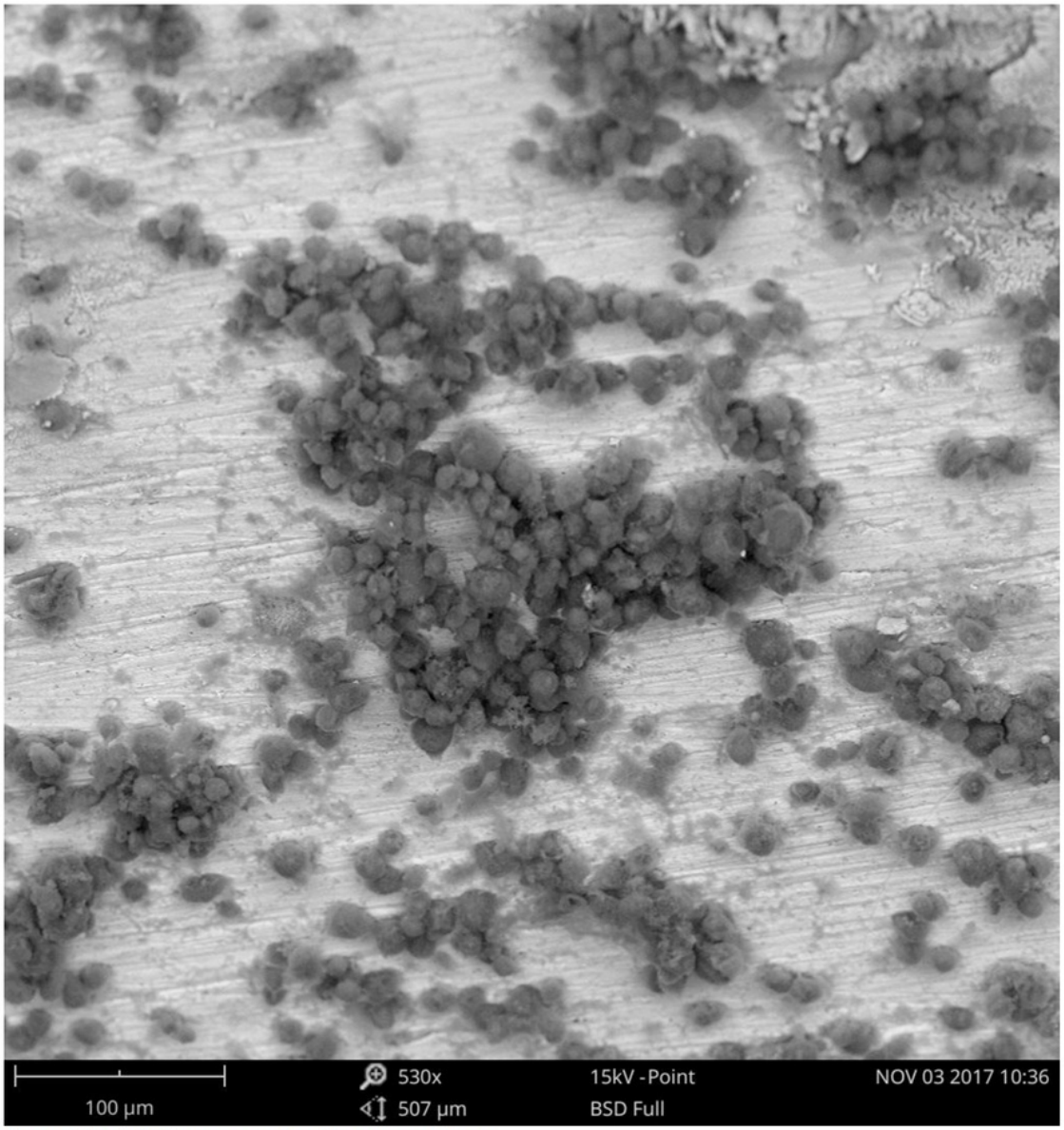

Figure 118 - SEM image of cell culture on sample 7

Sample 12

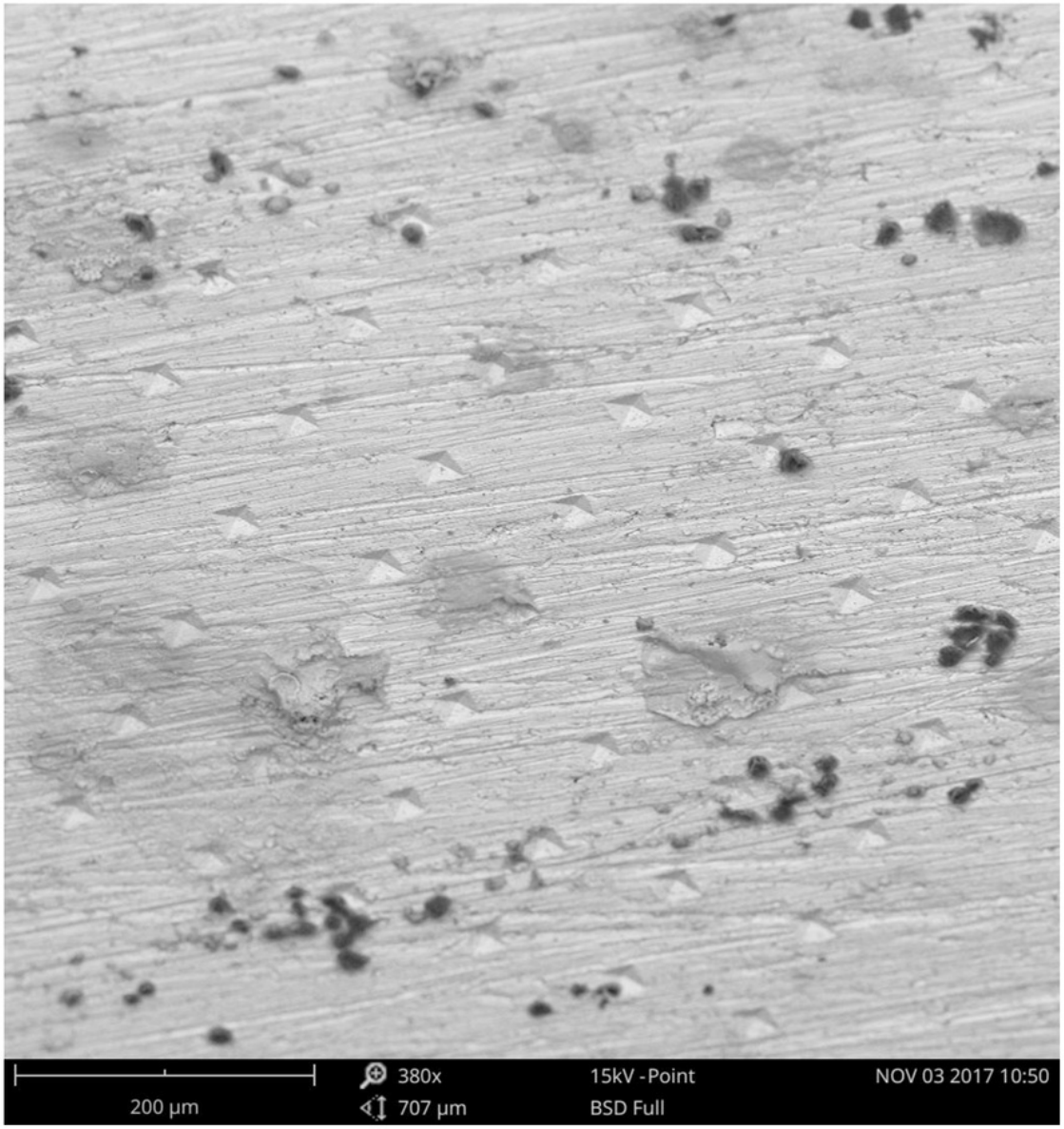

Figure 119 - SEM image of cell culture on sample 12

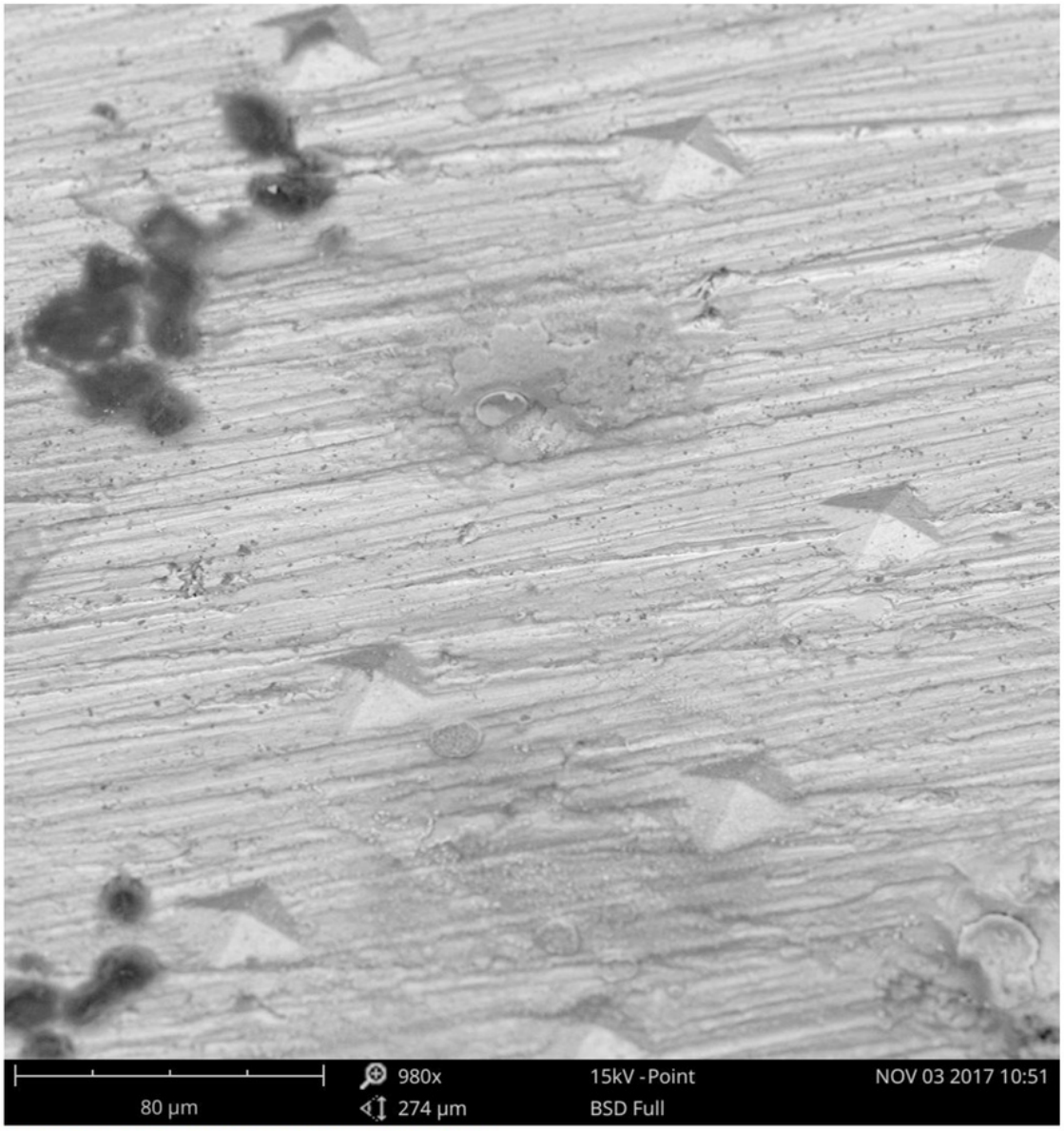

Figure 120 - SEM image of cell culture on sample 12

Sample 13

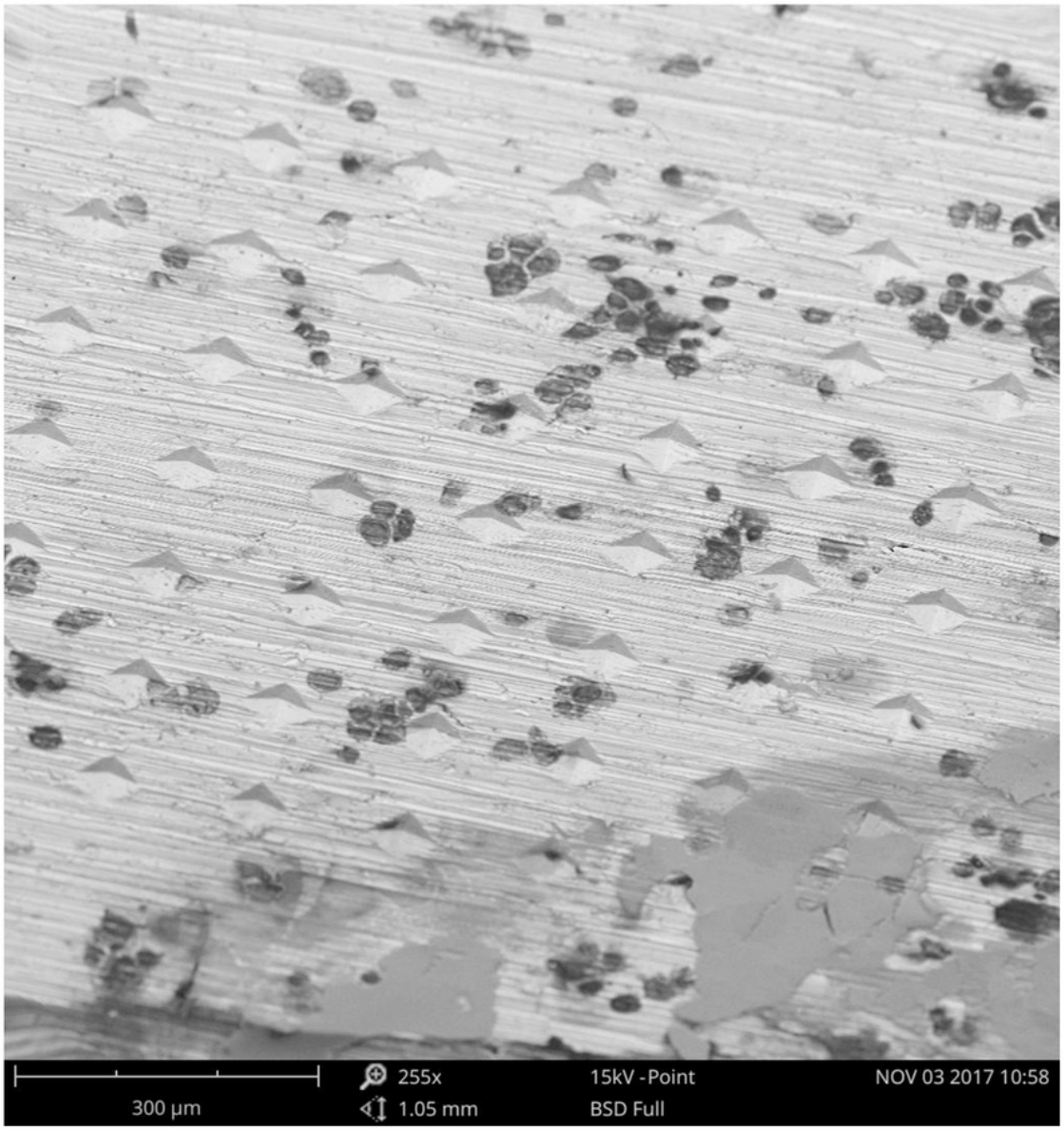

Figure 121 - SEM image of cell culture on sample 13

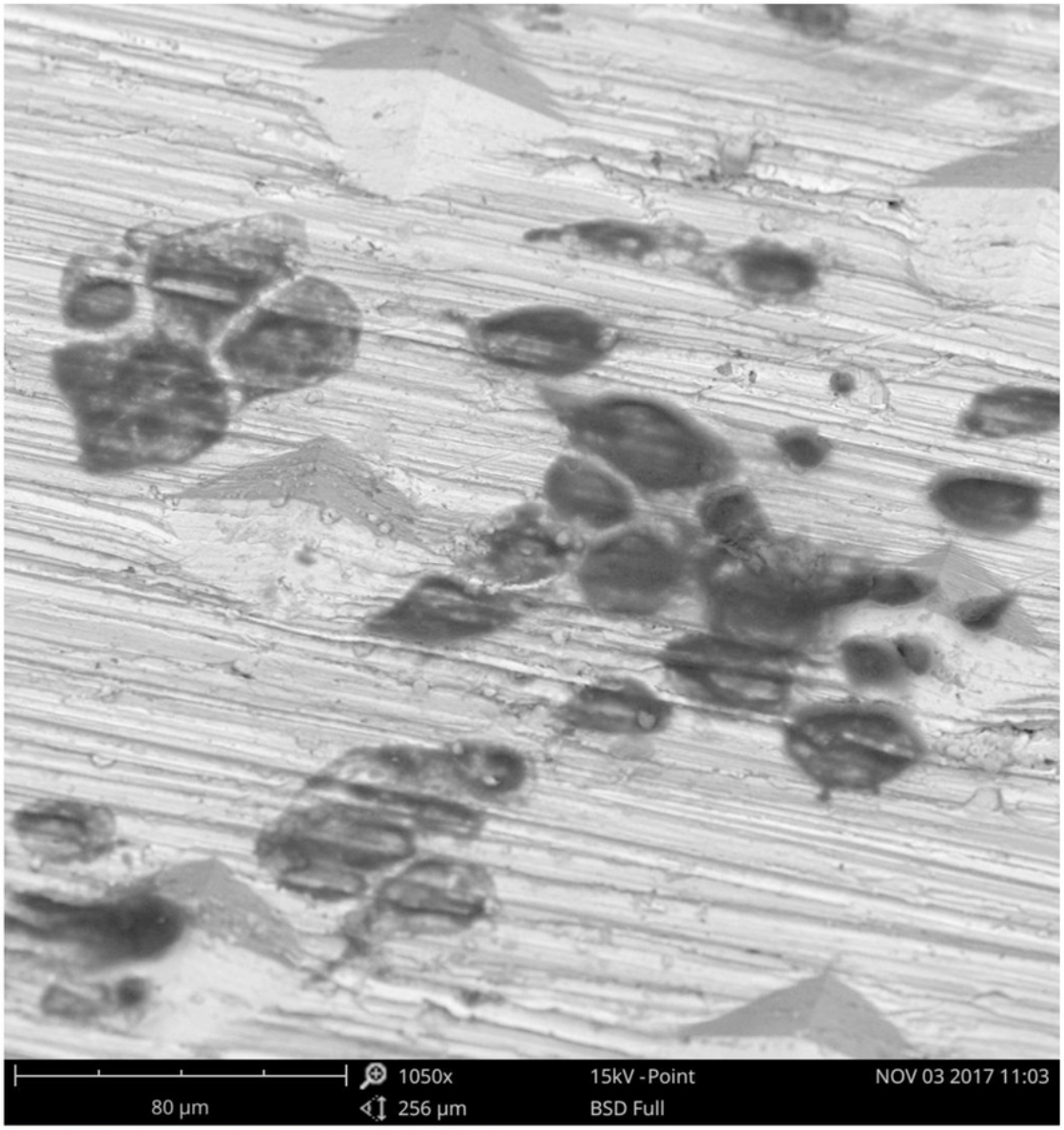

Figure 122 - SEM image of cell culture on sample 13

Sample 16

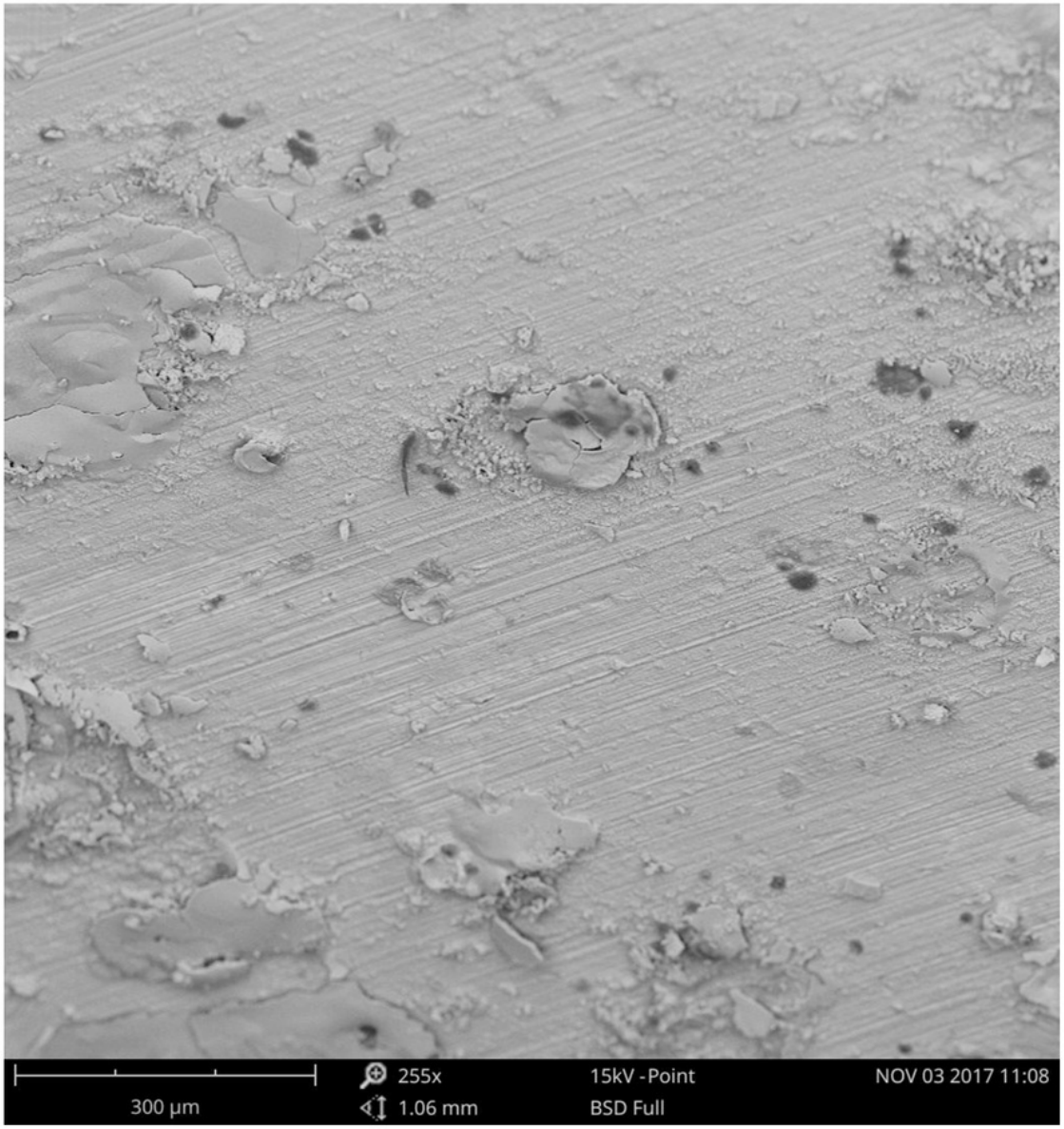

Figure 123 - SEM image of cell culture on sample 16

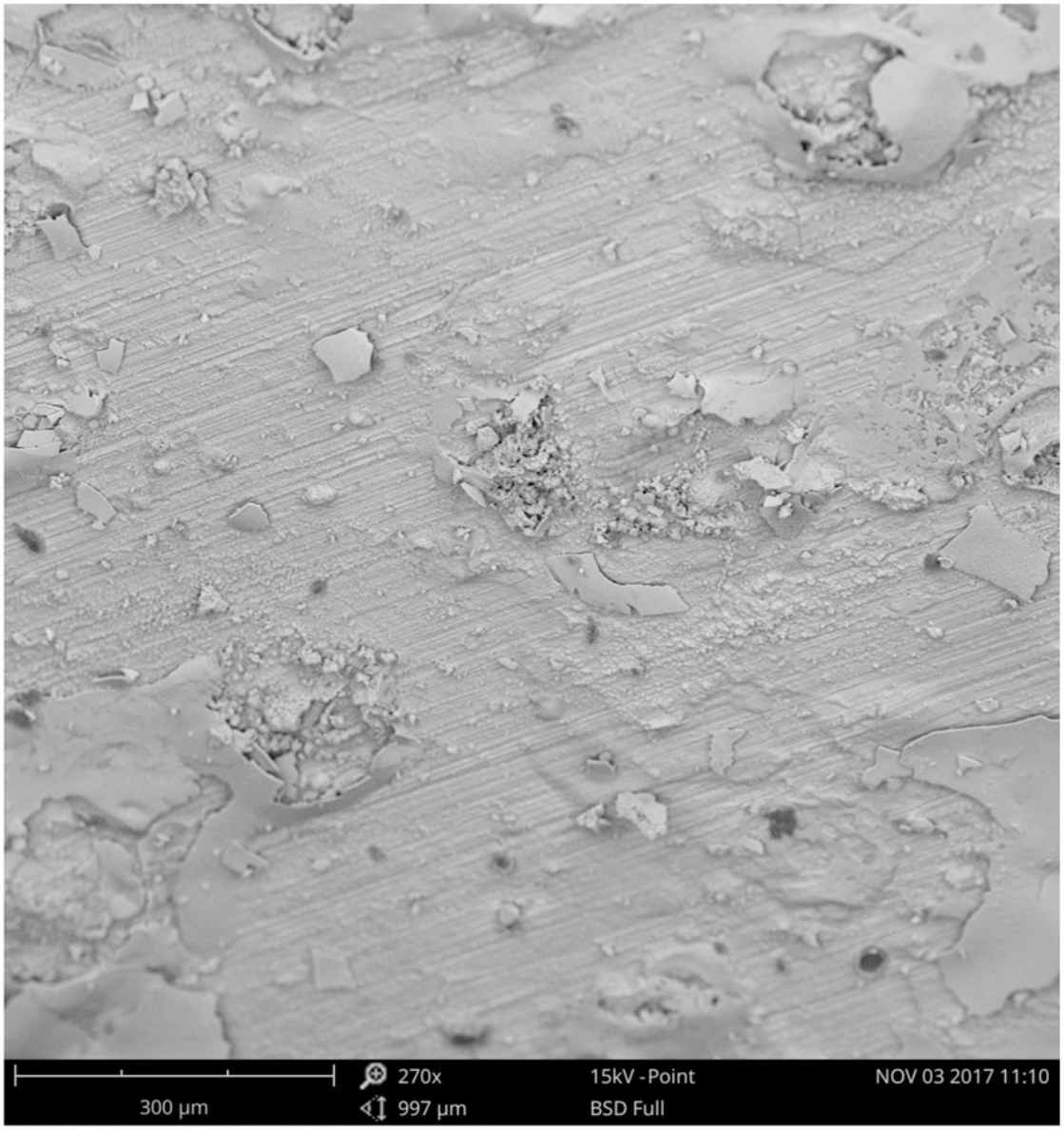

Figure 124 - SEM image of cell culture on sample 16

Sample A

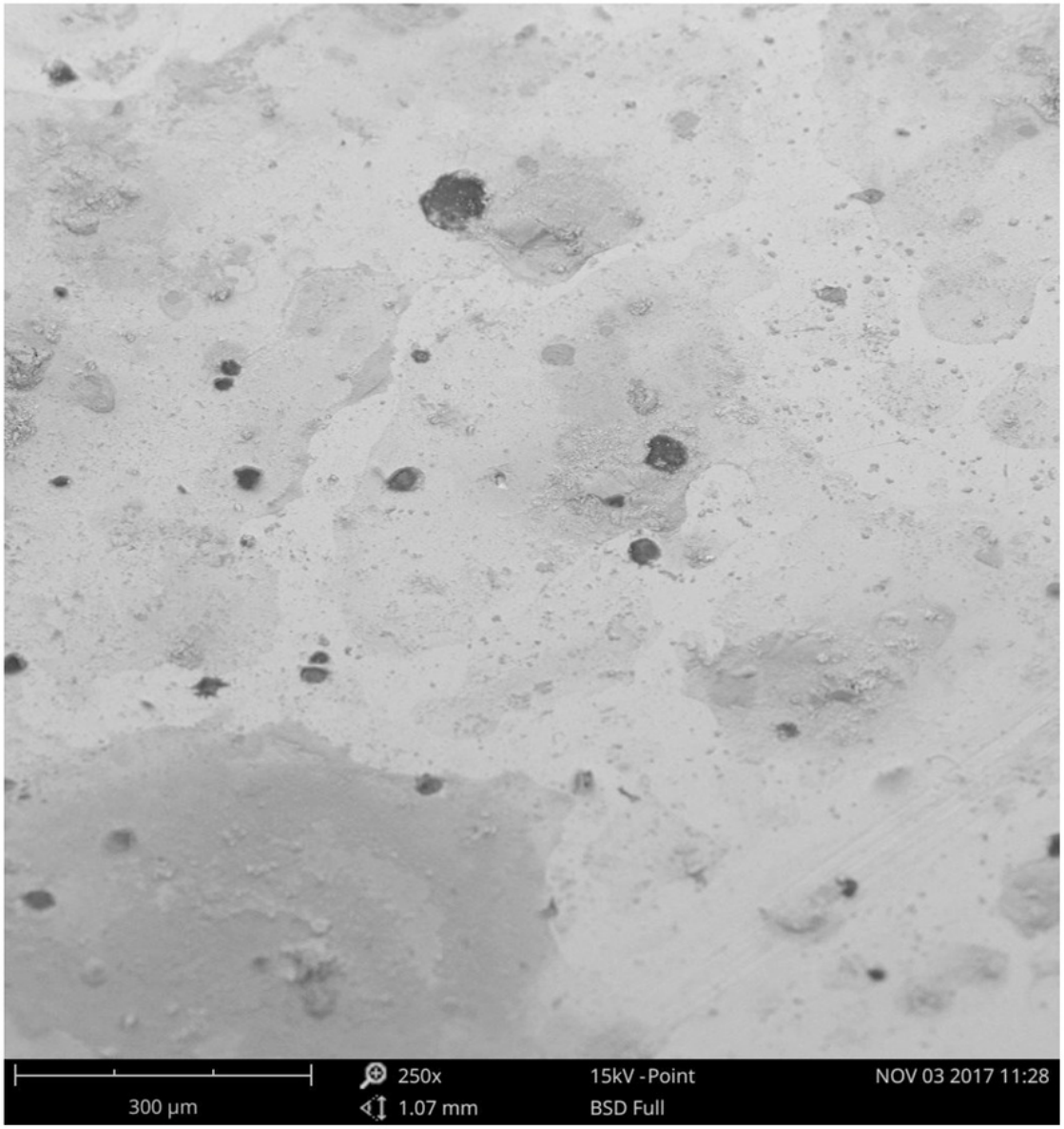

Figure 125 - SEM image of cell culture on sample A

Figure 126 - SEM image of cell culture on sample A

Sample B1

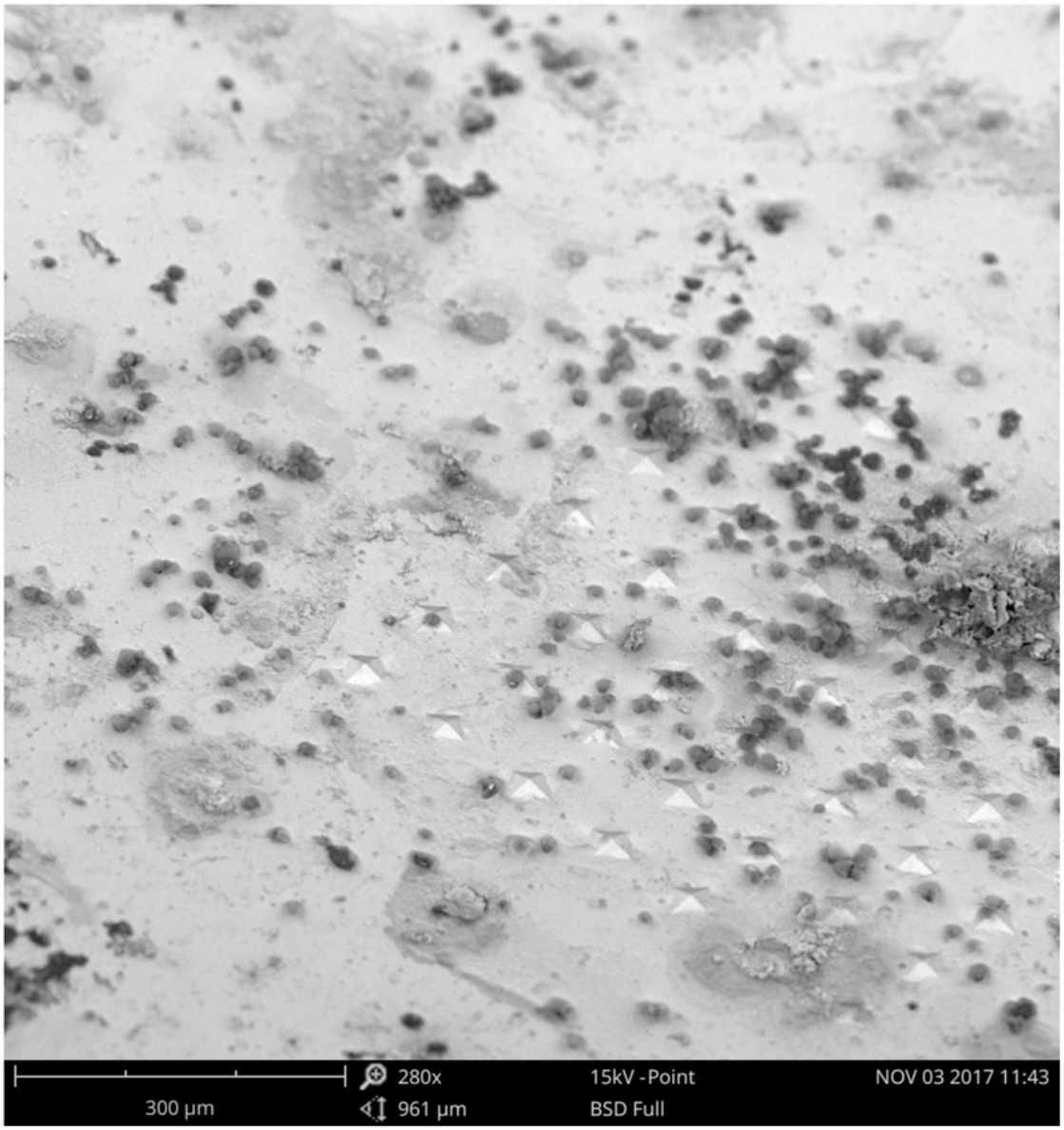

Figure 127 - SEM image of cell culture on sample B1

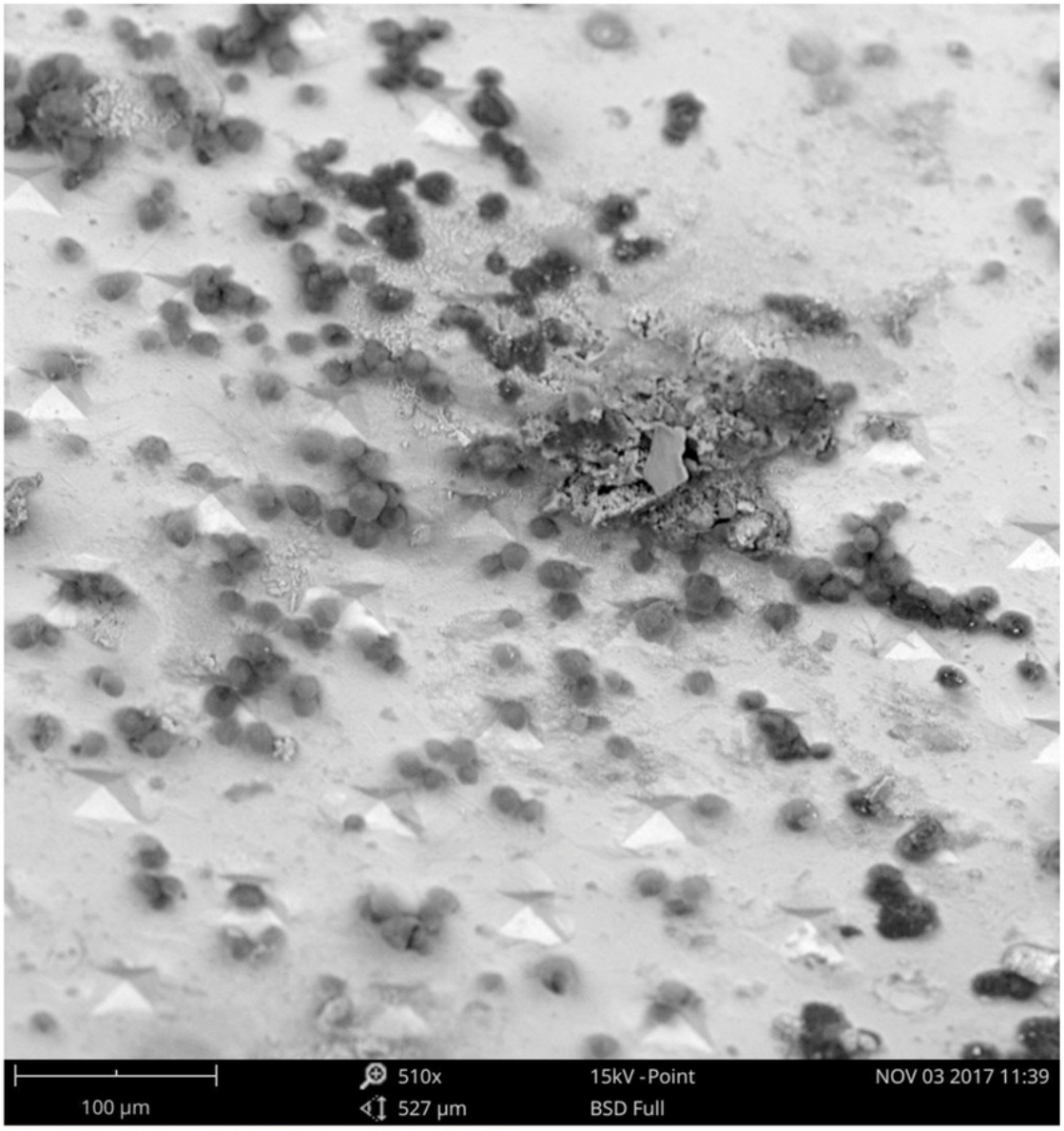

Figure 128 - SEM image of cell culture on sample B1

Sample B2

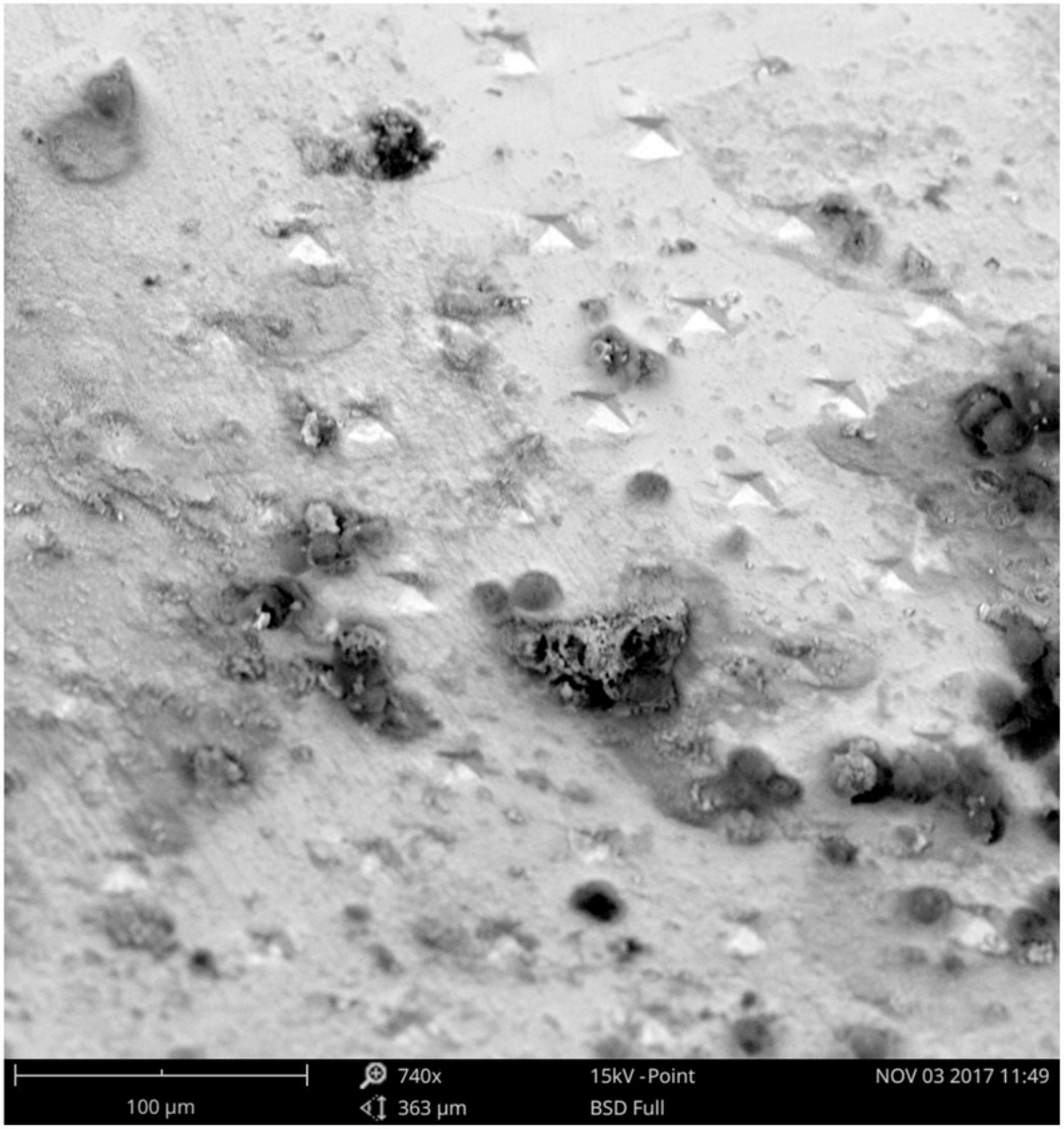

Figure 129 - SEM image of cell culture on sample B2

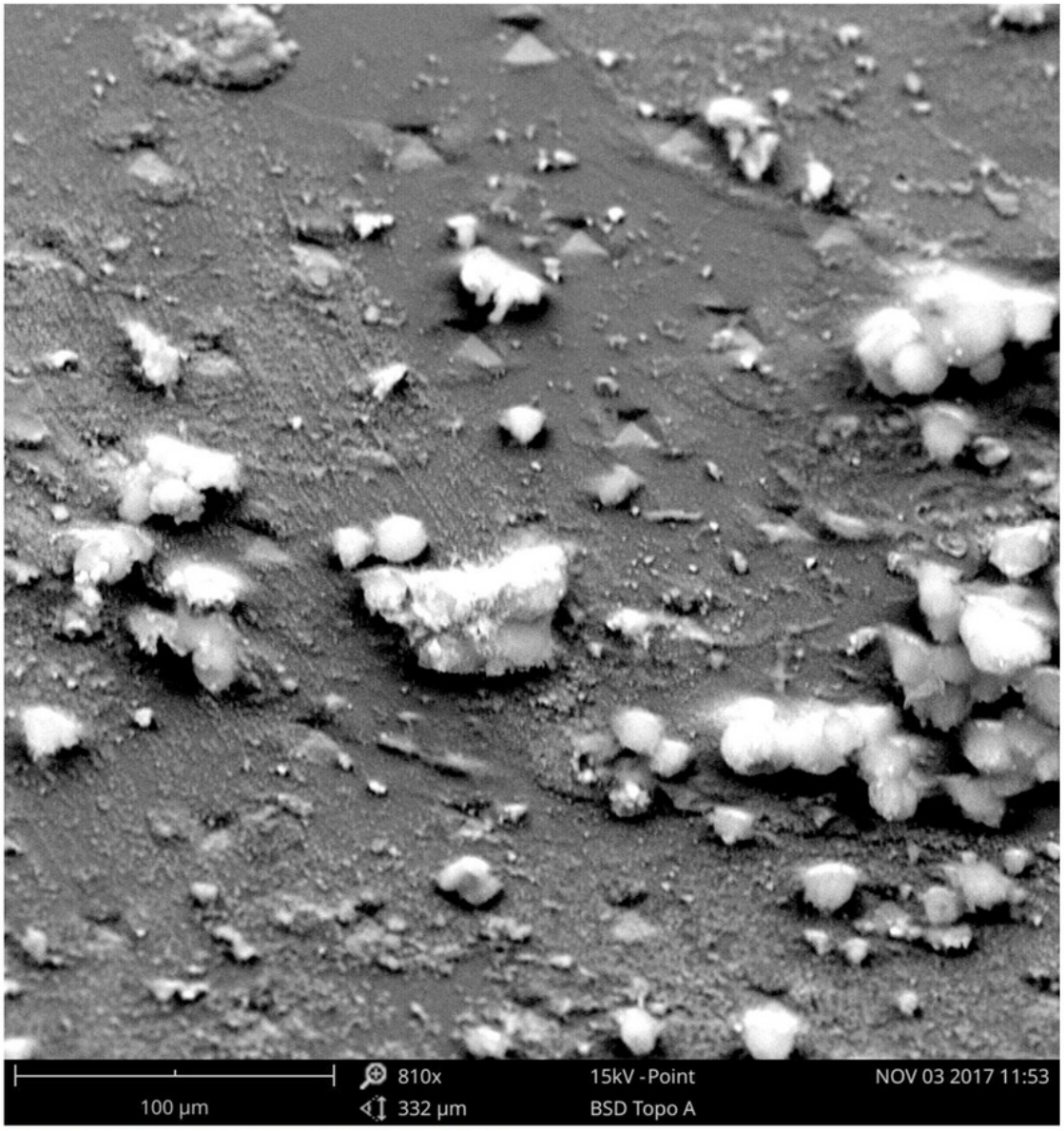

Figure 130 - SEM image of cell culture on sample B2

Sample B3

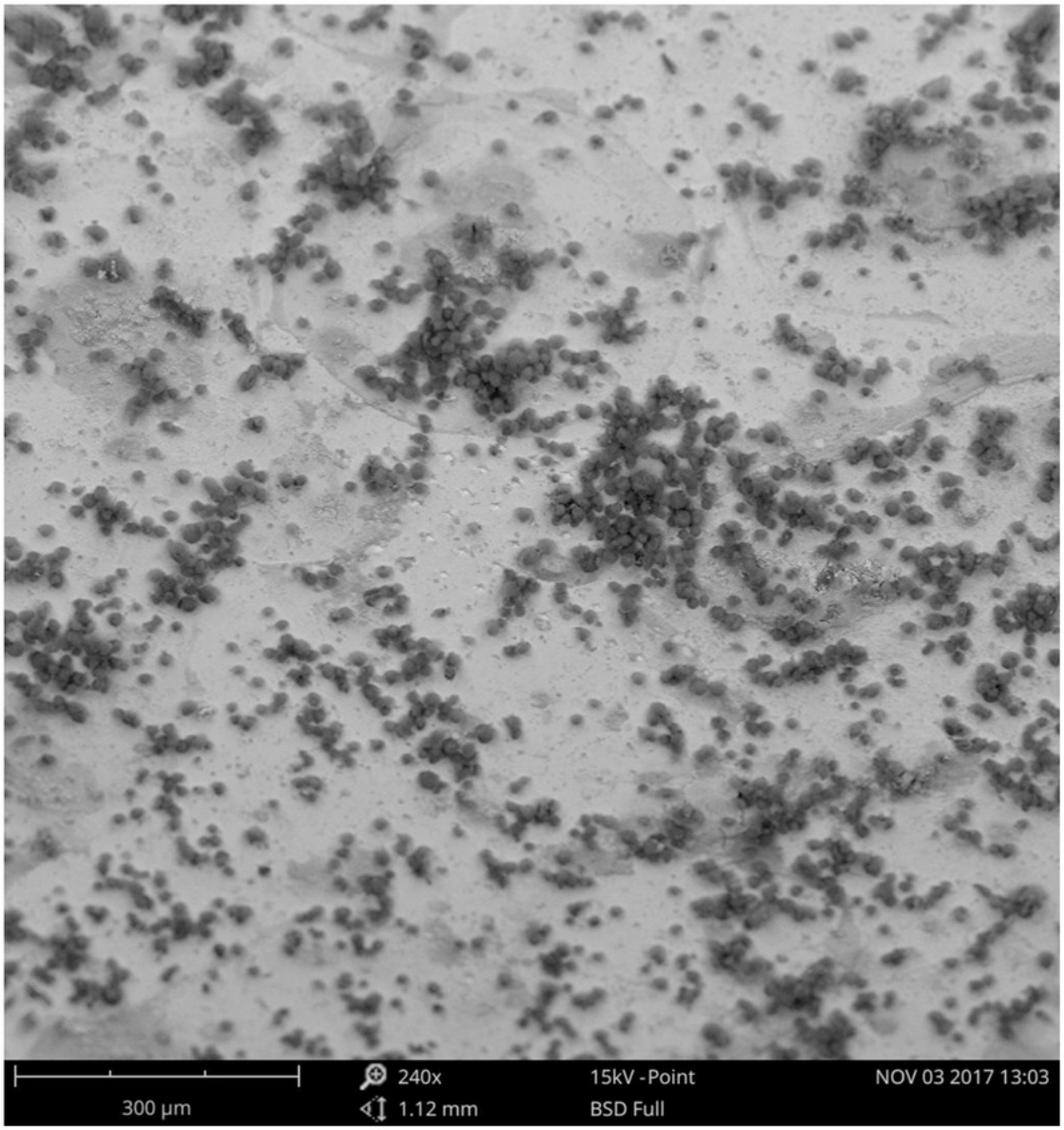

Figure 131 - SEM image of cell culture on sample B3

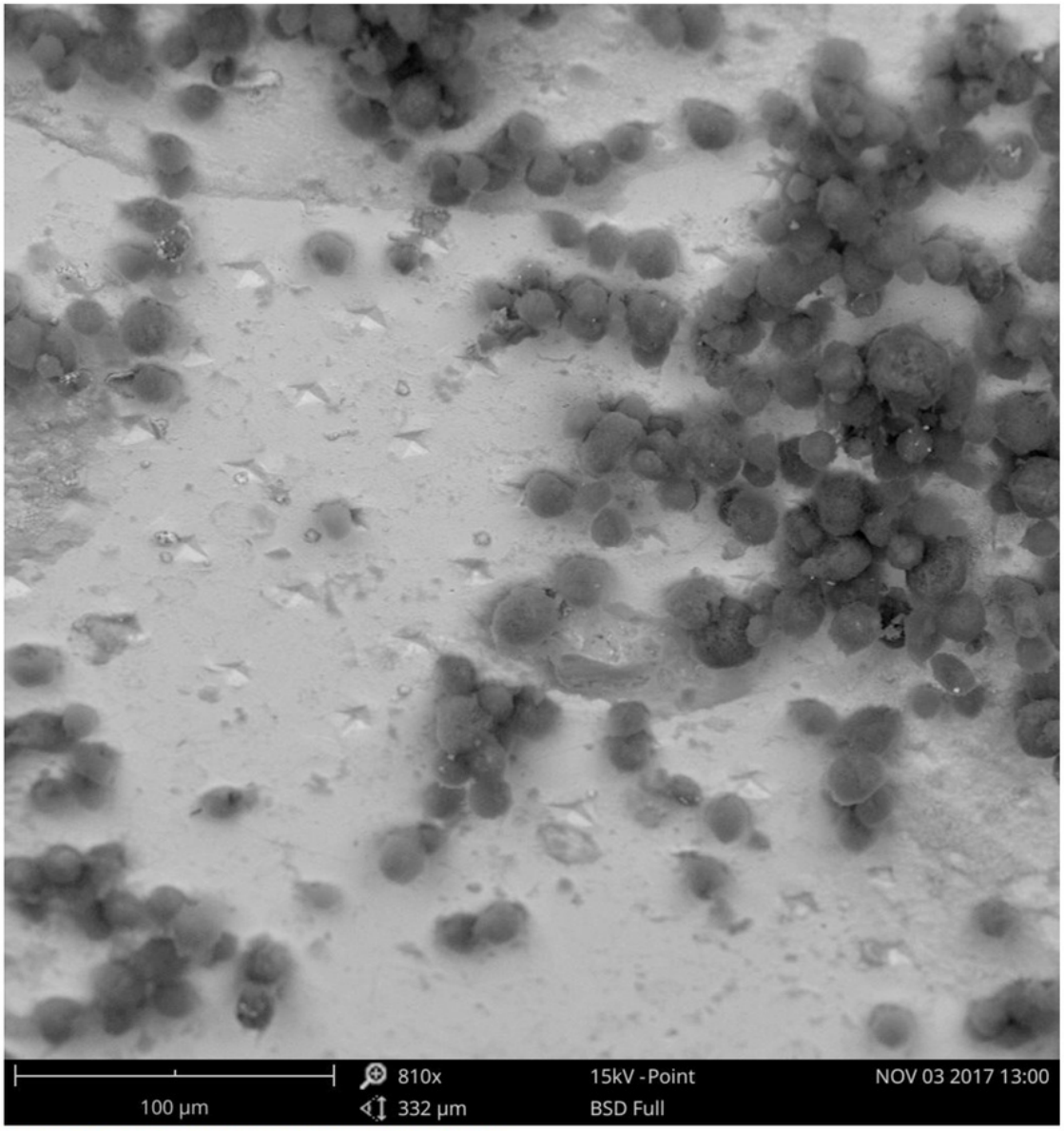

Figure 132 - SEM image of cell culture on sample B3

Sample C1

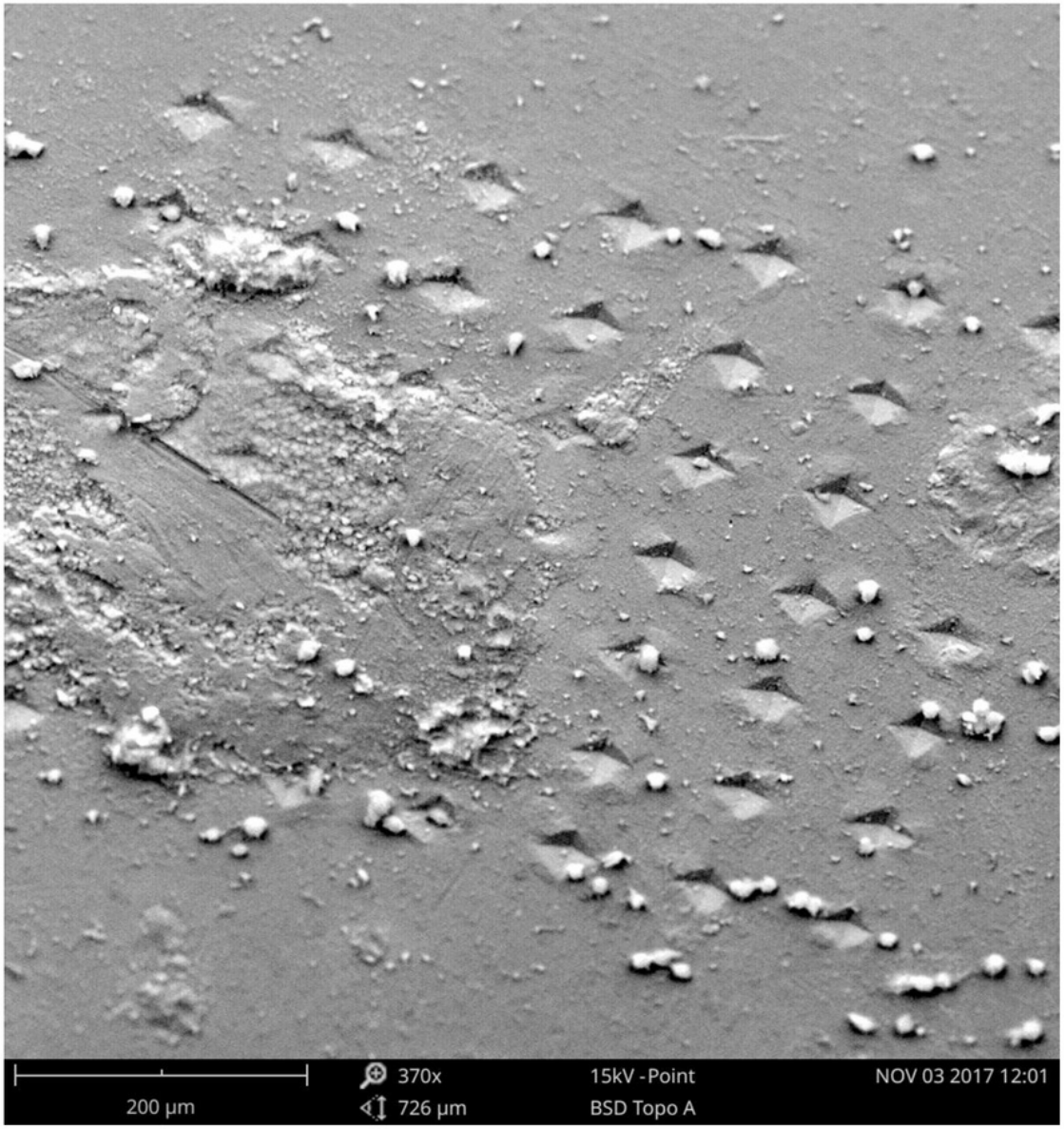

Figure 133 - SEM image of cell culture on sample C1

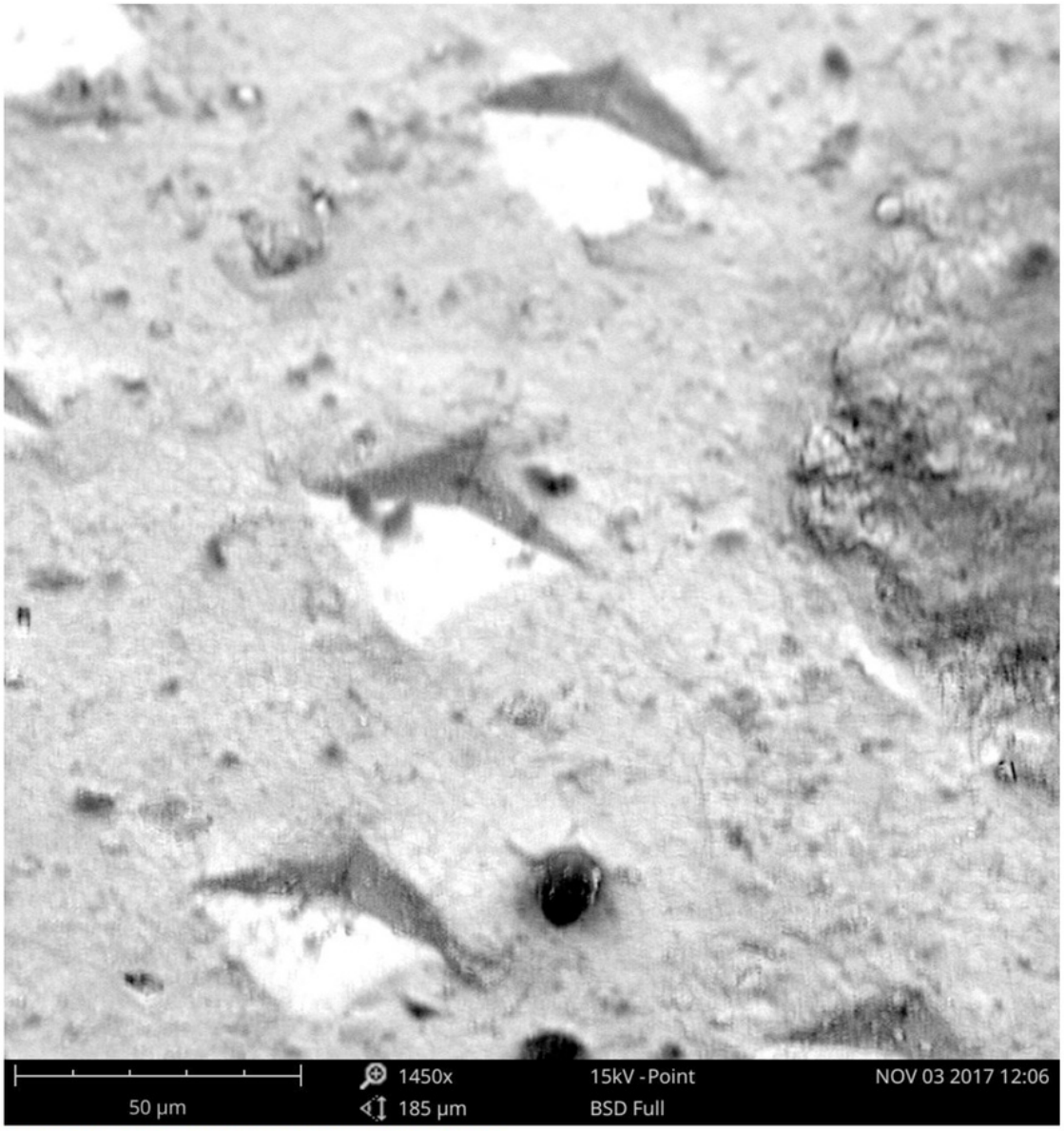

Figure 134 - SEM image of cell culture on sample C1

Sample C2

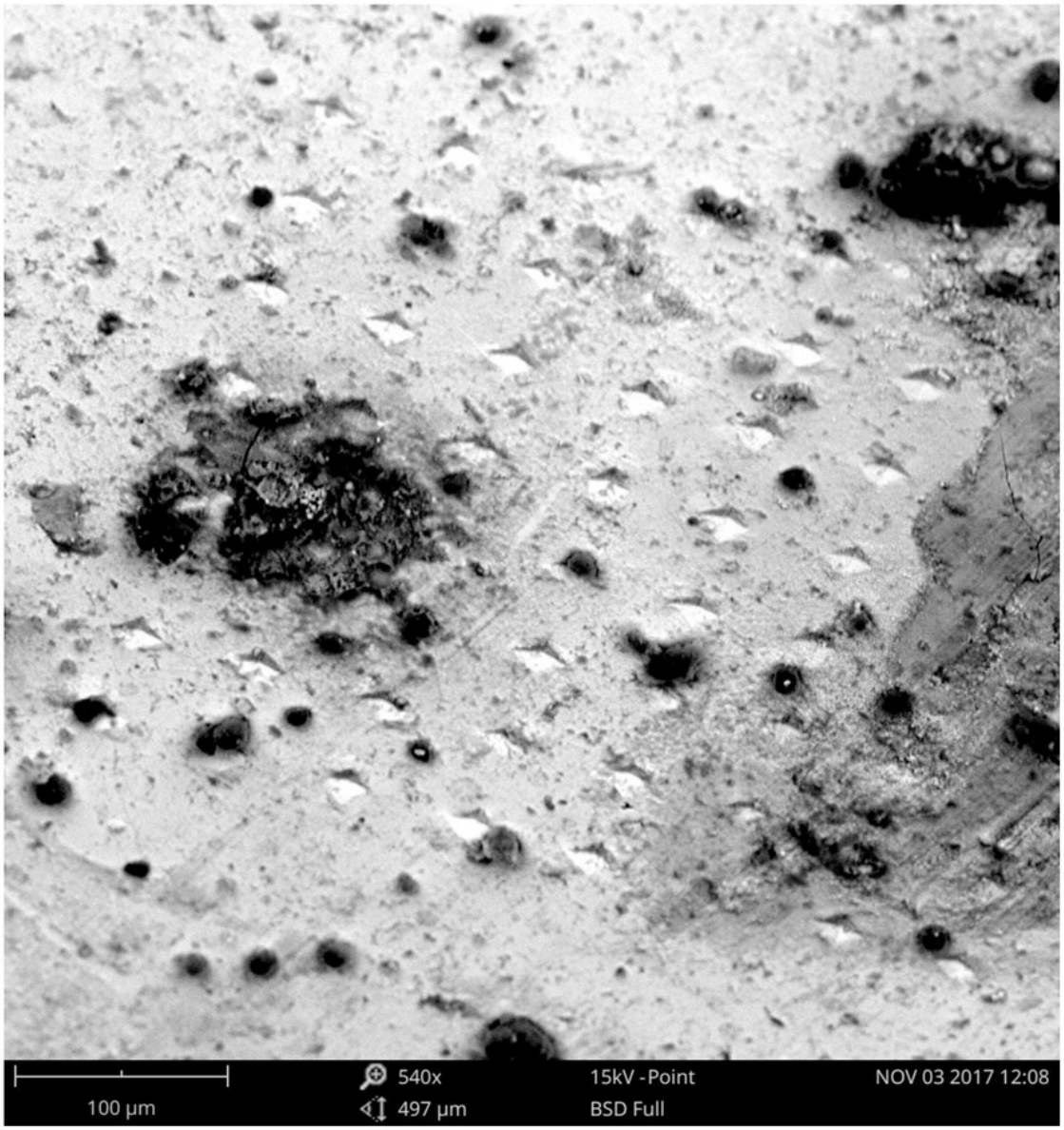

Figure 135 - SEM image of cell culture on sample C2

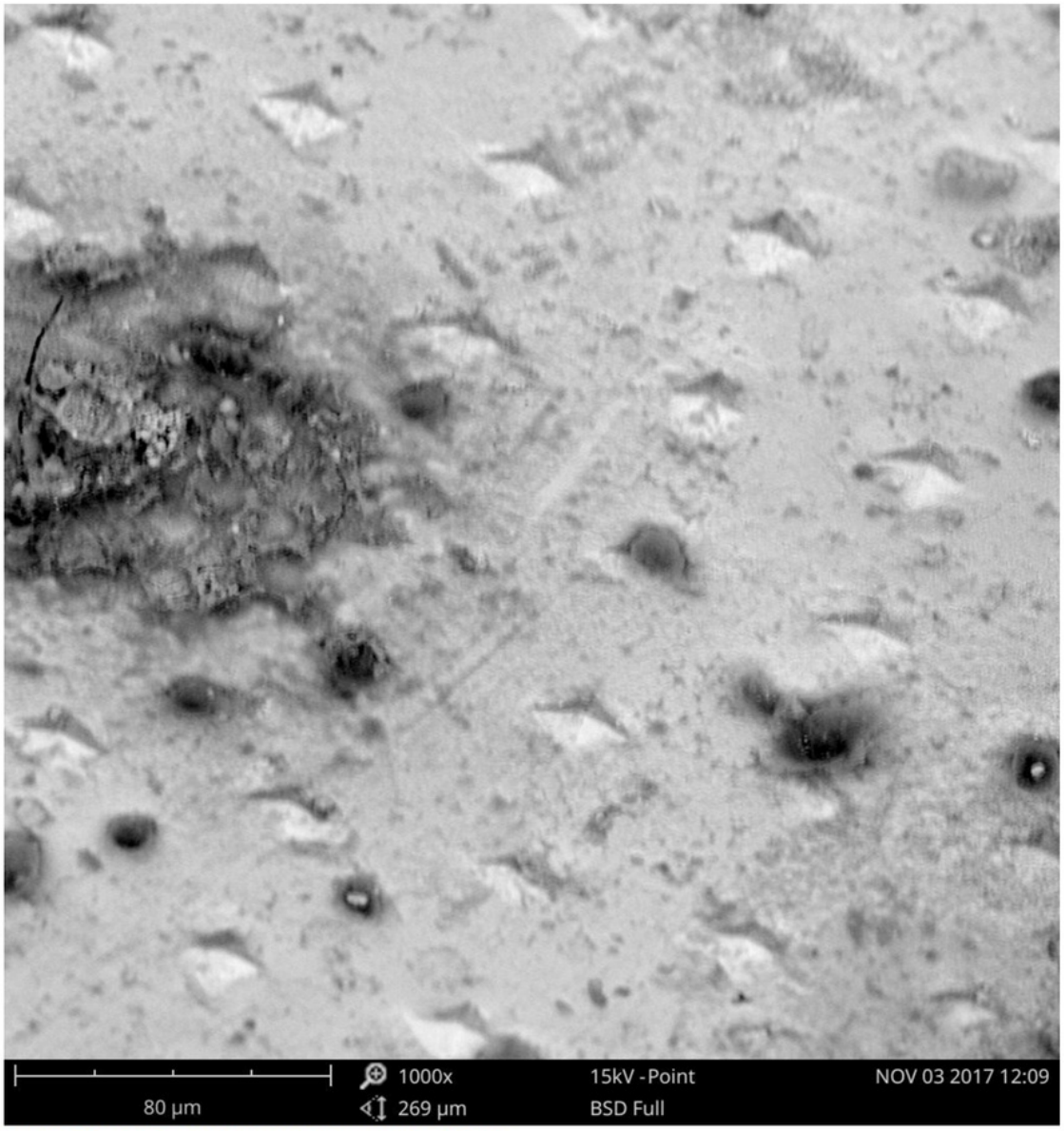

Figure 136 - SEM image of cell culture on sample C2

Sample C3

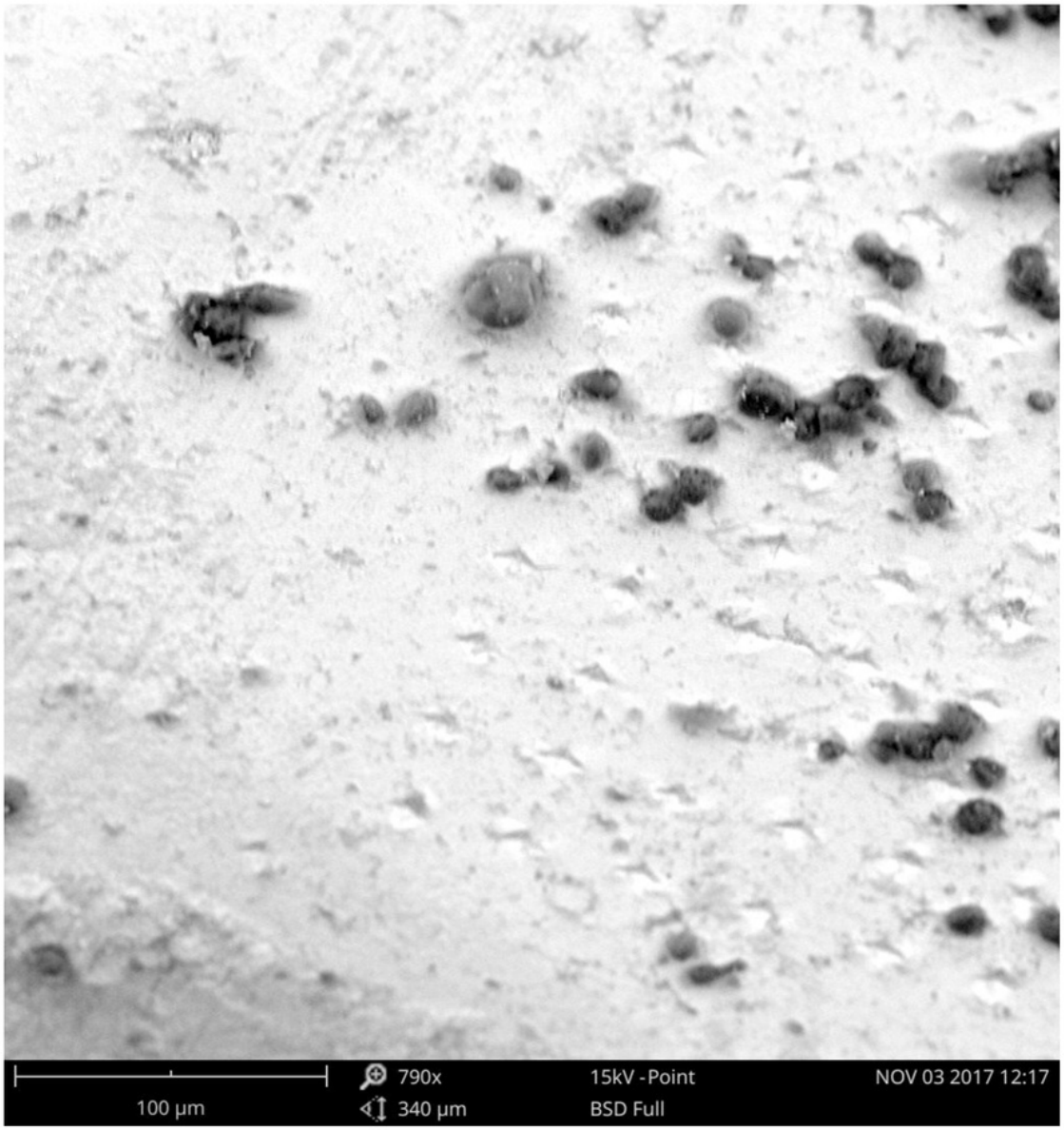

Figure 137 - SEM image of cell culture on sample C3

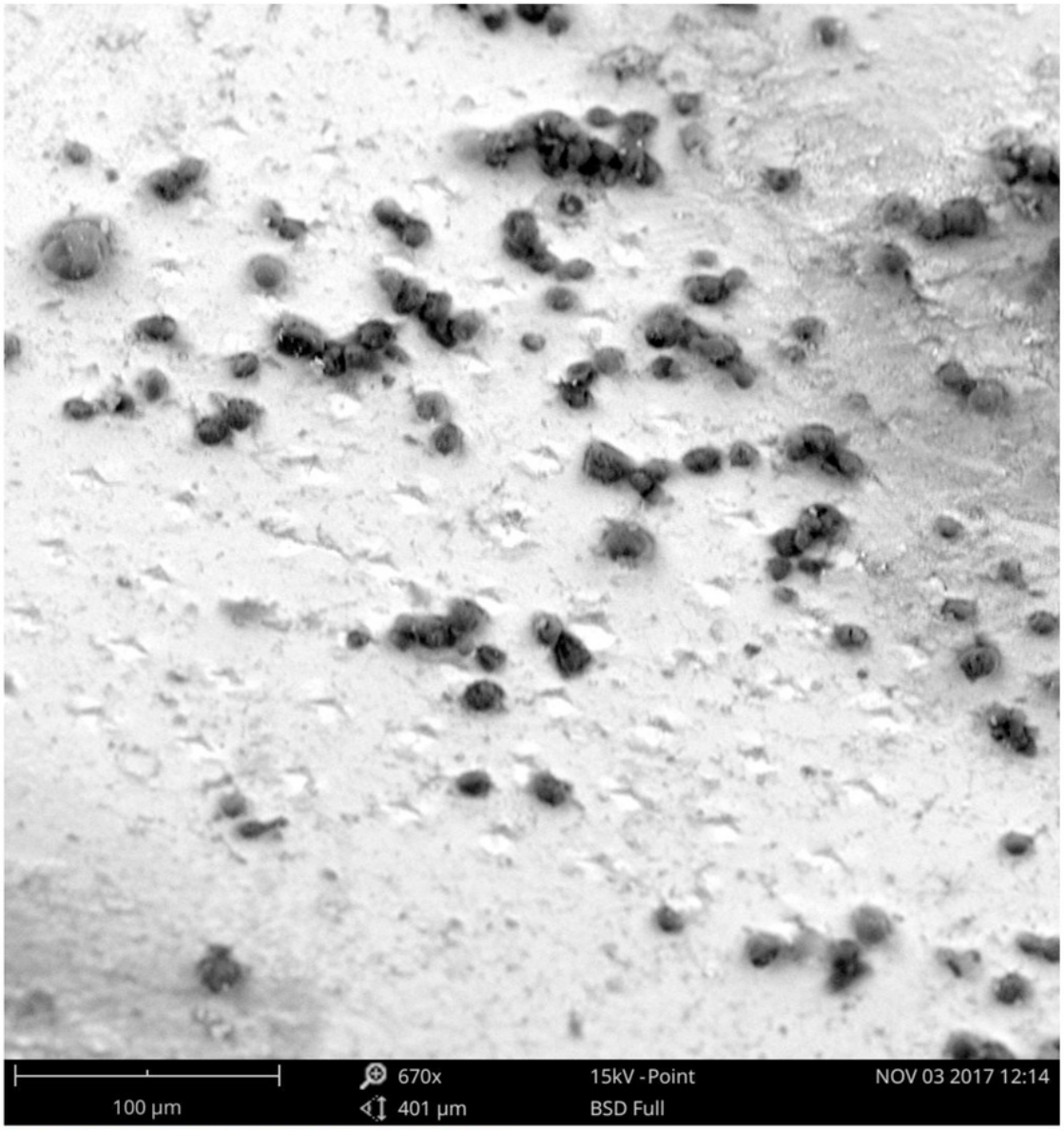

Figure 138 - SEM image of cell culture on sample C3

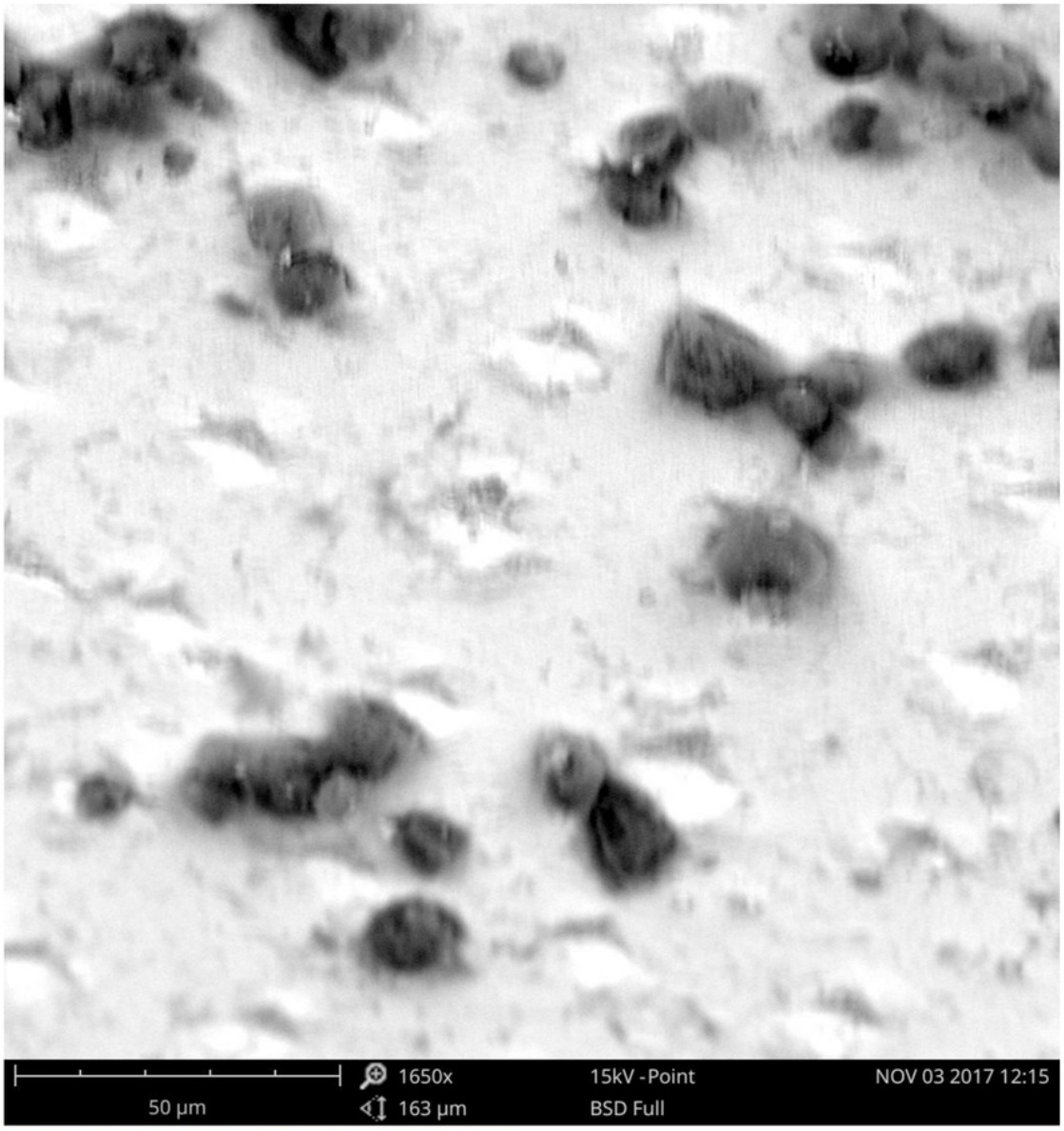

Figure 139 - SEM image of cell culture on sample C3

Sample D1

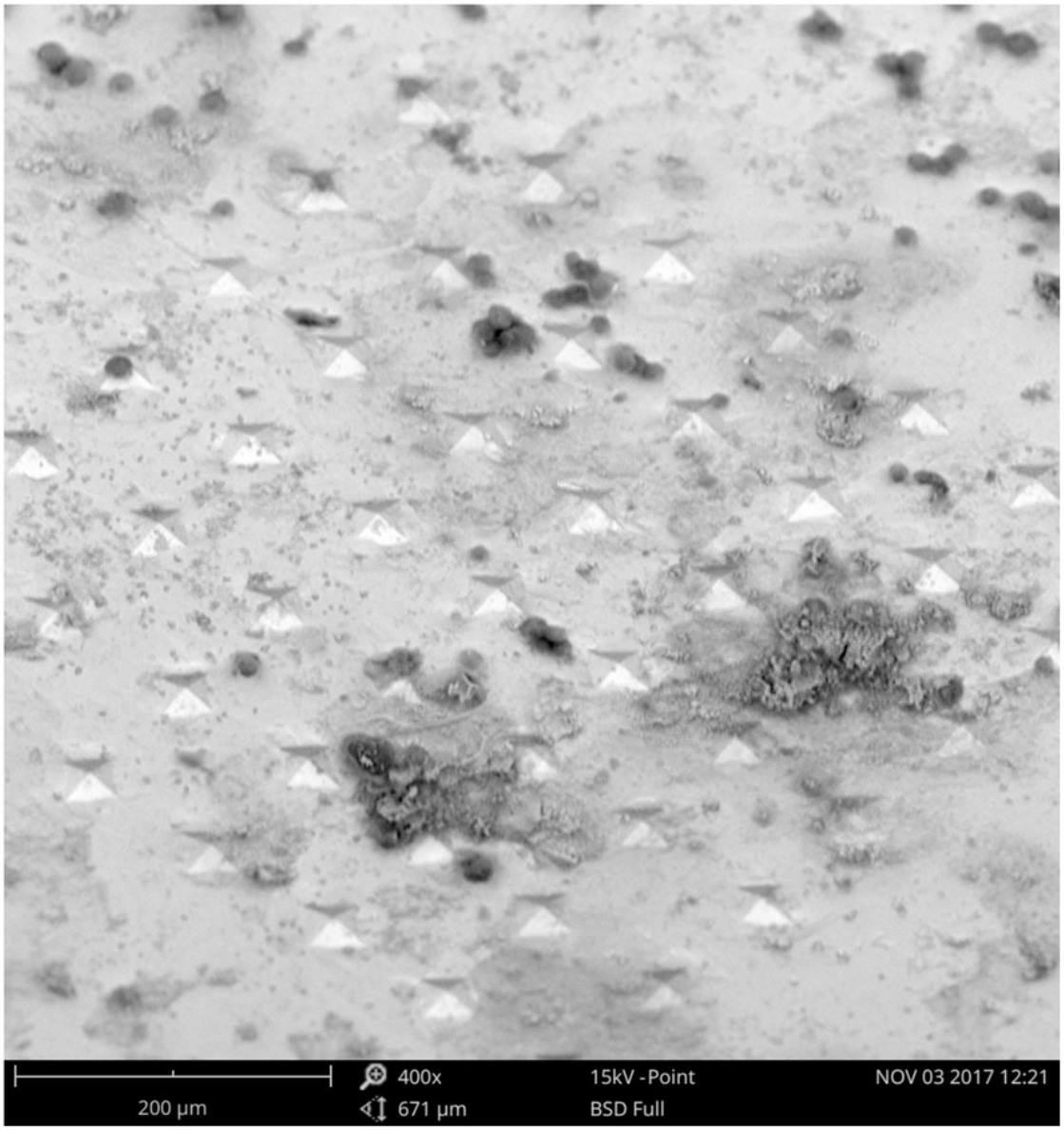

Figure 140 - SEM image of cell culture on sample D1

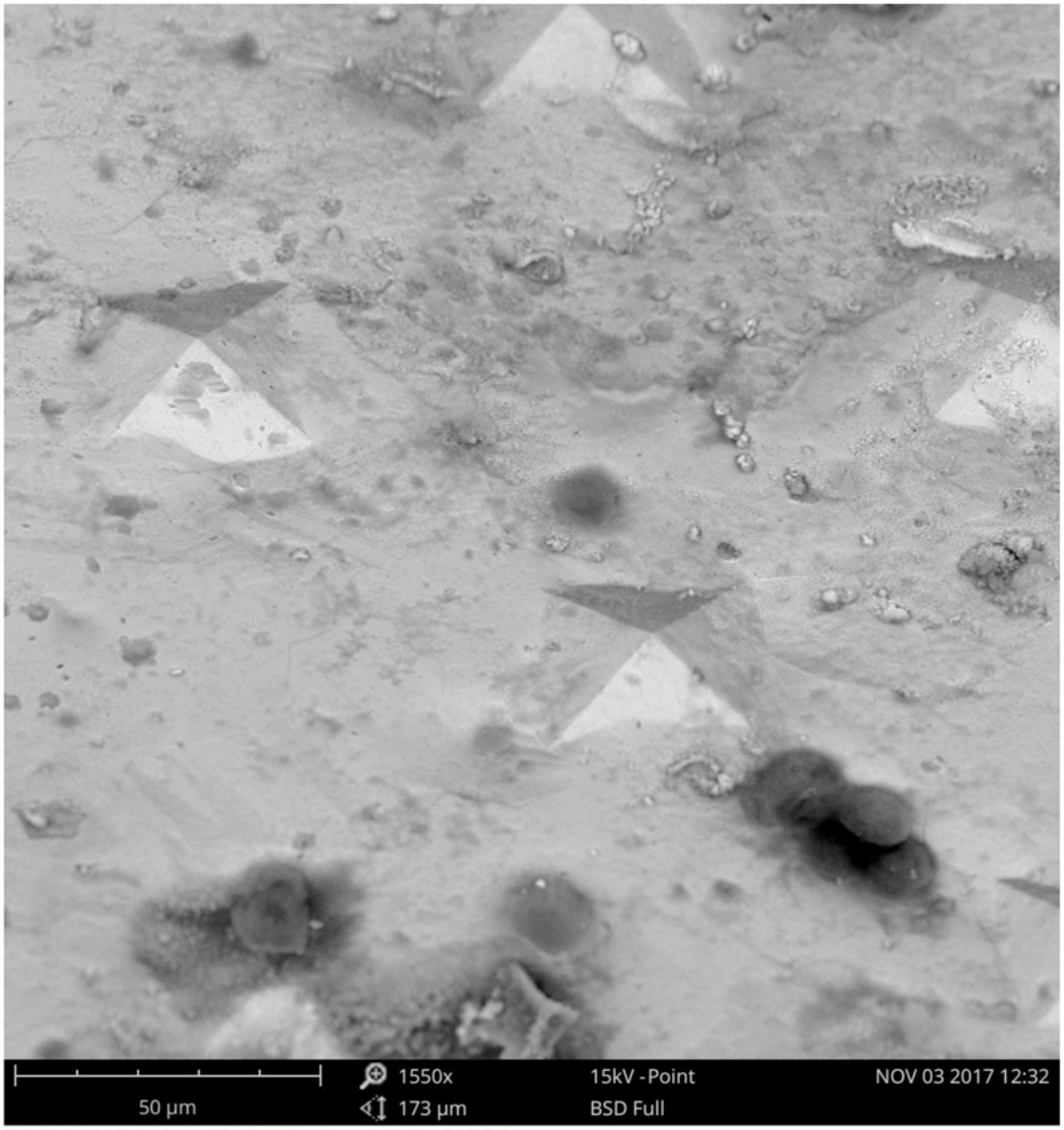

Figure 141 - SEM image of cell culture on sample D1

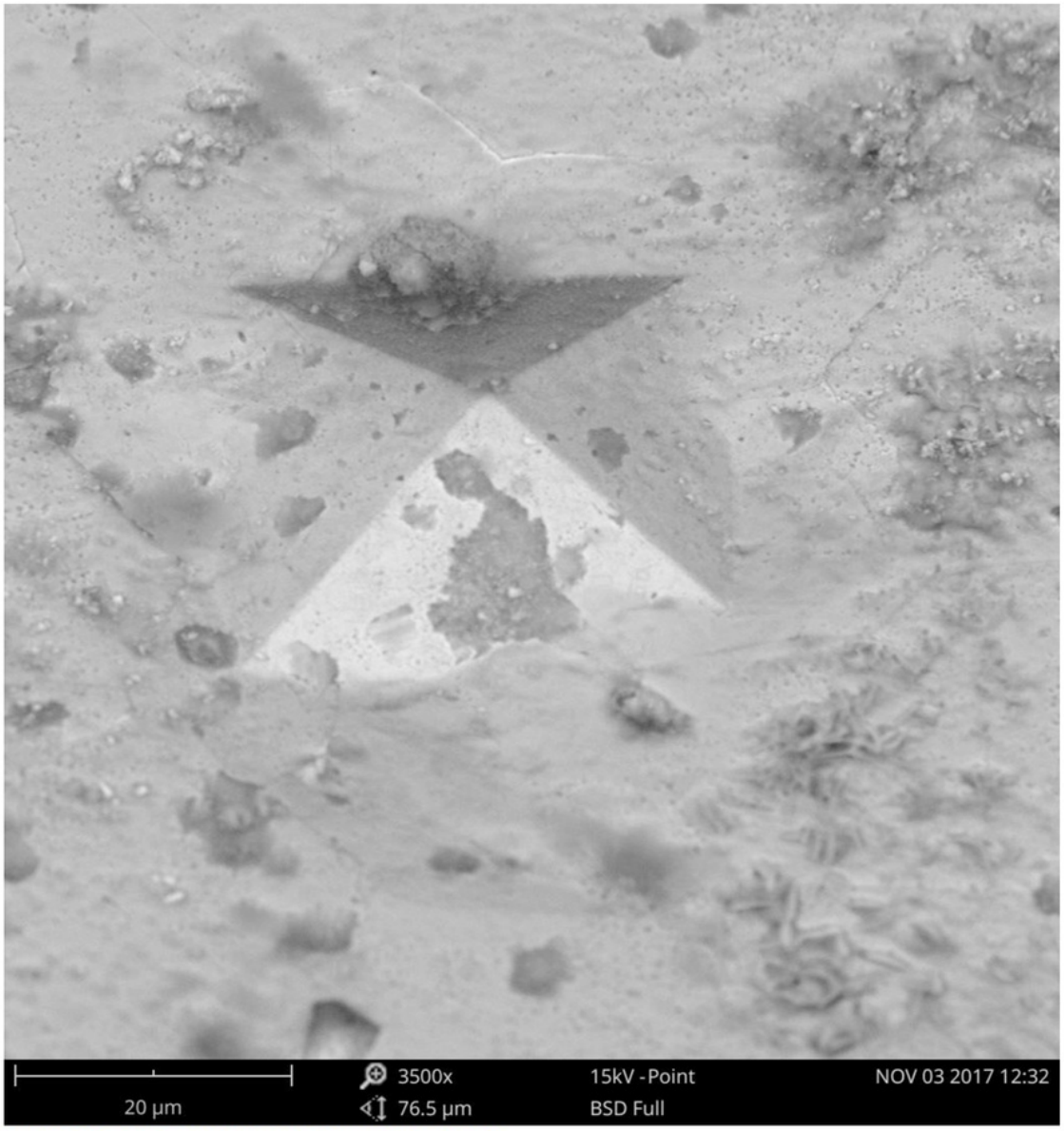

Figure 142 - SEM image of cell culture on sample D1

Sample D2

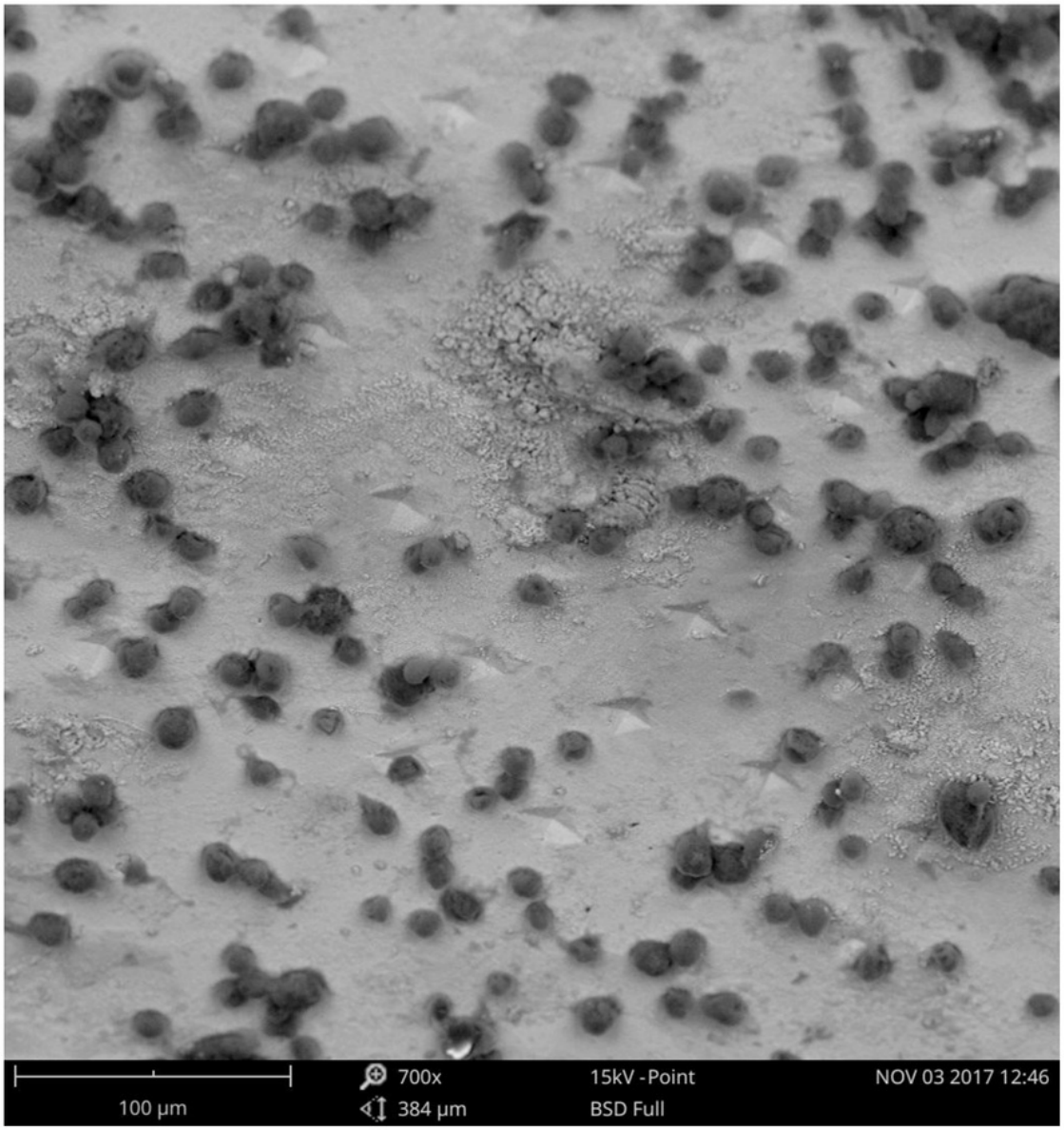

Figure 143 - SEM image of cell culture on sample D2

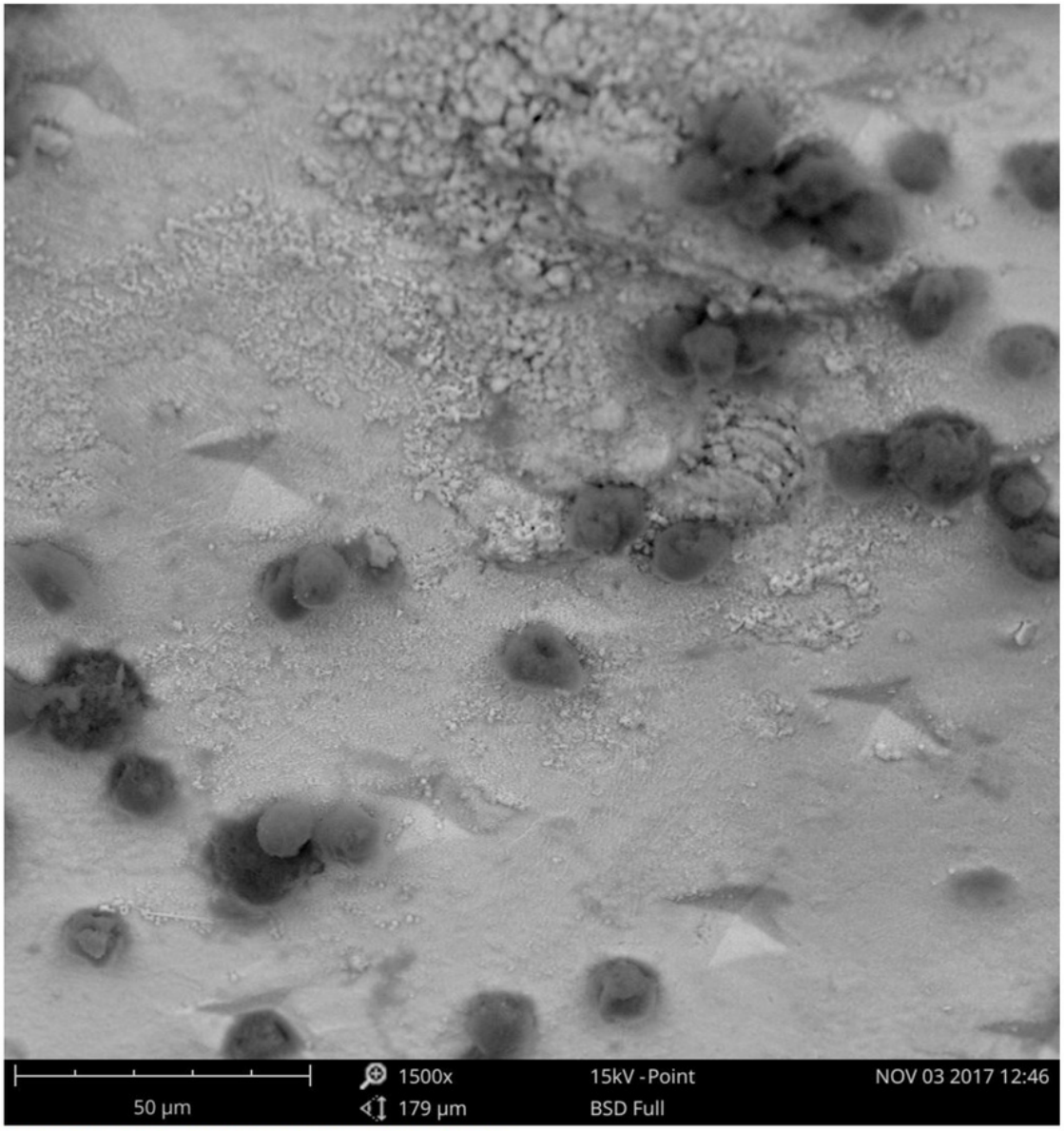

Figure 144 - SEM image of cell culture on sample D2

Sample D3

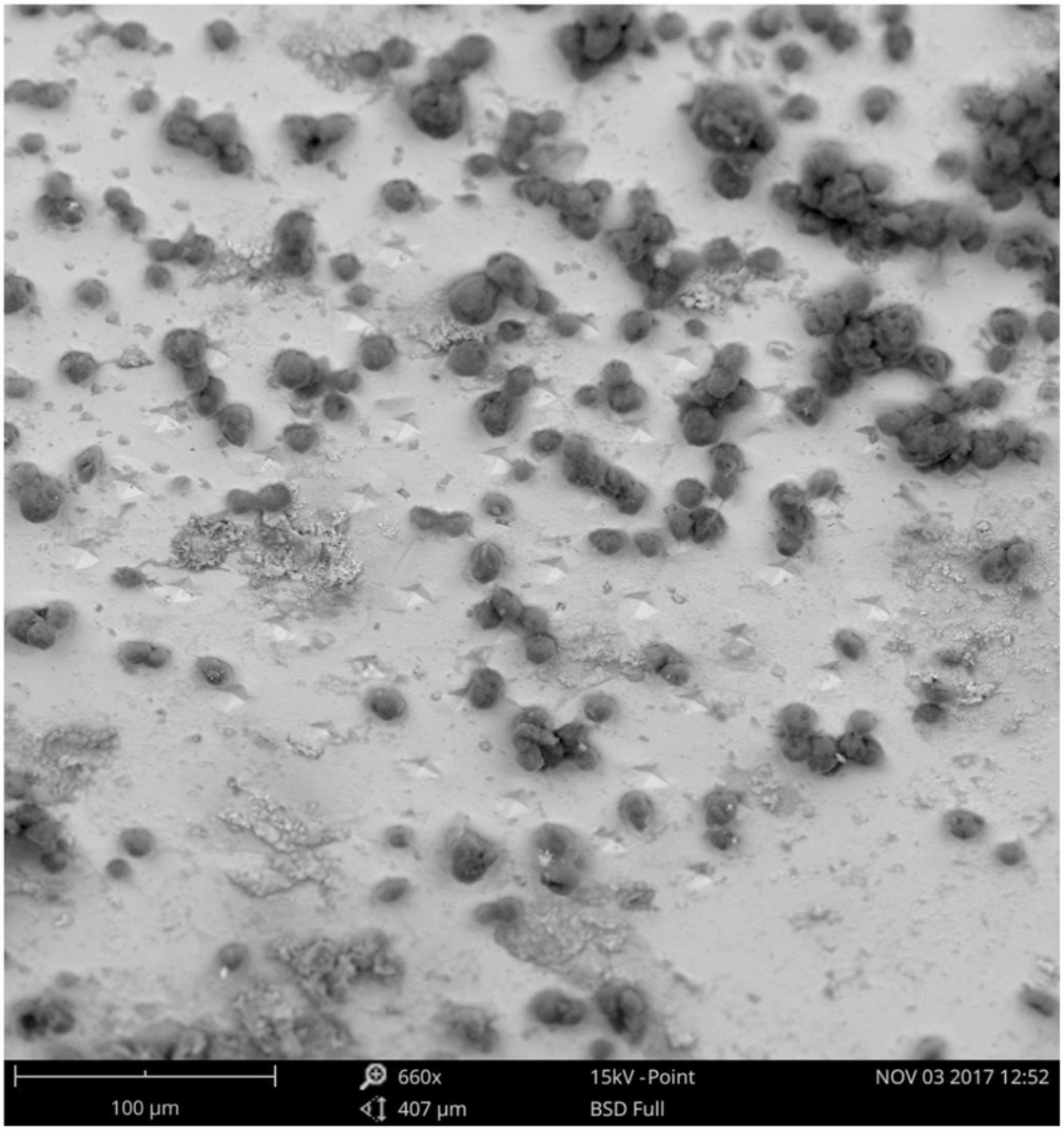

Figure 145 - SEM image of cell culture on sample D3

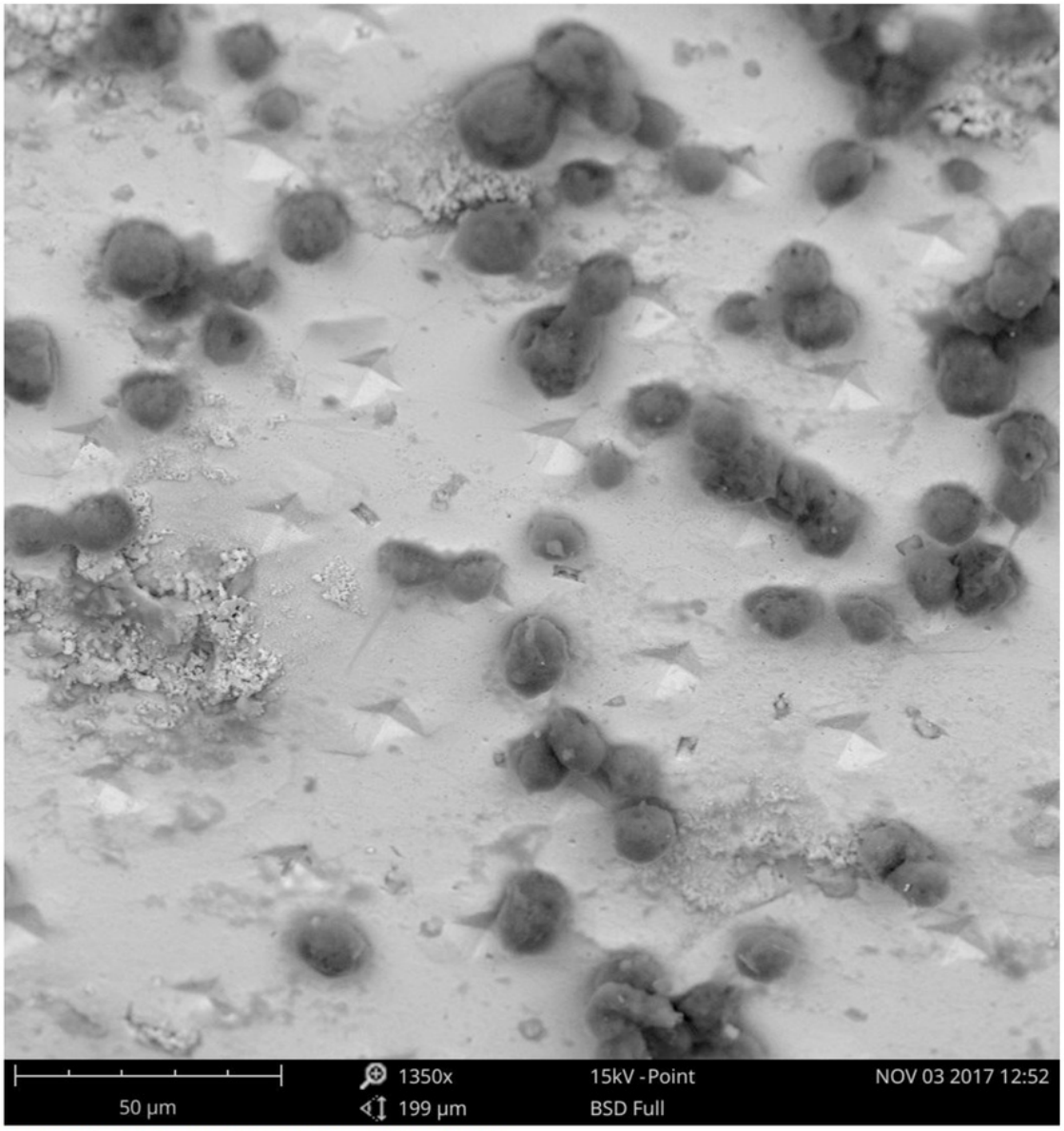

Figure 146 - SEM image of cell culture on sample D3

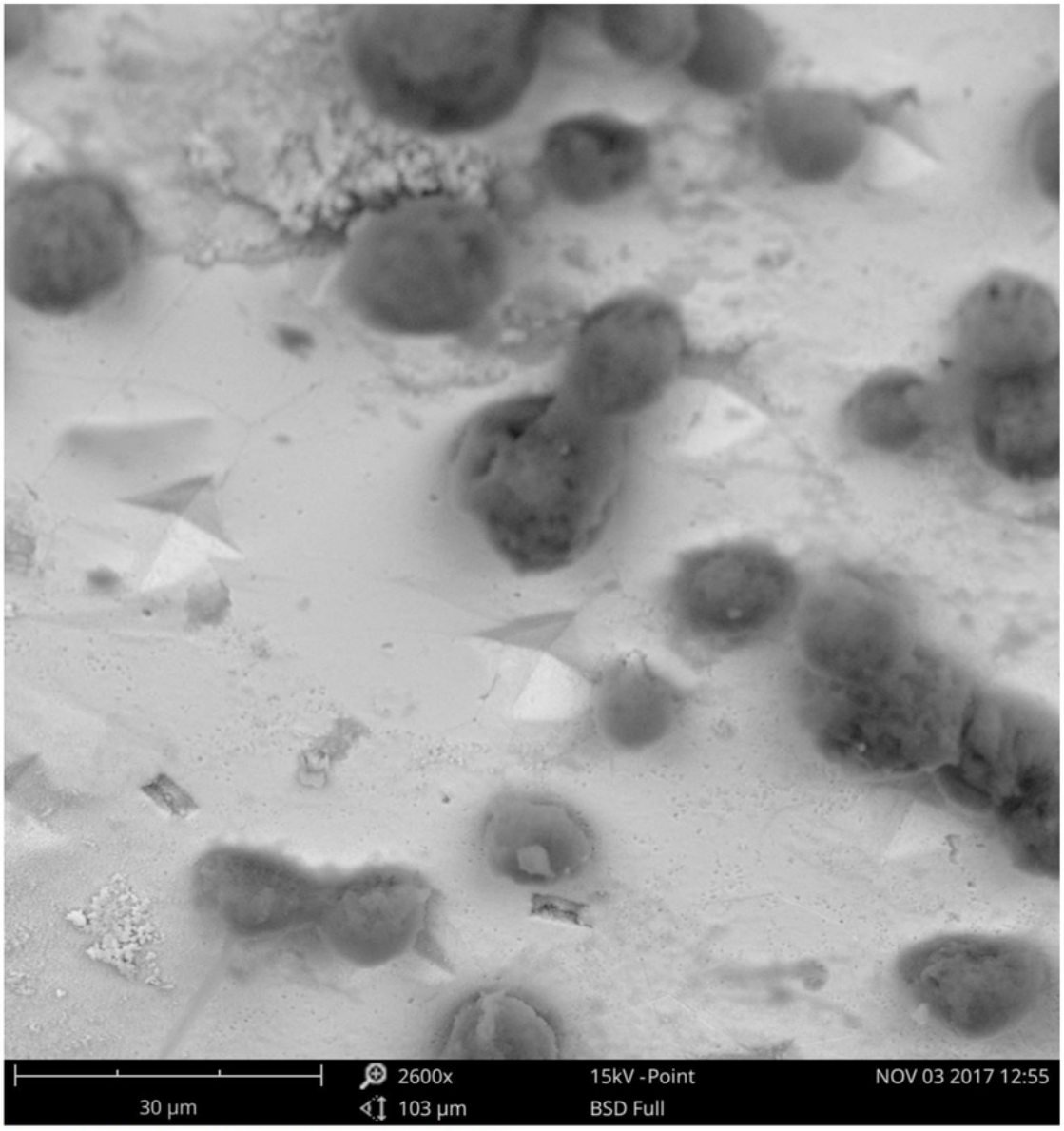

Figure 147 - SEM image of cell culture on sample D3